Dissertation

Master in Civil Engineering – Building Construction

Performance-based design of bolted steel structures

Hernán Alberto Coloma Peralta

Leiria, July 2018

Dissertation

Master in Civil Engineering – Building Construction

Performance-based design of bolted steel structures

Hernán Alberto Coloma Peralta

Dissertation developed under the supervision of professor Hugo Filipe Pinheiro Rodrigues, adjunct professor at the School of Technology and Management of the Polytechnic Institute of Leiria.and professor Byron Armando Guaygua Quillupangui at Central University of Ecuador

Leiria, July 2018

1. Dedication.

This work is dedicated to my family, girlfriend, and friends that has been my major inspiration in my life their support and love have guide me to this journey giving me the force to continue and overcome all prove that I have faced.

2. Thanks.

I would like to thanks the IPL's teachers for shearing their knowledge and support during the master and I want to thanks specially to my advisor Professor Hugo Filipe Pinheiro Rodrigues for his friendship, guide and advice that make possible this thesis.

I would like to thanks engineer Alex Farinango and Sedemi company for provide the information and characteristic of the study case.

I would like to thanks to the Universidad Central del Ecuador and SENESCYT for the given opportunity.

Finally, I would like to thanks to the most important people in my life my family, girlfriend and friends. During the develop of this thesis, they encourage me to give my maximum effort.

3. Abstract

In the last decade, the philosophy of seismic design has change from the force-based design to performances based design due to the advantage that presents. Also, the performance based the design presents less simplification of the force method representing in a more accurate form the real behavior of the structure. One method of this new philosophy is the direct displacement-based design (DDBD); this method permits to take in count in more exact form the nonlinear behavior than the force method. The DDBD can be used to design new structures and analyze the retrofit of structures of concrete, steel, composed and timber. In the case of steel structure, the formulas used represent a bilinear behavior of the material and the yield displacement proper of the steel structural system. This displacement method can be used with deferent demands optimizing the design.

Another technique used in the performed based design is the pushover analysis. This method can be used to design new structures, evaluated design, optimizing design and retrofit the structures. The pushover considers in a more accurate form the nonlinear behavior of the structure, and it show the fail mechanism; it can analysis if the structure presents the condition of strong column weak beam. Also, it can be determining the ductility and the damping of the structure.

Another concert that engineers have nowadays is the design higher structures that satisfy high demands. In order to reaches the performance that require this demand seismic protection systems are used such as damper and insulators. In this project, the fluid viscous dampers are study; the advantages that present their used and the behavior faced a seismic event using time history analysis.

Finally, it is designing a Fluid viscous dampers in study case to analysis the performance achieved and the advantage presented in the structure.

Keywords:

- Performance-based of in steel structures
- Direct displacement-based design steel frame structures.
- Pushover steel frame structures.
- Fluid viscous damper.

4. List of figures

5. List of tables

6. Lista de siglas

- Δi = Floor displacements at level i
- δi = Normalized inelastic mode of level i
- δc = Critical distortion
- Hi = Height of level i
- Hn = Height of roof level
- DL = Dead Load
- LL =Live Load
- W = Reactive mass
- b section width
- bw width of web of flanged beam
- C constant
- Cm centre of mass
- E modulus of elasticity
- E force induced by seismic action
- Es steel modulus of elasticity
- Fsec secant modulus of elasticity of confined concrete at peak strength
- F force
- fd damping force
- Fel seismic force corresponding to elastic spectrum
- Fm maximum force
- ft tension strength
- fyh yield strength of hoop or spiral transverse reinforcement
- fyo maximum feasible steel strength
- fu steel ultimate stress
- G shear modulus; gravity load
- g acceleration due to gravity, 9.805m/s
- H height
- He effective height of SDOF approximation to multi-storey building
- Ht height of mass / in building design
- Hs storey height
- h section depth
- hb beam section depth
- hc column section depth
- I importance factor in force-based design; section moment of inertia
- I multiplier applied to design seismic intensity level
- It moment of inertia of beam section
- lc moment of inertia of column section
- K structure stiffness
- ka assessed structure stiffness at limit state
- Ke structure effective stiffness for DDBD
- Ki initial (elastic) stiffness
- k lr lateral stiffness of lead-rubber bearing
- Ks structure secant stiffness
- L length

- Lb beam length
- Lc distance from critical section to contraflexure point
- LP plastic hinge length
- m mass
- me effective mass participating in the fundamental mode
- n number of storeys in multi-storey building
- OTM overturning moment
- PGA peak ground acceleration
- R force-reduction factor applied to elastic spectrum in force-based design
- reduction factor applied to displacement spectrum for damping
- force-reduction factor related to ductility
- Sa(T) period-dependent response acceleration coefficient from response spectrum
- T period
- T seismic tension force in column of frame
- tb period at end of maximum spectral response acceleration plateau
- Tc corner period in displacement response spectrum
- Te effective period for DDBD
- V shear force; shear strength
- Vc column shear force
- Vy yield shear force

Content table

1. Introduction

Introduction

1.1. Introduction

The force-based design has been the most used method for the seismic design of structures in which the structure is designed for equivalents static forces due to the action seismic event. In order to get the equivalent forces, the period of the structure is assumed based in the structural system, material, and height of the building. Using the calculated period, the based shear is obtaining from an acceleration design spectrum that takes in account the characteristics of the foundation soil, importance of the structure, irregularities and an assumed inelastic behavior by using a factor (behavior factor “q” in Europe or response reduction factor “R”). The based shear is distributed as a lateral load acting in each floor, and the distribution is according a modal analysis.

A control in this method is the inelastic inter-story drifts limited by a country code; if the drift is exceeding the limited, the stiffened and strength of the structural elements must be increased. The problems presented in this method are the assumptions made such as the constant stiffens, ductility based in the structural system used instead of the characteristics of the structure, simply inelastic behavior consider, and calculation of the structure period with empirical equation. These assumptions and simplification can lead to results that are far away of the real behavior of the structure.

In the last decades, researches and engineers have proposed and implemented seismic analysis methods based in displacement instead of acceleration overcoming the problems presented in the force method. The displacement method is based in the performance of the structure facing a demand. In this method, the ductility and period are computed based in the characteristic of the structure. Also, the structure can be designed to have different performances to different levels of hazards (Ghorbanie-Asl, 2007).

The performance is an indicator of the damage level that will occur after the seismic event in the building in structural and nonstructural elements. The performances are achieved with target displacements; the minimum performance is the life safety for residential structures for and operational building for special structures.

Motivation and objectives.

1.2.

In the last decade, earthquakes with great magnitude has occurred in different countries killing, and injuring thousands of people for example (Vega, 2015):

- 19/09/2017 Mexico (7.1 magnitude) killing 369 people.
- 24/08/2016 Italy (6.2 magnitude) killing 300 people.
- 16/04/2016 Ecuador (7.8 magnitude) killing 650 people.
- 25/04/2015 Nepal (7.8 magnitude) killing around 9000 people.

The most common method useed to design structures is based in forces; this method has present deficiencies exposed in these earthquake. The more notable problems with the forces design are the use of factors to consider the ductility, over-strength and plastic behavior of the structure. Nowadays, the designers have to face larger and taller structures than building in the past; also, many structures have to accomplished new requirements such as zero dame in non-structural elements. These factors indicated the necessity of design methods that characterize in more realistic way the behavior of the structure. The performance-based design is a more realist approach. The Direct Displacement-Based Design (DDBD) and pushover are methods in this approached. Also, in order to get a better performance of the structures damping and isolations systems are used; this system can be used in new structure and rehabilitation. The DDBD and pushover are going to be analysis as method of the performance-based design in this thesis. Also, it is going to be use the fluid viscous damper to improve the performance of the structures.

The objectives of the thesis are

- To exhibit the advantages of the seismic design based on displacements over the force design in steel structure frames.
- To determine the performance of a structure designed by displacements and designed by force obtaining the ductile, capacity curve, performance point and plastic behavior in both cases.
- To increase the performance of a structure establishing the influence in the plastic behavior with the implementation of the fluid viscous dampers in a steel frame structure.

- To define the performance in a study case and implement fluid viscous instead of shear walls reaching a target drift.
- To verify the non-linear behavior of the study case with shear walls and with FVDs instead of the shear walls using a non-linear dynamic analysis (time history analysis)

1.3. Organization of the thesis

This work is divided in six chapters in the next paragraph is explained the content of each chapter in a summary way.

- Chapter one describes of the performance-based design. Motivation of the theme of the thesis and the objectives of it.
- Chapter two presents the theory of the Direct Displacement-Based Design and parameters necessary for this method. It is designed a regular steel frame structure (special moment frame) by the displacement and force method comparing the obtained results
- Chapter three implements of the fluid viscous dampers (FVDs) reaching a target drift. Theory and parameters necessary to compute the damping coefficients of the dampers are exposed, and it is explained the nonlinear dynamic analysis (Fast nonlinear analysis FNA) based.
- Chapter four performances a nonlinear static analysis (pushover) in the model's design by displacements and forces with different lateral load patterns. Obtaining the ductile, capacity curve, performance point and plastic behavior in both cases.
- Chapter five is the study case in which is performed an analysis pushover including the effects of the high modes. A nonlinear dynamic analysis (FNA) will be done on the study case removing the shear walls obtaining the maximum drift then it will be incorporate the FVDs to reach the objective target. Another nonlinear dynamic analysis will be done in the structure with the dampers obtaining the performance of the structure.
- Chapter six are the conclusion obtained of the project.

2. Direct Displacement Based Design (DDBD)

Direct Displacement Based Design (DDBD)

2.1.

In the decade of 1992 to 1994, Nigel Priestley, Mervyn Kowalsky and Bob Park developed an innovative seismic analysis method based in displacement focused in the performance of the structure (Priestley, Calvi, & Kowalsky,, 2007); nowadays, this method is known as Performance-based design). The Direct Displacement Based Design (DDBD) is a performance-based seismic design method where a structure of multi degree of freedom of liberty (MDOF) is analysis as an equivalent structure of simple degree of freedom (SDOF), and it is carried to a target displacement; the equivalent structure has an effective mass (me) and effective height (he) based in the original mass and height of the structure.

The SDOF has an effective stiffness equal of the secant stiffness (ke) of the bilinear stiffness model of the structure that takes in count the inelastic behavior of the structure.

The bilinear model is composed of the initial stiffness (ki) of the elastic behavior and the decreasing of the stiffness equal to the initial stiffness affected multiply by a coefficient. In the case of the DBDD, the effective stiffness is of a single degree of freedom.

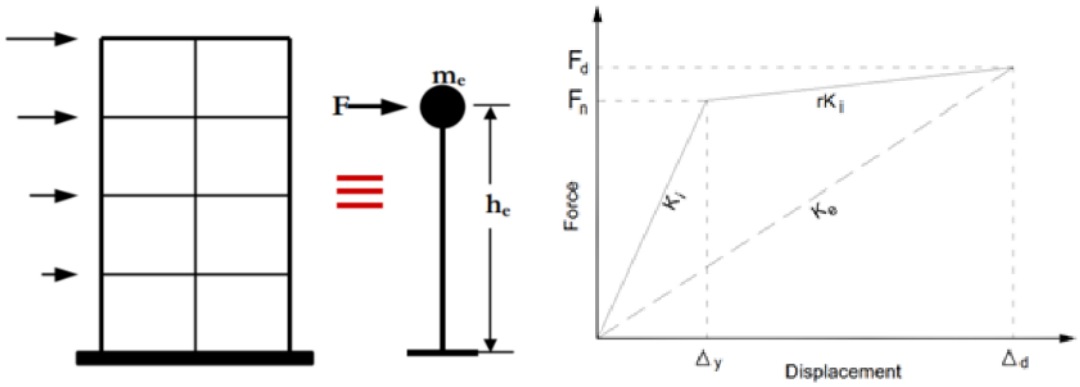

Figure 1. a) Equivalent structure b) Secant or effective stiffness. Source: Timothy Sullivan; Progettazione basata sugli spostamenti per le Costruzioni in Acciaio: stato dell'arte

The equivalent damping (ξ_{eq}) has to provide a mechanism capable to dissipate the energy taking in count the lineal behavior (5% elastic damping) and nonlinear behavior (hysteretic damping); the computation of the ξ_{eq} considers the material, structural system and

the displacement ductility (μ); similarly, the equivalent damping is related to the structures ductility. After it is obtained the equivalent damping, a damping reduction factor is determined to obtain the displacement spectra corresponding to the calculated equivalent damping. (KARIMZADA, 2015)

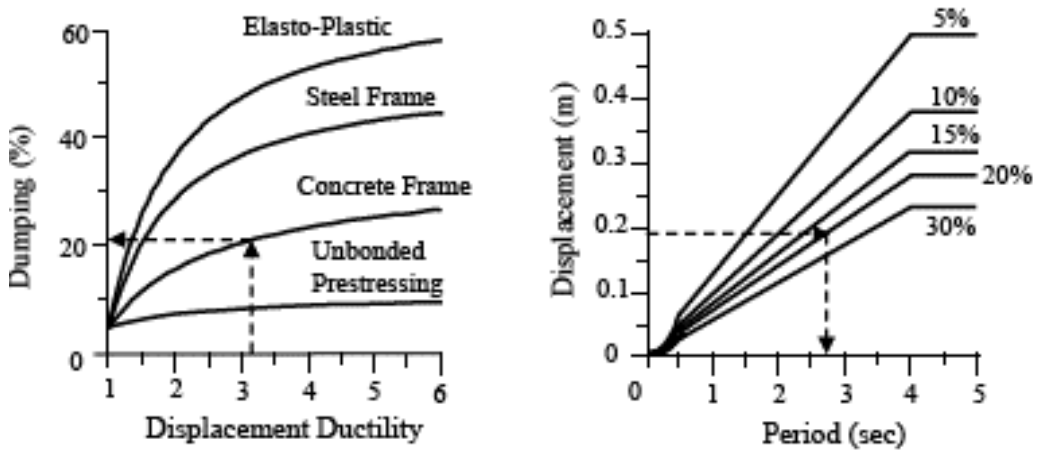

Figure 2. a) Equivalent Damping vs. Ductility b) Design Displacement Spectra. Source. (KARIMZADA, 2015)

Form the target displacement (Δ_d), a line parallel to the x axel is draw until it intersects the displacement spectra corresponding to the equivalent damping finding the structure effective period (T_{eff}) like in Figure 2; the effective stiffness can be calculated with effective period (T_{eff}).

Knowing the effective period (T_{eff}) and the target displacement (Δ_d), the base shear (V_B) is determined; the found base shear is distributed in each floor according to the height and mass of the floor. In order to consider the effects of the contribution of the highest modes, the force assigned to the last floor is equal to the ten percent of the base share. Also, the DBDD can consider the effects of torsion, P-Delta, high modes, and irregularities by affecting the effects with a coefficient or applying modified formulas in the process.

Finally, the structure is design with the different combinations that involves the gravitational, wind, earth pressure and seismic load ensuring an adequate design of the building.

2.2. Application of the DBDD theory

The theory of the DBDD will be applied to a regular structure in plane and height, with a fixed foundation, and bolted connection (rigid connection – moment resistant connection). The predesign of the structure was according the AISC 360-16, AISC 358-16 and AISC 341-16; the sections of the structures are classified as high ductility sections according the AISC 341 (AISC Seismic Provisions for Structural Steel Buildings). The seismic parameters such acceleration spectra and displacement spectra were obtaining from the Ecuadorian Construction Code "NEC - SE – DS" (Norma Ecuatoriana de la Contruccion); likewise, the live load, dead load, load combination, and factors were taken from the NEC - SE – CG. The Ecuador.

2.2.1. Structure geometry

The structure has a floor area of 21x21m (441m^2) divided in three bays of seven meter in direction of X axel and Y axel; the total height of structure is a seven-floor building with 21.5m^2 of total height in which the first floor has 3.5 meters, and the other floors have 2 meters of height.

The structural elements are hot rolled steel sections that accomplish the requirements of high ductility for seismic actions exposed in the Eurocode and American standards (AISC and ASCE).

Structural elements type of the predesign:

Master beam VM1: W450X43 (450X120X8X10)
Master beam VM1: W350X30 (350X100X6X8)
Principal beams VP: W430X48 (430X140X8X10
Secondary beams: W200X14 (200X80X4X8)
Columns: HSS 460X460X25

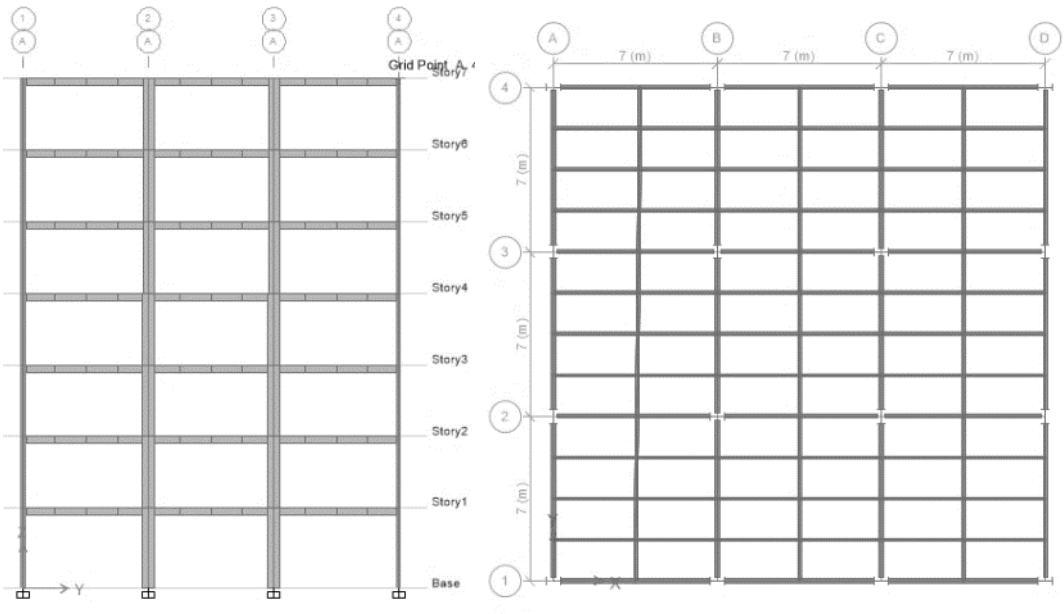

Figure 3. Elevation and plan view. Source: author

2.2.2. Structure mechanical and seismic characteristics

Structure type: Special moment frame (AISC 341-16).

Column – Beam connection: Bolted Flange Plate (BFP) Moment Connection.

Material: Steel A-36.

Table 1.

Steel mechanical properties.

Type of steel:		**A36**
Fy =	36	Ksi
	248	Mpa
	25310357	Kg/m2
E =	29000	Ksi
	199948	Mpa
	20388898630	Kg/m2

Beam type: W (Profile I)

Column type: HSS (Tubular profile)

Load applied according NEC15:

- **Dead load**

Table 2.

Dead load description.

Steel deck. Thickness=0.65mm and Height=55mm	7	Kg/m^2
Filling concrete thickness of the steel deck	200	Kg/m^2
Floor finishing.	30	Kg/m^2
Walls	150	Kg/m^2
Ceiling	13	Kg/m^2
∑DL=	**400**	**Kg/m^2**

Table 3.

Live load description.

Department	200	Kg/m^2
	200	**Kg/m^2**

Seismic parameter:

- **Location:** Quito (Highlands)
- **Seismic zone:** V
- **Factor according the site of implantation of the structure:** Z=0.4; η=2.48
- **Characterization of seismic hazard:** High
- **Soil type:** C;

  r =1

  Fa=1,20

  Fd=1,11

  Fs=1,11
- **Structure importance:** Residential I=1
- **Plan and elevation factor:** $\Phi_P = \Phi_E = 1$
- **Response reduction factor:** R=8

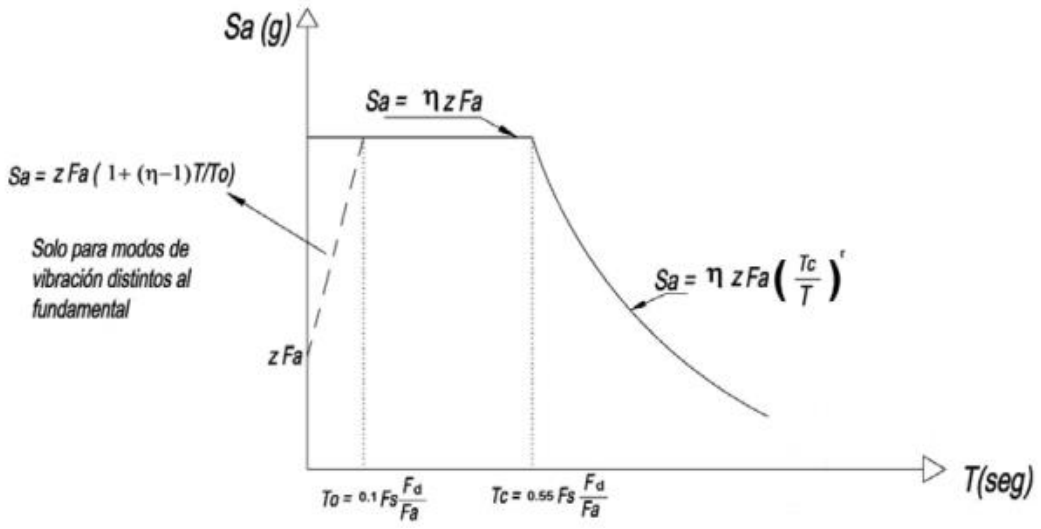

Figure 4. Elastic acceleration spectra according NEC 15 Source: Norma Ecuatoriana de la construccion

2.2.3. DBDD analysis.

2.2.3.1. Property calculations of equivalent single degree of freedom system

- **Design displacement of the substitute structure.**

The design displacement (Δ_d) if the SDOF is computed according the mass distribution, height of each floor, inelastic mode shape, and critical displacement or drift. The critical displacement must be taken based in the ductility of the structural elements, desire performance to achieve, and the maximum drift specify in the local building code; in this case, the critical displacement was calculated with the maximum drift stipulated in the NEC-SE–DS.

The design displacement depends of the displacement shape of the real structure; the displacement shape considers the plastic behavior due to the formation of the plastic hinges and plasticization of the steel fibers in the first mode (Chopra & Goel, 2001)

Seismic or reactive mass calculation: The seismic mass considers that the totally of the dead load and twenty-five percent of the live load. The analysis will be performed in the frame of the axes three.

$$W = DL + 0.25LL$$ Equation 1. (Reactive mass)

Table 4.

Self-weight.

Element	Weight (Kg/m)	Length (m)	Weight (Kg)
VM1	43	84	3612
VM2	30	63	1890
VP1	48	84	4032
VS	14	189	2646
C1	343	48	16485

Table 5.

Seismic or reactive mass

Distance X (m)	Distance Y (m)	Plant area (m^2)	Dead load (Kg/m^2)	Live load (Kg/m^2)	Self-weight (Kg)	Reactive mass (Kg/m^2)	Reactive mass (Kg)
21	7	147	480	200	33946	530	111856,2

- **Critical displacement and inelastic mode shape.**

The critical displacement based in the local code (NEC) due to the high ductility of the steel profile allows strains or deformations bigger than the maximum drift of the NEC; the maximum drift according to the NEC is 0.02 for force based designed and 0.025 for direct based displacement design that cover the performance level of life safety found in the FEMA 356.

The equations developed in 2006 by the professor Priestley, Calvi and Kowalsky were used to determine the inelastic mode shape. The floor displacement is proportional to the distortion of the analyzed floor, critical displacement, and inverse to the critical distortion; the critical distortion is the maximum distortion that in the majorities of cases is the distortion of the first floor.

$$\Delta_c = \max\ drift\ x\ H$$ Equation 2. (Critical displacement)

$$\delta_i = \left(\frac{H_i}{H_n}\right)$$ Equation 3. (Normalized inelastic mode shape less than four floors)

$$\delta_i = \frac{4}{3}\left(\frac{H_i}{H_n}\right)\left(1 - \frac{H_i}{4H_n}\right)$$ Equation 4. (Normalized inelastic mode shape more than four floors)

$$\Delta_i = \delta_i \left(\frac{\Delta_c}{\delta_c}\right)$$ Equation 5. (Floor displacements at level i)

ddb

Parameters for the calculation of design displacement of the substitute structure

Δc =	0,0875	m					
Stories	**Hi (m)**	**Di**	**mi(DL+0.25LL) (Kg s²/m)**	**Δi (m)**	**Δimi**	**Δi²mi**	**miΔiHi**
7	21,50	1,00	23151	0,42	9728,84	4088,32	209170,05
6	18,50	0,90	23151	0,38	8760,69	3315,13	162072,79
5	15,50	0,79	23151	0,33	7666,26	2538,58	118827,07
4	12,50	0,66	23151	0,28	6445,55	1794,50	80569,42
3	9,50	0,52	23151	0,22	5098,56	1122,84	48436,36
2	6,50	0,37	23151	0,16	3625,30	567,69	23564,42
1	3,50	0,21	23151	0,09	2025,75	177,25	7090,11
Σ			**162060**		**43350,95**	**13604,31**	**649730,22**

$$\Delta_d = \frac{\sum_{i=1}^{n}(m_i\Delta_i^2)}{\sum_{i=1}^{n}(m_i\Delta_i)}$$ Equation 6. (SDOF design displacement)

$$\Delta_d = 0.3138\ m$$

- **Effective mass and height.**

The effective height of the SDOF for frame systems is around seventy percent of the total height of the original structure. The effective mass contemplates the mass participating in the first mode of vibration of the structure; in the case of frame systems the mass is in the range of eighty percent of the total reactive mass.

$$H_e = \frac{\sum_{i=1}^{n}(m_i\Delta_i H_i)}{\sum_{i=1}^{n}(m_i\Delta_i)}$$ Equation 7. (Effective height)

$$H_e = 14.99m\ (\ 69.67\%\ of\ H_n)$$

$$m_e = \frac{\sum_{i=1}^{n}(m_i \Delta_i)}{\Delta_d}$$ Equation 8. (Effective mass)

$$m_e = 138140.40\,\frac{kg\ S^2}{m}\ (85.24\ \%\ of\ the\ reactive\ mass)$$

- **Ductility and Equivalent Viscous damping.**

The equivalent viscous damping is the sum of the elastic damping commonly equal to five percent in concrete and steel structures plus the hysteretic damping. The hysteresis damping reflects the inelastic behavior of the structural elements and system. In the case of steel frame systems, the bilinear with a factor r equal to 0.2 can be consider or an elastoplastic model can be considering. (Priestley, Calvi, & Kowalsky,, 2007)

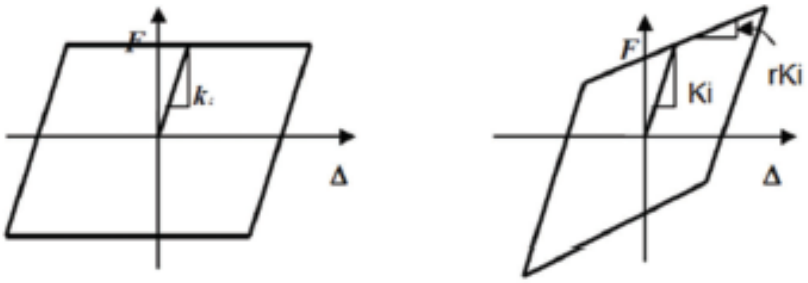

Figure 5. Elastoplastic and bilinear inelastic behavior model. Source: Book Displacement-based Seismic Design of structures

In order to compute the ductility of the structure is necessary to determine the yield displacement. In the case of steel frames, the yield displacement can be assumed as constant. A displacement spectrum is generating from the elastic displacement spectrum of five percent of damping by dividing the values of the original displace spectrum to a reduction factor for elastic.

$$f_{ye} = 1.1\ f_y$$ Equation 9. (Design yield strength)

f_{ye} = 39,6 ksi = 273,0324564 Mpa = 27841393 Kg/m^2

$$\varepsilon_y = \frac{f_{ye}}{E}$$ Equation 10. (Design yield strength)

$$\varepsilon_y = 0.001366$$

$$\phi_y = 0.65\frac{\varepsilon_y L_b}{h_b}$$ Equation 11. (Yield drift steel frames)

$$\phi_y = 0.01243$$

$$\Delta_y = \phi_y H_e$$ Equation 12. (Yield displacement steel frames)

$$\Delta_y = 0.1862\text{m}$$

$$\mu = \frac{\Delta_d}{\Delta_y}$$ Equation 13. (Ductility)

$$\mu = 1.685$$

$$\xi = 0.05 + 0.577\left(\frac{\mu-1}{\mu\pi}\right)$$ Equation 14. (Equivalent viscous damping steel frames)

$$\xi = 0.122\ (12.2\%)$$

$$R_\xi = \left(\frac{0.07}{0.02+\xi}\right)^{0.5}$$ Equation 15. (Damping modifier)

$$R_\xi = 0.709$$

- **Target period**

The target period of the substitute structure can be found from the new displacement spectra of the equivalent damping or with formulas based in the T_c and Δ_c that are the corner period and corner displacement. The equivalent period just computed, also represents the frame's target period, that could be either achieved by increasing the column or the beam sizes, depending on the beam to column capacity ratio already realized. The design process ends with the computation of the target structure stiffness K_{eq} (Villani, 2009). The displacement and acceleration spectra were gotten according the NEC.

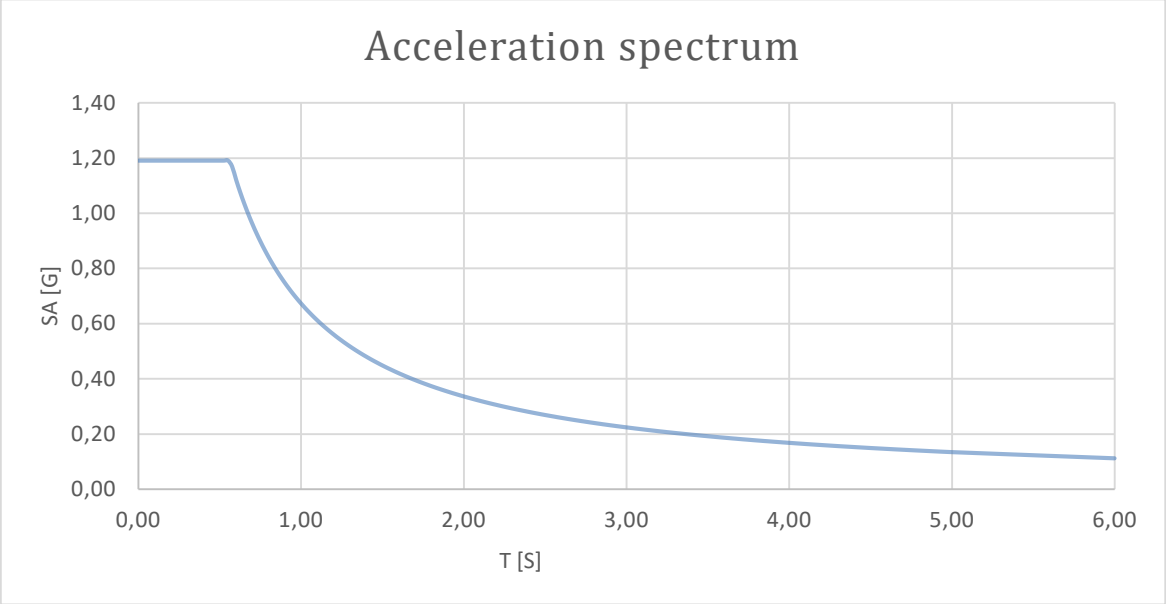

To	0,10	**Tc**	0,56	**TL**	2,66

Figure 6. Acceleration spectrum according NEC 15

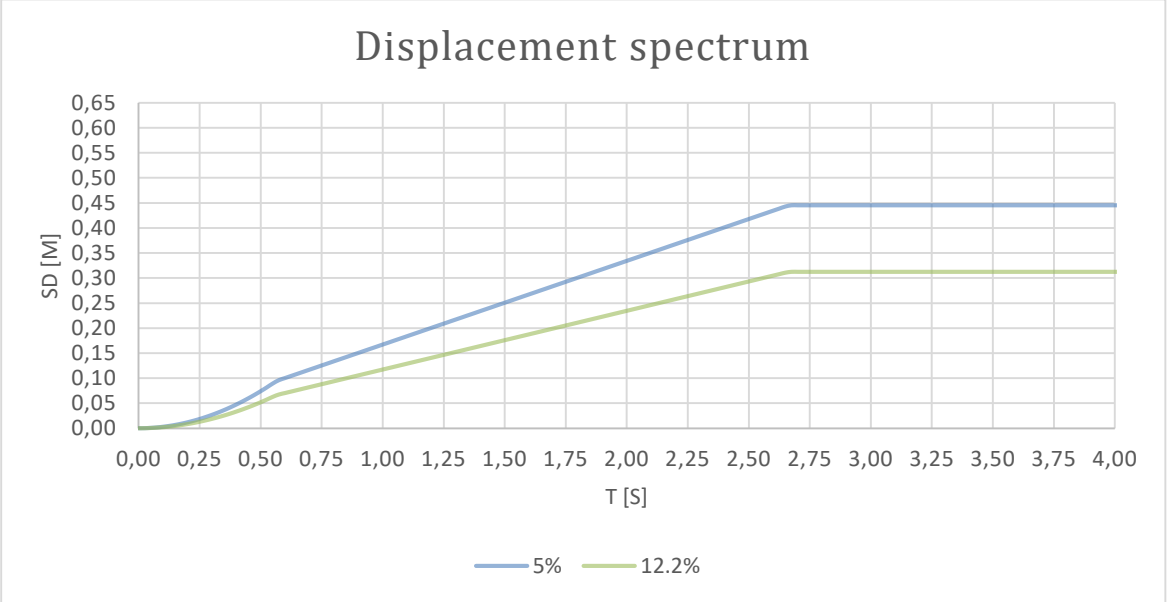

To	0,10	**Tc**	0,56	**TL**	2,66

Figure 7. Displacement spectrum according NEC 15

$\Delta_{c,5\%} = S_{d,5\%}(T_L)$ Equation 16. (Corner displacement for damping 5%)

$\Delta_{c,5\%} = 0.445$ m

$\Delta_{c,\xi} = \Delta_{c,5\%} R_{\xi}$ Equation 17. (Corner displacement for equivalent damping)

$\Delta_{c,12.2\%} = 0.315$ m

$\Delta_d < \Delta_{c,\xi} < \Delta_{c,5\%}$ Equation 18. (Check of the displacement obtained with the equivalent)

$0.3138 < 0.31546 < 0.4458$

$T_e = T_L \frac{\Delta_d}{\Delta_{c,\xi}}$ Equation 19. (Target period)

$T_e = 2.87$ seg

- **Effective stiffness and base shear.**

The effective stiffness is computed by inverting the equation for the period of a single degree of freedom oscillator. Knowing the equivalent stiffness and the design displacement, the based shear can be determined (Fernandex, 2015).

$K_e = \frac{4\pi^1 m_e}{T_e^2}$ Equation 20. (Effective stiffness)

$K_e = 662368$ Kg/m

$V_b = K_e \Delta_d$ Equation 21. (Base shear)

$V_b = 207863$ Kg (13% of the reactive mass)

2.2.3.2. Floor lateral forces and base overturning moment calculation.

The base shear is distributed to the floors where are discretized the masses of the multi degree of freedom. The ten percent of base shear is assigned to the roof, and the rest of the nighty percent is distribution to the rest of the floors in proportional to the height, masses, displacement of the floor.

$$F_i = F_t + 0.9\,V_b \frac{m_i \Delta_i}{\sum_{i=1}^{n}(m_i \Delta_i)}$$ Equation 22. (Shear distribution)

$$F_i = 0.1 V_{b_t} + 0.9\,V_b \frac{m_i \Delta_i}{\sum_{i=1}^{n}(m_i \Delta_i)}$$ Equation 23. (Roof shear distribution)

$$F_i = 0.9\,V_b \frac{m_i \Delta_i}{\sum_{i=1}^{n}(m_i \Delta_i)}$$ Equation 24. (Other floors shear distribution)

Table 6.

Shear distribution.

Stories	**Δimi**	**Fi**	**Vi**
	Kg m	**kg**	**Kg**
7	9729	62770	62770
6	8761	37806	100576
5	7666	33083	133659
4	6446	27815	161474
3	5099	22002	183476
2	3625	15645	199121
1	2026	8742	207863
Σ	**43351**	**207863**	

$OTM = \sum F_i \; H_i$ Equation 25. (Base Overturning Moment)

Table 7.

Overturning moments

Stories	**Hi**	**Fi**	**OTM**
	(m)	**Kg**	**Kg-m**
7	21,5	62770	0
6	18,5	100576	188310
5	15,5	133659	490038
4	12,5	161474	891015
3	9,5	183476	1375437
2	6,5	199121	1925867
1	3,5	207863	2523230
Base	0	0	3250750

2.2.3.3. P-Δ Effect

In steel structures the P-Δ effect must be consider if the stability index is great than 0.05 for values less than 0.05 this effect can be ignoring.

Moreover, another aspect to consider is that 0.3 is the maximum value of the stability index; if the value is great than 0.3, the structure must be redesign to increase the stiffness of the structure.

Taking in count the P-Δ, the base shear and overturning moment must be increased depending of the structural material. A simple method to reflect the P-Δ effect in the base shear distribution and overturning moments is to multiply the values of this parameters by a coefficient. The coefficient is equal to the increased base shear by the P-Δ effect divided by the based shear without P-Δ effect

$$\theta_\Delta = \frac{P\Delta_d}{VH_e} \text{ or } \theta_\Delta = \frac{P\Delta_d}{OTM}$$ Equation 26. (Stability index)

θ_Δ=0.1564 (first formula)

$$V_{b(P-\Delta)} = F = K_e\Delta_d + C\frac{P\Delta_d}{H_e}$$ Equation 27. (Based shear increased by P-Δ effect)

$V_{b(P-\Delta)}$ = 435746 Kg

$$A = \frac{V_{b(P-\Delta)}}{V_b}$$ Equation 28. (Amplification factor)

A= 1.16

$$F_{i(P-\Delta)} = F_iA$$ Equation 29. (Increased lateral floor by P-Δ effect)

Table 8.

Increased lateral floor by P-Δ effect

Stories	$Fi_{(P-\Delta)}$	$Vi_{(P-\Delta)}$
	kg	**Kg**
7	73017	73017
6	43978	116995
5	38484	155478
4	32356	187834
3	25594	213428
2	18199	231627
1	10169	241796
Σ	**241796**	

$OTM_{i(\mathrm{P}-\Delta)} = OTM_i\ A$ Equation 30. (Increased overturning by P-Δ effect)

Table 9.

Overturning by P-Δ effect

Stories	$OTM_{(P-\Delta)}$
	Kg-m
7	0
6	219051
5	570035
4	1036469
3	1599971
2	2240256
1	2935136
Base	3781420

2.3. Comparison of results obtained from DBDD with FBD.

In order to compare de displacement method with the forced and displacement methods, the elements of the structure were design with the lateral force obtained by the direct based

design and the linear static seismic lateral force (forced method) according the AISC 360, 341, and 358.

The structure is classified as a special moment frame which was a reduction seismic response modification factor (R) equal to 8. Also in both cases, the maximum drift was 0.025; the two analysis included the P-delta effect.

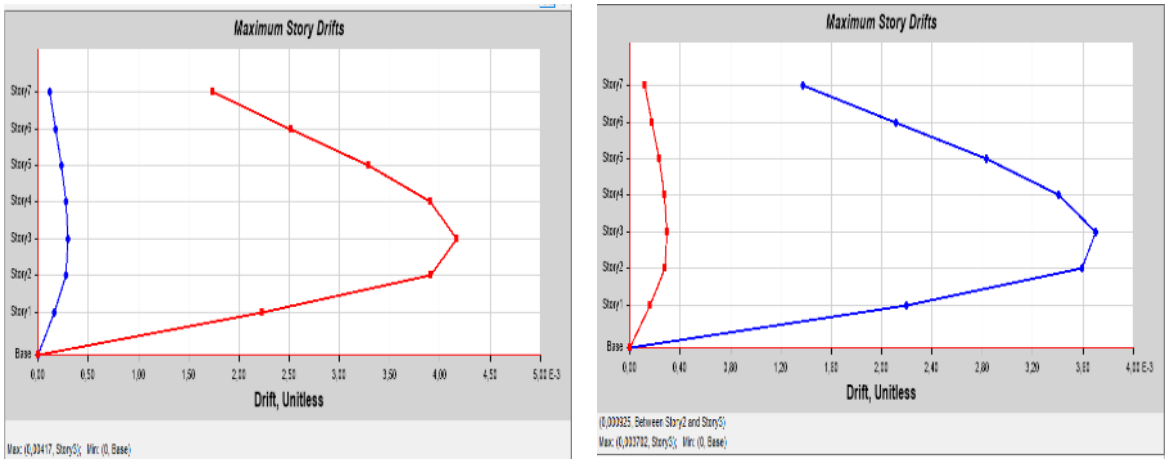

Figure 8. Maximum drift in force design a) Lateral force in X B) Lateral force in Y

$\Delta_{max} = 0.78\, R\, \Delta$ Equation 31. (Maximum inelastic interstory drift according NEC 15)

$$\Delta = 0.025$$

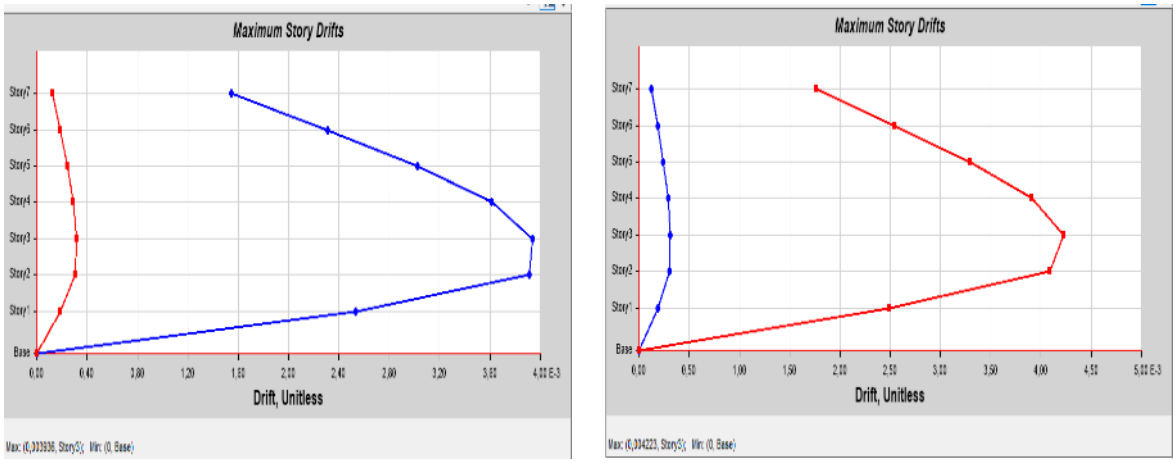

Figure 9. Maximum drift in displacement design a) Lateral force in X B) Lateral force in Y

$$\Delta_{max} = 0.78\, R\, \Delta = 0.025$$

2.3.1. Quantity of steel obtained.

All structural elements are classified as high ductility section, and the design satisfy limit state design (LRF) for ultimate and serviceability limit state. The final sections are present in table 10.

Table 10.

Final element sections.

	DBDD				**BFD**			
	Web		**Flange**		**Web**		**Flange**	
Element	**h**	**t_h**	**b**	**t_b**	**h**	**t_h**	**b**	**t_b**
	cm	**cm**	**cm**	**cm**	**cm**	**cm**	**cm**	**Cm**
C1	60	2	35	2	65	2	35	2
VM1	50	1	20	1,2	45	0,8	18	1,5
VM2	35	0,8	12	1	40	0,8	12	1
VP1	50	1	20	1,5	45	0,8	24	1,5
VS	16	0,4	9	0,6	17	0,4	9	0,6

Table 11.

Total weight for force and displacement design

	Total Weight	
Element Type	**DBDD**	DBF
	kgf	**kgf**
Column	90230,1	98112,84
Beam	121705,31	119116,71
Σ	**211935,41**	**217299.55**

Table number 12 shows that the structure design with the displacement method presents a 2.54% less material than the traditional force design.

2.3.2. Base shear and lateral forces.

The base shear distribution in the lateral force has a triangular configuration due to the regularity of the building; in the case of the displacement method the story force was obtained by DBDD. The lateral forces are equal for the axes X and Y. The lateral forces were applied with a 5% of eccentric that stipule the Ecuadorian and international codes.

Table 12.

Comparison of lateral forces between displacement and force method.

			DBDD	BFD	
Story	**Location**	**Elevation**	**Force**	**Force**	**Variation**
		m	**tonf**	**tonf**	**%**
Story7	Top	21,5	73,159	51,732	41,421
Story6	Top	18,5	44,063	44,983	-2,046
Story5	Top	15,5	38,558	36,962	4,317
Story4	Top	12,5	32,419	29,111	11,363
Story3	Top	9,5	25,644	21,528	19,121
Story2	Top	6,5	18,234	14,167	28,706
Story1	Top	3,5	10,189	7,161	42,281
		Σ	242,266	205,644	

The base shear in the displacement methods is 17.8% greater than the obtained with the force method; similarly, the story forces are greater in all stories except the story six where the force decrees two percent. The reduction in the story six is product of the consideration of the high mode.

3. Fluid viscous damper

Introduction

All the structures that are submitted to dynamic actions such as seismic events responses to them dissipating the seismic input energy; this balance of energy is expressed in equation **3.1.** 33.

$$E_i = E_k + E_s + E_h + E_\xi$$ Equation 32. (Balance energy equation)

The input energy from the seismic event (E_i) is equal to the kinetic energy (E_k), elastic deformation energy (E_s), plastic deformation energy dissipated kwon as hysteretic (E_h), and the viscous damping dissipation (E_ξ) proper of the structure and by the additional system (Colunga, 2003). The most common solution that the engineers select to balance the equation is to increase the elastic and inelastic response by incising the structural element cross sections and the quantity of steel. In the last decades, the used of dampers and isolation system increasing the viscous damping. The additional systems dampers and insulators can be classified in three classes:

- **Passive Control Systems:** These systems are mechanical devices which does not require a power source to active; on other hand, their functioning start with the deformation, or acceleration of the structure that produce a movement of the devices dissipating energy. Their functioning cannot be controlled, and it only depends of the response of the structure. The passive systems are the cheapest system of the three classes of system; in this group are the mechanisms that working with the yielding of mild steel, viscoelastic action in rubber-like materials, sloshing of fluid, shearing of viscous fluid, orificing of fluid, and sliding friction (Symans, Constantinou, Taylor, & Garnjost, 2012)

- **Active Control Systems**: Electro-hydraulic compose of movement sensors, process data system and hydraulic components. The devices started at the same moment in which the seismic event stars; the sensor sent a signal and the quantity of displacement after the system of process data calculate the necessary for to be applied in the hydraulic system to counter the seismic effects, and the hydraulic

system applies the calculated force. These systems need a large external power sources, and their maintenance cost are high.

- **Semi-Active Control Systems:** These systems require small quantities of external power. The semi-active system acts as an active control system with small seismic vent or wind effect, and they act as a passive system with strong seismic events.

3.2. Fluid viscous dampers

The fluid viscous dampers (FVD) are a passive energy dissipation; also, the FVD are used in a complement in the isolation system too. These dampers are more common used in the rehabilitation to achieve a determine performance with a define demand; in the last two decades the system has been implemented in design of new building obtaining smaller transversal section in the structural element, better performance and less developing of plastic hinge during the seismic events, wind storms, or blasts (Teresa, 1999).

The fluid viscous dampers increase the critical damping ration of the structure that commonly is equal to five percent in structures without complement systems reducing the dynamic response of the system; theses system takes the majority of the input energy remaining the majority of the structure inside of the elastic limits, and only a few plastic hinges.

3.2.1. Fluid viscous dampers parts and working.

The FVDs is composed of a stainless-steel piston rod with a bronze orifice head and a self-contained piston displacement accumulator. The damper cylinder is filled with a compressible viscous fluid (silicone or oil) which is generally non-toxic, non-flammable, thermally stable and environmentally safe. (Narkhede & Sinha, 2012)

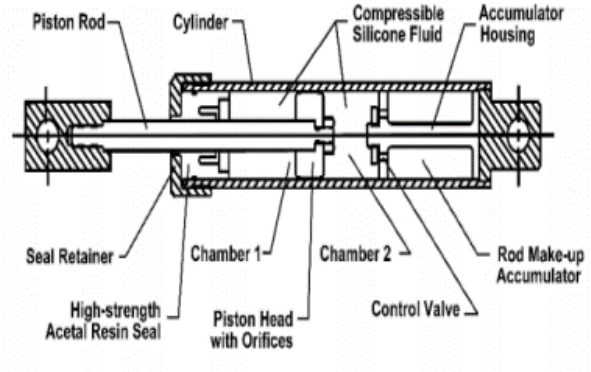

Figure 10**.** Longitudinal section of fluid viscous damper

During the seismic event, the fluid flow through orifices due to the difference of pressure between the two cavities inside the FVDs. The flow of the fluid produces friction between the fluid, the piston and the walls of the chamber, and the movement of the fluid produces an increasing of the temperature (Heat) inside of the damper. Also, the compressive behavior prudes a change of the volume simulating a spring with a restoring force. The energy dissipation in this system is in form of heat that is dissipates into the atmosphere, friction and the compression in the fluid.

The force in the viscous damper is given by, $F = C.V^{\alpha}$ where F is the output force, V the relative velocity across the damper, C is the damping coefficient and α is a velocity constant exponent which is usually a value between 0,3 and 1,0. Fluid viscous dampers can operate over temperature fluctuations ranging from –40°C to +70°C. (SaiChethan, Srinivas, & Ranjitha, 2017)

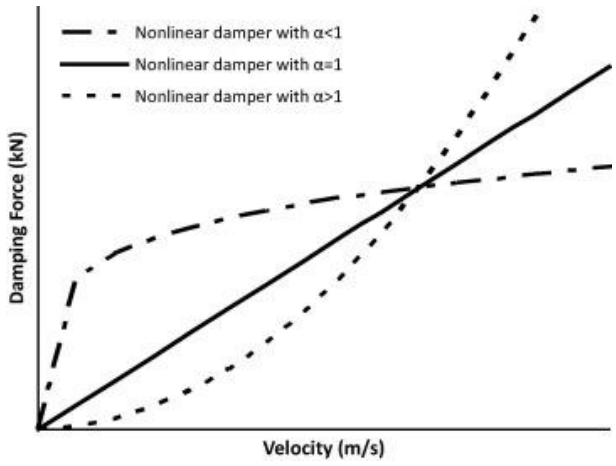

Figure 11. Force-velocity relationship FVDs

The response of the fluid viscous damper is out of phase with the structure movement and tension, so the devices do not add stress to the structure. The dampers are velocity dependent. The maximum tensions are developed at maximum lateral displacement, and the velocity is zero at that point. The maximum velocity is reached when the structure pass through rest position. (Brown, M. Uno, Thompson, & Stratford, 2015)

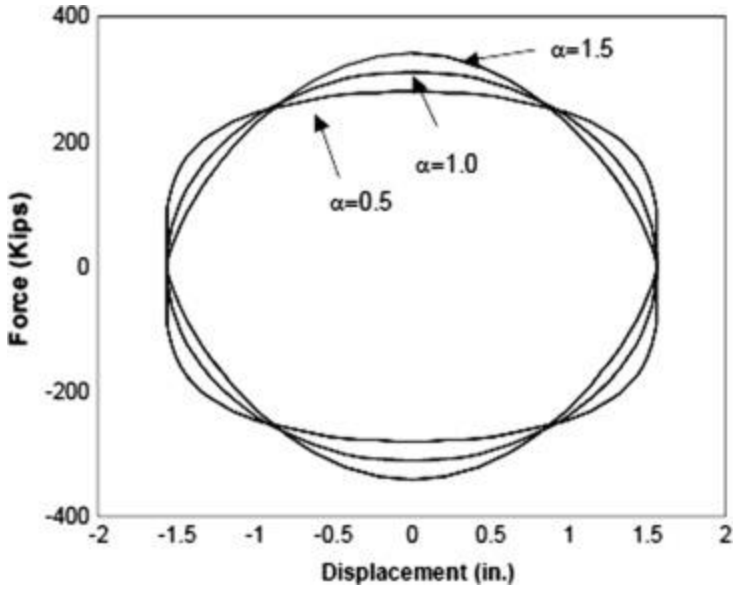

Figure 12. Force displacement relationship

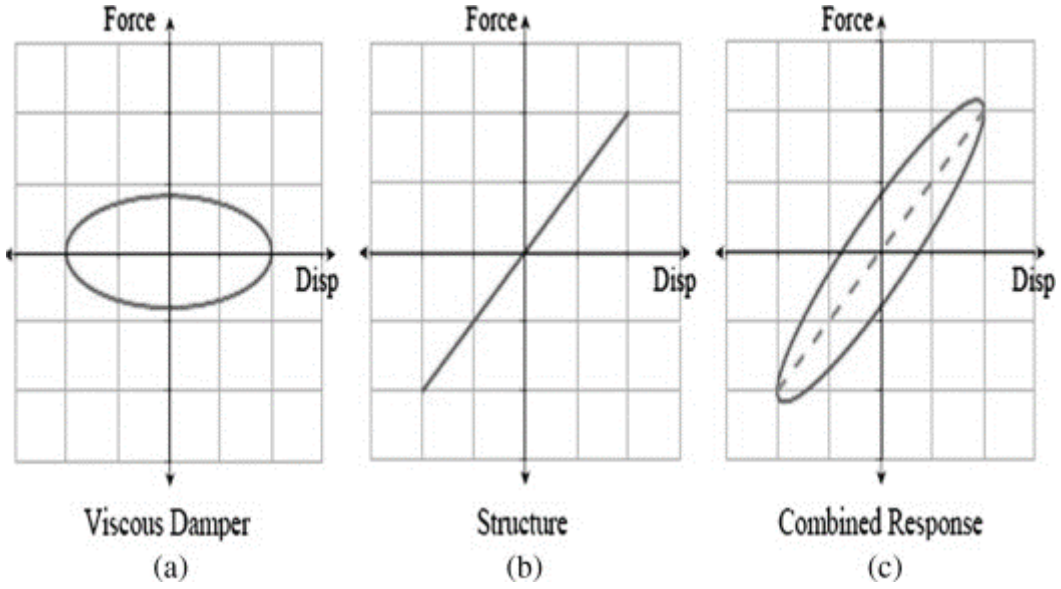

Figure 13. Hysteretic curve

3.2.2. Fluid viscous dampers configuration and location.

The configuration of the FVDs has a great influence in the efficiency of the force develop by the device. The angle that form the braced with the horizon axis, vertical axis or with the other components of the brace that contain the damper. In the figure 12 are present the consideration to take in count in the configuration of the dampers.

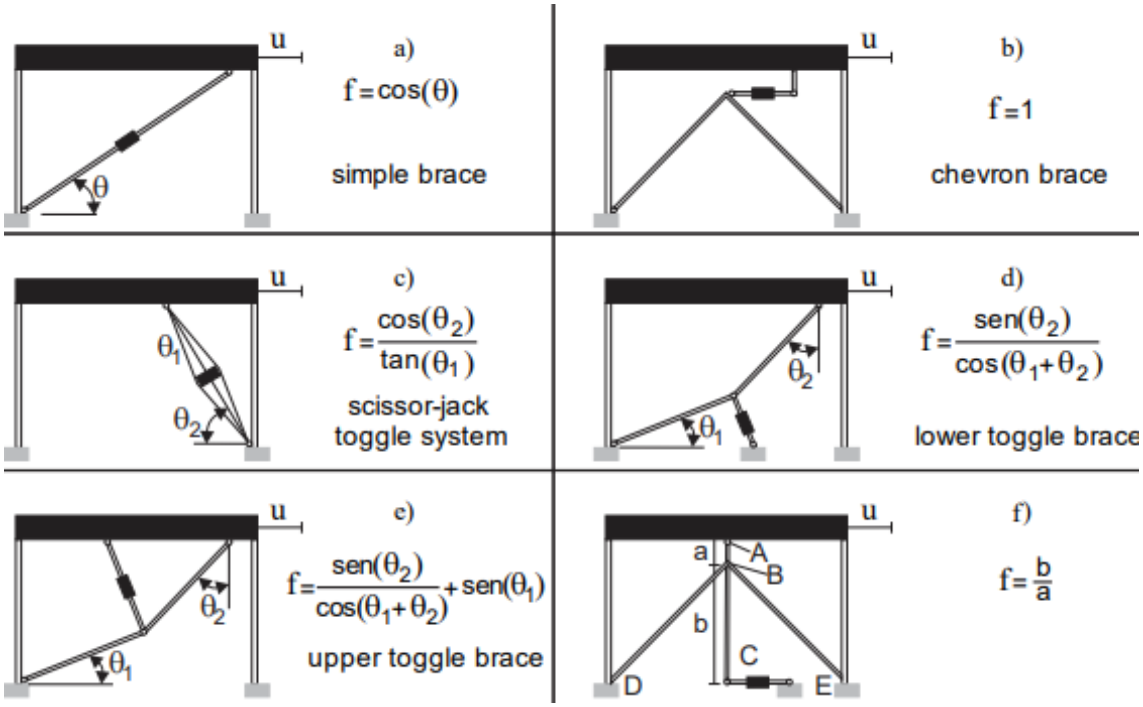

Figure 14. FVDs efficiency by their configuration. Source: (Castro & Sánchez, 2016)

Analyzing table figure 12, the configuration chevron has one of the better efficiencies sending the total horizontal force developing in the system to the structure, but if it considers the vertical component of the seismic effect, the chevron configuration is not able to counter in any percentage the vertical component giving to the other configurations an advantage. Another aspect to consider, it is the quantity of steel used in which the better configuration is the simple brace. The code ASCE 7 in the chapter eighteen gives recommendation for the location of the dampers:

- It is recommendable that the structure does not present irregularities.
- In every level, it must be at least two dampers in the direction to reinforce.
- The dampers must be located in every level of the structure.

- It is recommendable that the location of the dampers will be symmetrical in order to not generate torsion.

In order to obtain the optimal location of the dampers, the design and analysis procedure should be an iterative process considering the architecture and used of the building.

3.2.3. Procedures for the design of the FVDs

The American Society of Civil Engineers in the code ASCE 7 in the chapter eighteen recommends the use of four procedures two non-lineal and two lineal. The ASCE 7 and the NEC allow the use of artificial records or accelerogram compatibles in the case of lacking accelerograms recorded in area of the study case.

For these cases, the non-linear response time-history will be used, and it was generated synthetic based in the geology and soil conditions of Quito and the area where was determine to implement the structure. Similarly, three synthetic accelerograms were generated for the non-lineal dynamic analysis that is the minimum establish in ASCE, NEC, and Eurocode.

3.2.4. Fast Nonlinear Analysis (FNA)

The Fast-Nonlinear Analysis (FNA) is a modal time history analysis that can be lineal or non-lineal. The modal analysis is done by modal superposition, and the obtaining of the N number of modal modes is with Ritz-vectors. The analysis only takes in count the nonlineal behavior in limited elements selected, and elements with concentrated damping, base isolation or energy dissipation.

$$M\ddot{u}(t) + C\dot{u}(t) + Ku(t) + R(t)_{NL} = R(t)$$ Equation 33. FNA general equation

In the equation 34, M, C and K are the mass, proportional damping and stiffness matrices, respectively. The elastic stiffness matrix K omit the stiffness of nonlinear elements. The $R(t)_{NL}$ is the global node force vector from the sum of the forces in the nonlinear elements and is computed by iteration at each point in time.

It can be added to equation 34 a matrix of arbitrary stiffness $K_e u(t)$ of random value in the both size of the equation if the structure is unstable without the nonlinear element.

The introduction of the effective stiffness elements will eliminate the introduction of long periods into the basic model and improve accuracy and rate of convergence for many nonlinear structures. (Wilson, 1995)

$$M\ddot{u}(t) + C\dot{u}(t) + (K + K_e)u(t) = R(t) - R(t)_{NL} + K_e\, u(t)$$ Equation 34. (FNA general equation 2)

Using the Ritz-vector, the modal analysis and the transformation to modal coordinates can be done obtaining equation 36.

$$I\ddot{Y}(t) + \Lambda\dot{Y}(t) + \Omega Y(t) = F(t)$$ Equation 35. (Ritz-vector equation)

The term F(t) is the lineal and nonlinear forces acting in the system.

$$F(t) = \Phi^T R(t) - \Phi^T R(t)_{NL} + \Phi^T K_e u(t)$$ Equation 36. (Total forces in the sys FNA)

The FNA reduces the computational time required for a nonlinear dynamic analysis of a large structure, with a small number of nonlinear elements, can be only a small percentage more than the computational time required for a linear dynamic analysis of the same structure. This allows large nonlinear problems to be solved quickly (Wilson, 1995)

3.2.5. Constants and coefficients determination of FVDs

In order to determine the dampers and their producing force, it is required to define the velocity coefficient, damping constants and necessary damping of the structure to reach the displacement target.

$$F = CV^{\alpha}$$ Equation 37. (FVD force.)

The viscous damping of the structure depends of the damping constants of the dampers, configuration of the FVD, and structure mass, relative displacement of the damper's extremes, angular frequency and the last story displacement in the fundamental mode. The equation 39 is taken from the FEMA 274, and solving the equation can define the damping coefficient.

$$\beta_H = \frac{\sum_j \lambda C_j \Phi_{rj}^{1+\alpha} \cos^{1+\alpha}\theta_j}{2\pi A^{1-\alpha}\omega^{2-\alpha}\sum_i m_i \Phi_i^2}$$ Equation 38. (Structure viscous damping)

$$\sum C_j = \frac{\beta_H 2\pi A^{1-\alpha}\omega^{2-\alpha}\sum_i m_i \Phi_i^2}{\lambda \sum_j \Phi_{rj}^{1+\alpha}\cos^{1+\alpha}\theta_j}$$ Equation 39. (Damping coefficient)

The maximum displacement is obtaining from the time history analysis, and the target displacement is taken from the local code. Determining the target and the maximum displacement, the target damping can be computed, and this damping will be the approached in the interactive process.

$$B = \frac{D_{max}}{D_{target}}$$ Equation 40. (Reduction factor B function of drift)

$$B = \frac{2.31 - 0.41\ln(\beta_0)}{2.31 - 0.41\ln(\beta_{eff})}$$ Equation 41. (Reduction factor B function of damping)

$$\beta_{damper} = \beta_{eff} - 5\%$$ Equation 42. (Viscous damping of the dampers.)

The parameter λ is function of the modal participation factor (Γ), and the velocity constant exponent (α). The parameter λ can be computed from a formula or a table in the FAME 274.

$$\lambda = 2^{2+\alpha}\,\frac{\Gamma^2(1+\frac{\alpha}{2})}{\Gamma(2+\alpha)}$$ Equation 43. λ (Formula.)

Table 13

Values of λparameter.

Exponent α	**Parameter** λ
0,25	3,7
0,5	3,5
0,75	3,3
1	3,1
1,25	3

$$A = \frac{g x \Gamma_i x S_a x T}{4 x \beta_{mD} x \pi^2}$$ Equation 44. (Roof response amplitude)

Finally, it is necessary to determine an adequate steel profile annex to the damper that does not bend of produce flexure reducing the efficiency of the FVD. The steel profiles HSS and pipes are the most common for this propose.

3.3 Fluid viscous dampers application.

The structures designed with the force and this placement method were design with a superior story drift that is defined in the code. The exceeded quantity will be reduced with damper. The force and displacement model are similar the analysis and design of the damper will be performed in one.

3.3.1. Non-lineal time history analysis without dampers.

According with the geological, geotechnical, and the soil type were generating three synthetic accelerogram. Three accelerogram is the minimum of the registers establish in the North American and Ecuadorian code.

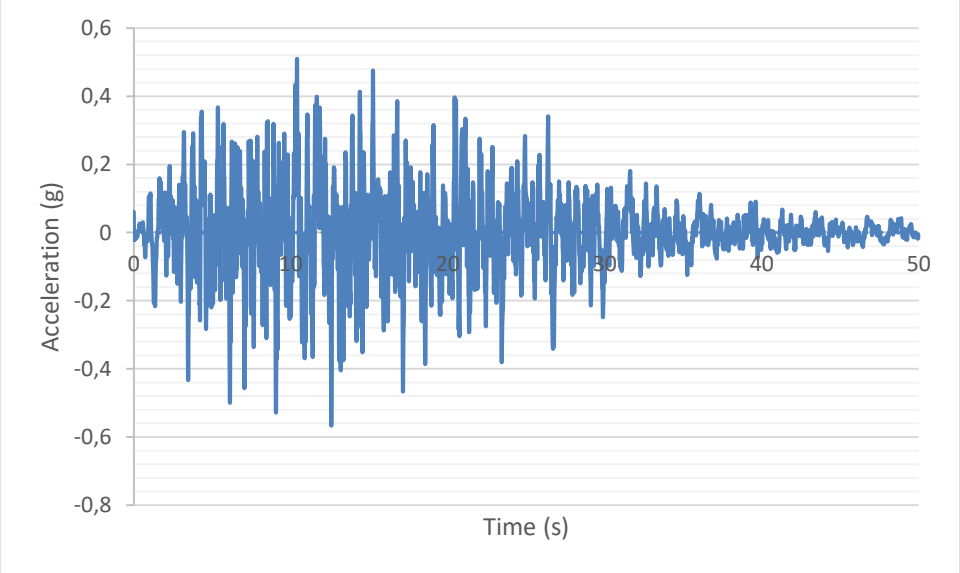

Figure 15. Artificial accelerogram 1.

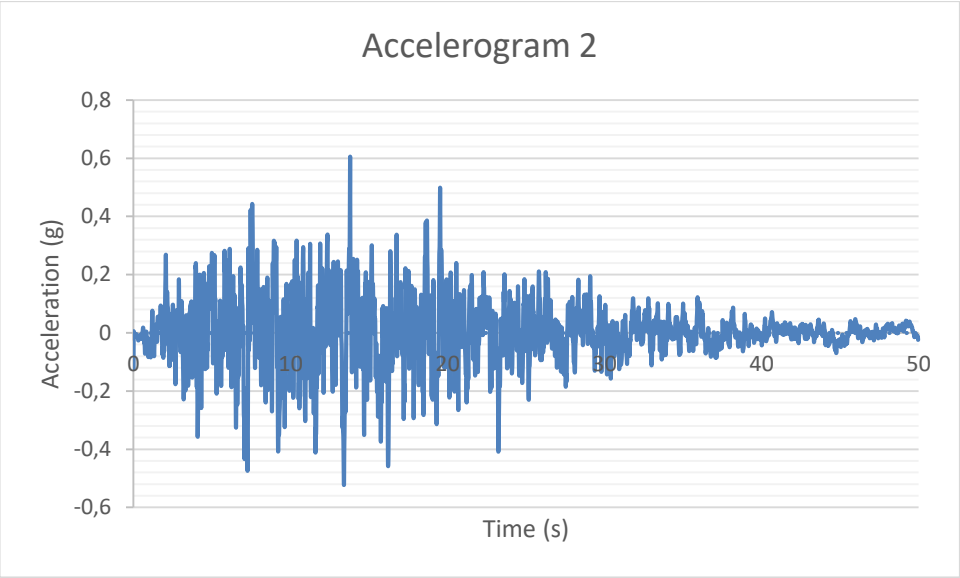

Figure 16. Artificial accelerogram 2.

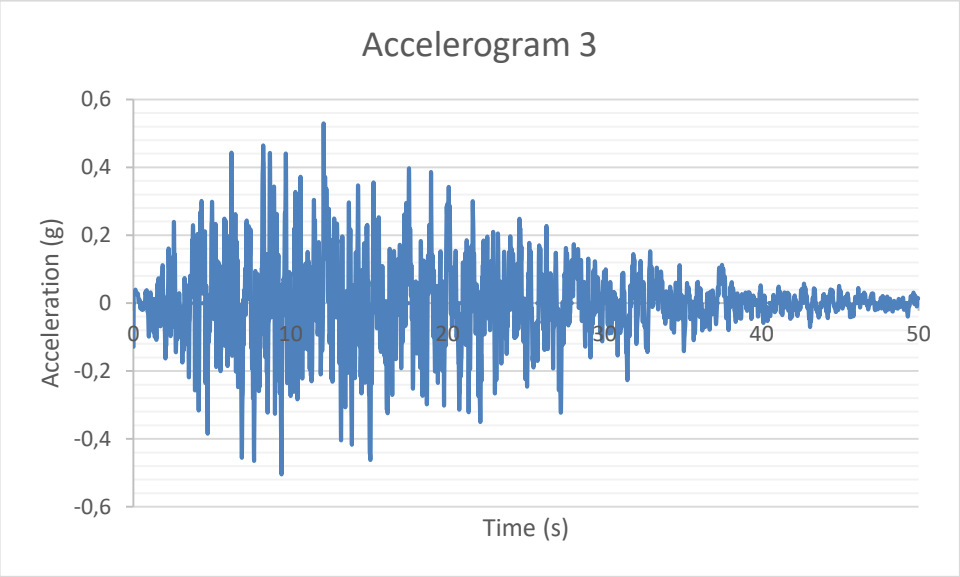

Figure 17. Artificial accelerogram 3.

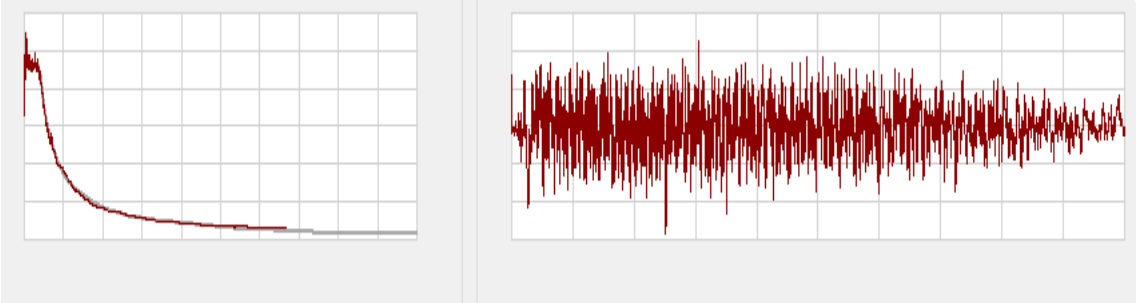

Figure 18. Matching accelerogram 1 with response spectra

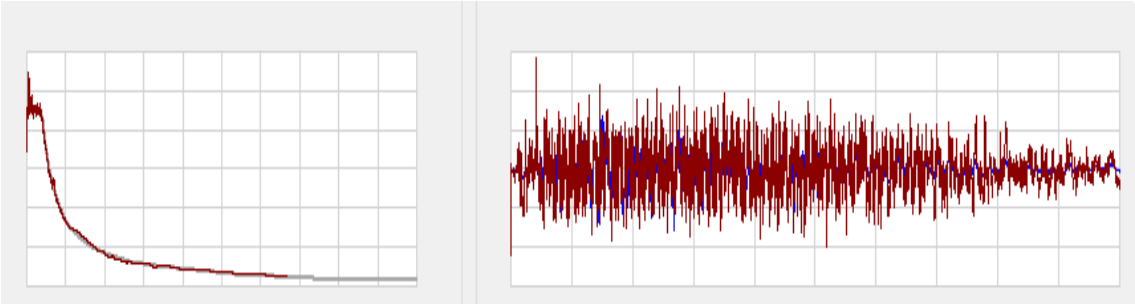

Figure 19. Matching accelerogram 2 with response spectra

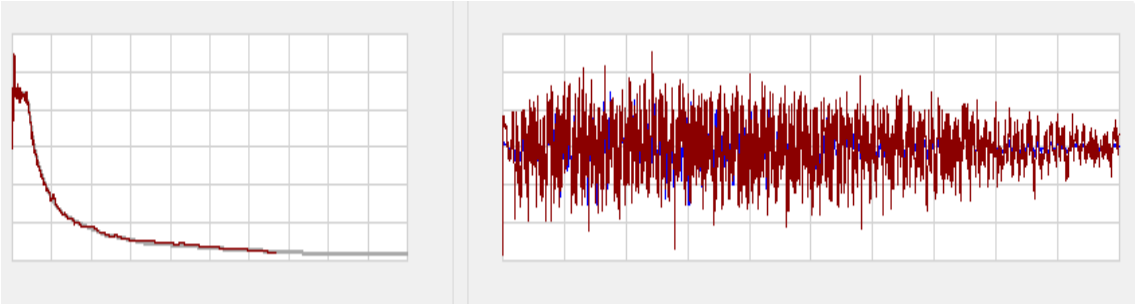

Figure 20. Matching accelerogram 3 with response spectra

Obtaining the artificial accelegrams, they were matching with the elastic spectra. In order to load case for the time history analysis with components X and Y, the accelerograms were combining taking the hundred percent for one direction and thirty percent in the perpendicular direction.

Table 14.

Maximum and minimum drifts X direction.

Story	TH1,1		TH1,2		TH1,3		TH1,4		TH1,5		TH1,6	
	Max	Min	Max	Min	Max	Min	Max	Min	Max	Min	Max	Min
Story7	0,0121	0,0111	0,0115	0,0138	0,0119	0,0117	0,0016	0,0019	0,0036	0,0035	0,0036	0,0033
Story6	0,0173	0,0171	0,0165	0,0190	0,0166	0,0166	0,0022	0,0026	0,0050	0,0050	0,0052	0,0051
Story5	0,0210	0,0217	0,0213	0,0226	0,0200	0,0209	0,0029	0,0031	0,0060	0,0063	0,0063	0,0065
Story4	0,0238	0,0239	0,0244	0,0252	0,0241	0,0245	0,0033	0,0034	0,0072	0,0074	0,0071	0,0072
Story3	0,0268	0,0256	0,0250	0,0260	0,0256	0,0278	0,0034	0,0035	0,0077	0,0083	0,0080	0,0077
Story2	0,0264	0,0255	0,0242	0,0241	0,0251	0,0268	0,0033	0,0033	0,0075	0,0080	0,0079	0,0076
Story1	0,0160	0,0154	0,0143	0,0147	0,0163	0,0157	0,0019	0,0020	0,0049	0,0047	0,0048	0,0046

Table 15.

Absolute maximum drifts X direction.

Story	Elevation m	TH1,1	TH1,2	TH1,3	TH1,4	TH1,5	TH1,6	Max
Story7	21,5	0,0121	0,0138	0,0119	0,0019	0,0036	0,0036	0,0138
Story6	18,5	0,0173	0,0190	0,0166	0,0026	0,0050	0,0052	0,0190
Story5	15,5	0,0217	0,0226	0,0209	0,0031	0,0063	0,0065	0,0226
Story4	12,5	0,0239	0,0252	0,0245	0,0034	0,0074	0,0072	0,0252
Story3	9,5	0,0268	0,0260	0,0278	0,0035	0,0083	0,0080	0,0278
Story2	6,5	0,0264	0,0242	0,0268	0,0033	0,0080	0,0079	0,0268
Story1	3,5	0,0160	0,0147	0,0163	0,0020	0,0049	0,0048	0,0163

Table 16.

Maximum and minimum drifts Y direction.

Story	TH1,1		TH1,2		TH1,3		TH1,4		TH1,5		TH1,6	
	Max	Min	Max	Min	Max	Min	Max	Min	Max	Min	Max	Min
Story7	0,002	0,0021	0,0043	0,0037	0,0041	0,0047	0,0136	0,0156	0,0147	0,0155	0,0142	0,0125
Story6	0,0027	0,0028	0,0056	0,0051	0,0056	0,0063	0,0188	0,0209	0,0201	0,0206	0,0186	0,0171
Story5	0,0033	0,0033	0,0068	0,0067	0,0073	0,0073	0,0242	0,0243	0,0247	0,0248	0,0228	0,0223
Story4	0,0037	0,0036	0,008	0,008	0,0083	0,0083	0,0276	0,0276	0,0272	0,0269	0,0267	0,0265
Story3	0,0037	0,0038	0,0086	0,0085	0,0082	0,0086	0,0274	0,0285	0,0273	0,0284	0,0286	0,0283
Story2	0,0032	0,0036	0,0084	0,008	0,0076	0,0076	0,0252	0,0254	0,024	0,0267	0,0279	0,0265
Story1	0,0019	0,0021	0,0047	0,0046	0,0043	0,0042	0,0143	0,0141	0,014	0,0154	0,0158	0,0152

Table 17.

Absolute maximum drifts Y direction.

Story	Elevation m	TH1,1	TH1,2	TH1,3	TH1,4	TH1,5	TH1,6	Max
Story7	21,5	0,0021	0,0043	0,0047	0,0156	0,0155	0,0142	0,0156
Story6	18,5	0,0028	0,0056	0,0063	0,0209	0,0206	0,0186	0,0209
Story5	15,5	0,0033	0,0068	0,0073	0,0243	0,0248	0,0228	0,0248
Story4	12,5	0,0037	0,0080	0,0083	0,0276	0,0272	0,0267	0,0276
Story3	9,5	0,0038	0,0086	0,0086	0,0285	0,0284	0,0286	0,0286
Story2	6,5	0,0036	0,0084	0,0076	0,0254	0,0267	0,0279	0,0279
Story1	3,5	0,0021	0,0047	0,0043	0,0143	0,0154	0,0158	0,0158

After performing the Time History Fast Non-Lineal Analysis in the structure, the maximum drifts were obtaining. In the X and Y axes, the absolute maximum drifts are equal to 0.278 and 0.286 respectively. In both cases, the maximum drift of the time history analysis

is greater than the maximum drift establishes in the Ecuadorian code and the obtaining of the static force analysis. The viscous damper will be used to get the target drift without changing the structural configuration of the building.

3.3.2. Determination of FVDs parameters.

The first pass is to calculate the reduction factor with the obtained maximum and with the target displacement. The reduction factor allows to get a first quantity of damping in the iterative that the devices will have to add to the system. It is necessary to reduce the self-damping of the structure that is taken five percent commonly.

$$B = \frac{D_{max}}{D_{target}}$$

$$B = \frac{0.278}{0.20} = 1.39 \text{ Reduction factor X axes}$$

$$B = \frac{0.286}{0.20} = 1.43 \text{ Reduction factor Y axes}$$

$$\beta_{eff} = e^{\frac{\left(\frac{0.41\ln(\beta_0)-2.31}{B}\right)+2.31}{0.41}}$$

$$\beta_{eff} = 15.47\% \text{ Factor X axis}$$

$$\beta_{damper} = 15.47 - 5 = 10.47\% \text{ Factor X axis}$$

$$\beta_{eff} = 16.77\% \text{ Factor Y axis}$$

$$\beta_{damper} = 16.77 - 5 = 11.77\% \text{ Factor Y axis}$$

Two models are going to be design with two different dampers. The first one is with a velocity constant equal to 0.5, and the second one with a constant equal to one known as lineal damper. In the two cases, the number of dampers placed are two for each direction accomplish with the requirements of the ASCE 7.

3.3.3. Nonlinear Viscous Dampers Parameters

In order to compute the damping coefficient, it is necessary to determine the constants of roof response amplitude, normalized modal displacement, λ factor and the modal participation factor. The damping coefficient necessary to define the roof response amplitude is taken form the table 18 6-1 of the ASCE 7. The dampers damping will add twelve percent more to the structure in both directions obtaining 17% damping of the structure.

T = 1.17 seg (Period of the mode)

$\beta_{mD} = 1.26$ (damping coefficient)

$\alpha = 0.5$

Table 18.

Parameters necessaries to compute the FVD damping coefficients Y direction.

Nivel	Modal shape φi	φi^2	φrj	Mass (Ton)	COSΘ	$\Sigma\varphi i^2 xmi$	$\Sigma\varphi rj^{1+\alpha}\cos^{1+\alpha}\Theta j$
1	0.11429	0.013	0.114	21.151	0.8575	0.28	0.03068
2	0.28571	0.082	0.171	21.151	0.8575	1.73	0.05636
3	0.48571	0.236	0.200	21.151	0.8575	4.99	0.07102
4	0.65714	0.432	0.171	21.151	0.8575	9.13	0.05636
5	0.82857	0.687	0.171	21.151	0.8575	14.52	0.05636
6	0.94286	0.889	0.114	21.151	0.8575	18.80	0.03068
7	1	1.000	0.057	21.151	0.8575	21.15	0.01085

$\Gamma = 1.292$

$\lambda = 2^{2+\alpha}\frac{\Gamma^2(1+\frac{\alpha}{2})}{\Gamma(2+\alpha)}$ $\quad\quad$ $\lambda = 3.496$

$A = \frac{g x \Gamma_i x S_a x T}{4 x \beta_{mD} x \pi^2}$ $\quad\quad$ $A = 0.211\ m$

$\sum C_j = \frac{\beta_H 2\pi A^{1-\alpha}\omega^{2-\alpha}\sum_i m_i \Phi_i^2}{\lambda \sum_j \Phi_{rj}^{1+\alpha}\cos^{1+\alpha}\theta_j}$ $\quad\quad$ $\sum C_j = 279.196\ Tn\frac{s}{m}$ (Per floor)

$C_Y = 140\ Tn\frac{s}{m}$ (In each damper)

T = 1.11 seg (Period of the mode)

$\beta_{mD} = 1.26$ (damping coefficient)

$\alpha = 0.5$

Table 19.

Parameters necessaries to compute the FVD damping coefficients X direction.

Nivel	Modal shape φi	φi^2	φrj	Mass (Ton)	COSΘ	$\Sigma\varphi i^2 xmi$	$\Sigma\varphi rj^{1+\alpha}\cos^{1+\alpha}\Theta j$
1	0.11429	0.013	0.114	21.151	0.8575	0.28	0.03068
2	0.28571	0.082	0.171	21.151	0.8575	1.73	0.05636
3	0.48571	0.236	0.200	21.151	0.8575	4.99	0.07102
4	0.65714	0.432	0.171	21.151	0.8575	9.13	0.05636
5	0.82857	0.687	0.171	21.151	0.8575	14.52	0.05636
6	0.94286	0.889	0.114	21.151	0.8575	18.80	0.03068
7	1	1.000	0.057	21.151	0.8575	21.15	0.01085

$\Gamma = 1.292$

$\lambda = 2^{2+\alpha}\frac{\Gamma^2(1+\frac{\alpha}{2})}{\Gamma(2+\alpha)}$ $\lambda = 3.496$

$A = \frac{gx\Gamma_i xS_a xT}{4x\beta_{mD}x\pi^2}$ $A = 0.212\ m$

$\sum C_j = \frac{\beta_H 2\pi A^{1-\alpha}\omega^{2-\alpha}\sum_i m_i\Phi_i^2}{\lambda\sum_j \Phi_{rj}^{1+\alpha}\cos^{1+\alpha}\theta_j}$ $\sum C_j = 302.46\ Tn\frac{s}{m}$ (Per floor)

$C_X = 151\ Tn\frac{s}{m}$ (In each damper)

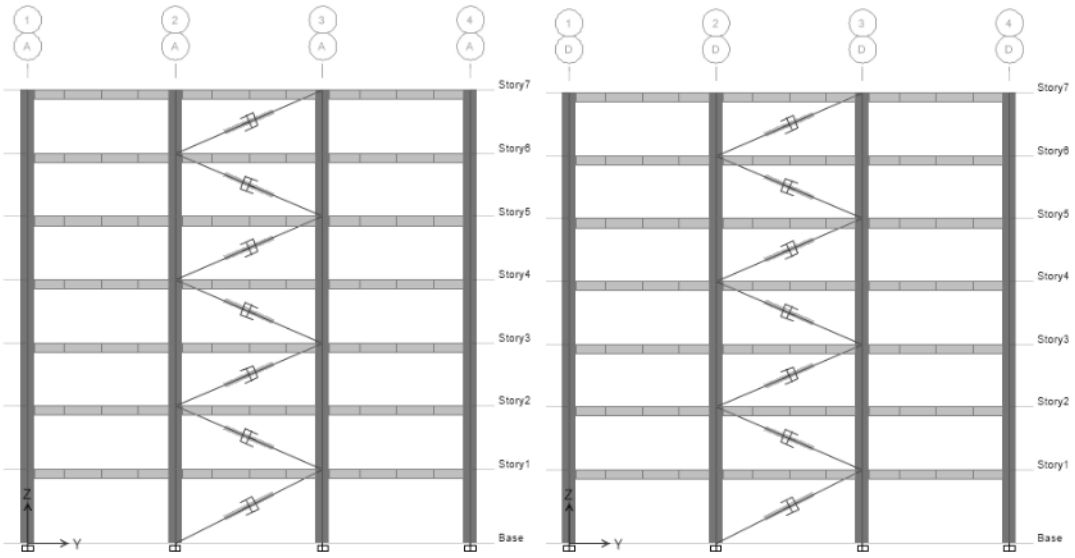

Figure 21. Location of FVDs Y direction.

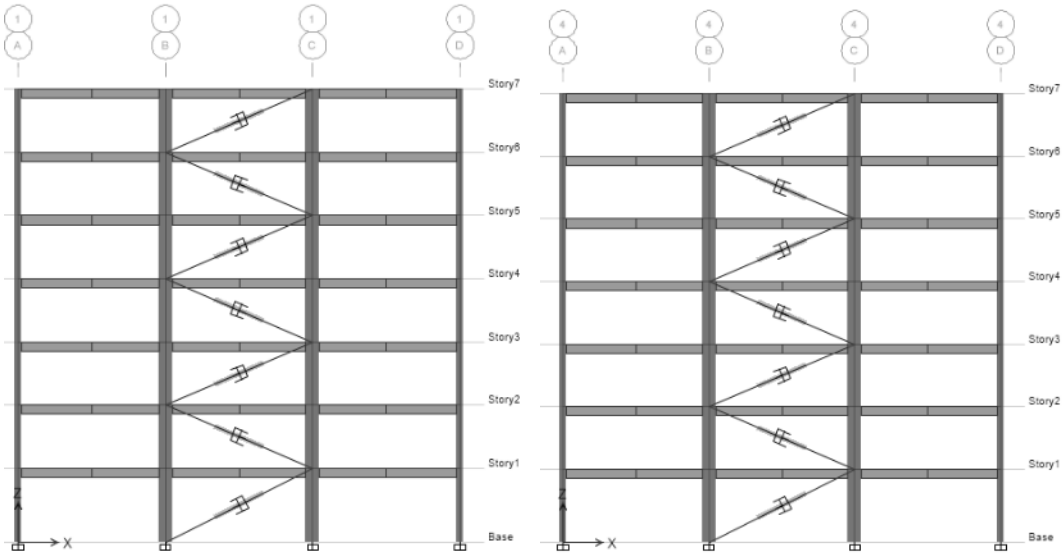

Figure 22. Location of FVDs X direction.

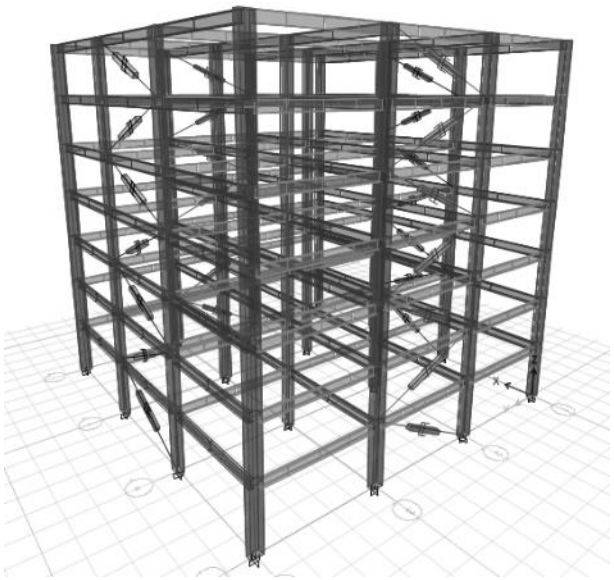

Figure 23. 3D view of Location of FVDs.

3.3.4. Results nonlinear Viscous Dampers

In the first tried, it was achieved a maximum drift of 0.0191 in TH1,1 and 0.0198 in TH1,4 in the directions X and Y respectively. These maximum drifts are lower than the

target drift define in the Ecuadorian code; the reduction of the maximum drifts is around 45% in both directions with the use of non-lineal viscous damper with a damping coefficient equal to 0.5.

Table 20.

Maximum and minimum drifts X direction with dampers.

Story	TH1,1		TH1,2		TH1,3		TH1,4		TH1,5		TH1,6	
	Max	Min	Max	Min	Max	Min	Max	Min	Max	Min	Max	Min
Story7	0,0059	0,0055	0,0054	0,0049	0,0056	0,0058	0,0004	0,0004	0,0011	0,0010	0,0014	0,0011
Story6	0,0095	0,0089	0,0088	0,0079	0,0090	0,0090	0,0007	0,0006	0,0020	0,0017	0,0025	0,0019
Story5	0,0137	0,0124	0,0122	0,0108	0,0124	0,0117	0,0011	0,0009	0,0029	0,0024	0,0036	0,0028
Story4	0,0173	0,0154	0,0150	0,0130	0,0150	0,0137	0,0014	0,0012	0,0037	0,0030	0,0047	0,0036
Story3	0,0191	0,0172	0,0164	0,0141	0,0162	0,0149	0,0016	0,0014	0,0040	0,0034	0,0053	0,0041
Story2	0,0185	0,0169	0,0158	0,0137	0,0152	0,0146	0,0017	0,0014	0,0039	0,0035	0,0053	0,0041
Story1	0,0109	0,0101	0,0094	0,0082	0,0089	0,0089	0,0010	0,0008	0,0024	0,0022	0,0032	0,0025

Table 21.

Absolute maximum drifts X direction with dampers

Story	Elevation m	TH1,1	TH1,2	TH1,3	TH1,4	TH1,5	TH1,6	Max
Story7	21,5	0,0059	0,0054	0,0058	0,0004	0,0011	0,0014	0,0059
Story6	18,5	0,0095	0,0088	0,0090	0,0007	0,0020	0,0025	0,0095
Story5	15,5	0,0137	0,0122	0,0124	0,0011	0,0029	0,0036	0,0137
Story4	12,5	0,0173	0,0150	0,0150	0,0014	0,0037	0,0047	0,0173
Story3	9,5	0,0191	0,0164	0,0162	0,0016	0,0040	0,0053	0,0191
Story2	6,5	0,0185	0,0158	0,0152	0,0017	0,0039	0,0053	0,0185
Story1	3,5	0,0109	0,0094	0,0089	0,0010	0,0024	0,0032	0,0109

Table 22.

Maximum and minimum drifts Y direction with dampers.

Story	TH1,1		TH1,2		TH1,3		TH1,4		TH1,5		TH1,6	
	Max	Min	Max	Min	Max	Min	Max	Min	Max	Min	Max	Min
Story7	0,0005	0,0004	0,0014	0,0013	0,0018	0,0014	0,0073	0,0068	0,0071	0,0061	0,0064	0,0069
Story6	0,0008	0,0007	0,0021	0,0020	0,0029	0,0022	0,0110	0,0101	0,0106	0,0090	0,0095	0,0096
Story5	0,0012	0,0010	0,0030	0,0028	0,0040	0,0031	0,0151	0,0135	0,0141	0,0119	0,0128	0,0122
Story4	0,0016	0,0013	0,0037	0,0035	0,0051	0,0038	0,0185	0,0161	0,0168	0,0138	0,0153	0,0147
Story3	0,0017	0,0015	0,0040	0,0039	0,0056	0,0042	0,0198	0,0172	0,0178	0,0143	0,0161	0,0161
Story2	0,0017	0,0014	0,0037	0,0038	0,0053	0,0039	0,0181	0,0171	0,0162	0,0131	0,0148	0,0156
Story1	0,0010	0,0008	0,0021	0,0022	0,0029	0,0023	0,0098	0,0100	0,0088	0,0072	0,0081	0,0089

Table 23.

Absolute maximum drifts Y direction with dampers.

Story	Elevation m	TH1,1	TH1,2	TH1,3	TH1,4	TH1,5	TH1,6	Max
Story7	21,5	0,0005	0,0014	0,0018	0,0073	0,0071	0,0069	0,0073
Story6	18,5	0,0008	0,0021	0,0029	0,0110	0,0106	0,0096	0,0110
Story5	15,5	0,0012	0,0030	0,0040	0,0151	0,0141	0,0128	0,0151
Story4	12,5	0,0016	0,0037	0,0051	0,0185	0,0168	0,0153	0,0185
Story3	9,5	0,0017	0,0040	0,0056	0,0198	0,0178	0,0161	0,0198
Story2	6,5	0,0017	0,0038	0,0053	0,0181	0,0162	0,0156	0,0181
Story1	3,5	0,0010	0,0022	0,0029	0,0100	0,0088	0,0089	0,0100

3.3.5. Linear Viscous Dampers Parameters

In this case, two damper in each direction per floor will be locates, and the damping coefficient is equal to one. The formula on the FDV damping coefficient is reducing due to the elimination of roof response amplitude term because it has exponential equal to zero such. The dampers damping will add twelve percent more to the structure in both directions obtaining 17% damping of the structure.

T = 1.17 seg (Period of the mode)

$\beta_{mD} = 1.26$ (Damping coefficient)

$\alpha = 1$

Table 24.

Parameters necessaries to compute the FVD damping coefficients Y direction.

Nivel	Modal shape φi	φi^2	φrj	Mass (Ton)	COSΘ	$\Sigma\varphi i^2 xmi$	$\Sigma\varphi rj^{1+\alpha}\cos^{1+\alpha}\Theta j$
1	0,11429	0,013	0,114	21,151	0,8575	0,28	0,00960
2	0,28571	0,082	0,171	21,151	0,8575	1,73	0,02161
3	0,48571	0,236	0,200	21,151	0,8575	4,99	0,02941
4	0,65714	0,432	0,171	21,151	0,8575	9,13	0,02161
5	0,82857	0,687	0,171	21,151	0,8575	14,52	0,02161
6	0,94286	0,889	0,114	21,151	0,8575	18,80	0,00960
7	1	1,000	0,057	21,151	0,8575	21,15	0,00240

$\Gamma = 1.292$

$\lambda = 2^{2+\alpha} \frac{\Gamma^2(1+\frac{\alpha}{2})}{\Gamma(2+\alpha)}$ $\lambda = 3.142$

$A = \frac{g x \Gamma_i x S_a x T}{4 x \beta_{mD} x \pi^2}$ $A = 0.211\ m$

$\sum C_j = \frac{\beta_H 2\pi A^{1-\alpha} \omega^{2-\alpha} \sum_i m_i \Phi_i^2}{\lambda \sum_j \Phi_{rj}^{1+\alpha} \cos^{1+\alpha} \theta_j}$ $\sum C_j = 785.48\ Tn\frac{s}{m}$ (Per floor)

$C_Y = 393\ Tn\frac{s}{m}$ (In each damper)

T = 1.11 seg (Period of the mode)

$\beta_{mD} = 1.26$ (Damping coefficient)

$\alpha = 1$

Table 25.

Parameters necessaries to compute the FVD damping coefficients X direction.

Nivel	Modal shape φi	φi²	φrj	Mass (Ton)	COSΘ	Σφi²xmi	Σφrj^1+α cos^1+α Θj
1	0,11429	0,013	0,114	21,151	0,85749	0,28	0,00960
2	0,28571	0,082	0,171	21,151	0,85749	1,73	0,02161
3	0,48571	0,236	0,200	21,151	0,85749	4,99	0,02941
4	0,65714	0,432	0,171	21,151	0,85749	9,13	0,02161
5	0,82857	0,687	0,171	21,151	0,85749	14,52	0,02161
6	0,94286	0,889	0,114	21,151	0,85749	18,80	0,00960
7	1	1,000	0,057	21,151	0,85749	21,15	0,00240

$\Gamma = 1.292$

$\lambda = 2^{2+\alpha} \frac{\Gamma^2(1+\frac{\alpha}{2})}{\Gamma(2+\alpha)}$ $\lambda = 3.142$

$A = \frac{g x \Gamma_i x S_a x T}{4 x \beta_{mD} x \pi^2}$ $A = 0.212\ m$

$\sum C_j = \frac{\beta_H 2\pi A^{1-\alpha} \omega^{2-\alpha} \sum_i m_i \Phi_i^2}{\lambda \sum_j \Phi_{rj}^{1+\alpha} \cos^{1+\alpha} \theta_j}$ $\sum C_j = 827.94\ Tn\frac{s}{m}$ (Per floor)

$C_X = 414\ Tn\frac{s}{m}$ (In each damper)

3.3.6. Results linear Viscous Dampers

In the first tried, it was achieved a maximum drift of 0.0184 in TH1,3 and 0.0190 in TH1,4 in the directions X and Y respectively. These maximum drifts are lower than the target drift define in the Ecuadorian code; the reduction of the maximum drifts is around 45% in both directions with the use of non-lineal viscous damper with a damping coefficient equal to 0.5.

Table 26.

Maximum and minimum drifts X direction with lineal dampers.

Story	TH1,1		TH1,2		TH1,3		TH1,4		TH1,5		TH1,6	
	Max	Min	Max	Min	Max	Min	Max	Min	Max	Min	Max	Min
Story7	0,0058	0,0054	0,0056	0,0050	0,0051	0,0054	0,0008	0,0007	0,0015	0,0016	0,0018	0,0016
Story6	0,0094	0,0085	0,0089	0,0080	0,0080	0,0083	0,0012	0,0011	0,0024	0,0025	0,0028	0,0026
Story5	0,0132	0,0117	0,0122	0,0109	0,0111	0,0110	0,0016	0,0015	0,0033	0,0033	0,0040	0,0035
Story4	0,0166	0,0143	0,0149	0,0132	0,0137	0,0133	0,0020	0,0018	0,0041	0,0040	0,0050	0,0043
Story3	0,0184	0,0157	0,0164	0,0142	0,0151	0,0146	0,0022	0,0019	0,0045	0,0044	0,0055	0,0047
Story2	0,0180	0,0156	0,0159	0,0137	0,0148	0,0143	0,0021	0,0019	0,0044	0,0043	0,0054	0,0047
Story1	0,0108	0,0097	0,0095	0,0083	0,0089	0,0089	0,0013	0,0011	0,0027	0,0027	0,0032	0,0029

Table 27.

Absolute maximum drifts X direction with lineal dampers.

Story	Elevation	TH1,1	TH1,2	TH1,3	TH1,4	TH1,5	TH1,6	Max
	m							
Story7	21,5	0,0058	0,0056	0,0054	0,0008	0,0016	0,0018	0,0058
Story6	18,5	0,0094	0,0089	0,0083	0,0012	0,0025	0,0028	0,0094
Story5	15,5	0,0132	0,0122	0,0111	0,0016	0,0033	0,0040	0,0132
Story4	12,5	0,0166	0,0149	0,0137	0,0020	0,0041	0,0050	0,0166
Story3	9,5	0,0184	0,0164	0,0151	0,0022	0,0045	0,0055	0,0184
Story2	6,5	0,0180	0,0159	0,0148	0,0021	0,0044	0,0054	0,0180
Story1	3,5	0,0108	0,0095	0,0089	0,0013	0,0027	0,0032	0,0108

Table 28.

Maximum and minimum drifts Y direction with lineal dampers.

Story	TH1,1		TH1,2		TH1,3		TH1,4		TH1,5		TH1,6	
	Max	Min	Max	Min	Max	Min	Max	Min	Max	Min	Max	Min
Story7	0,0010	0,0008	0,0018	0,0019	0,0022	0,0019	0,0072	0,0064	0,0071	0,0060	0,0061	0,0064
Story6	0,0014	0,0012	0,0027	0,0028	0,0032	0,0028	0,0107	0,0095	0,0104	0,0089	0,0090	0,0093
Story5	0,0019	0,0016	0,0036	0,0037	0,0043	0,0038	0,0145	0,0127	0,0139	0,0117	0,0121	0,0124
Story4	0,0022	0,0019	0,0044	0,0045	0,0053	0,0046	0,0176	0,0153	0,0165	0,0138	0,0146	0,0151
Story3	0,0024	0,0019	0,0047	0,0049	0,0057	0,0050	0,0190	0,0166	0,0176	0,0143	0,0156	0,0165
Story2	0,0022	0,0018	0,0043	0,0048	0,0053	0,0049	0,0176	0,0162	0,0162	0,0131	0,0145	0,0158
Story1	0,0012	0,0010	0,0024	0,0027	0,0029	0,0029	0,0097	0,0095	0,0088	0,0072	0,0080	0,0091

Table 29.

Absolute maximum drifts X direction with lineal dampers.

Story	Elevation m	TH1,1	TH1,2	TH1,3	TH1,4	TH1,5	TH1,6	Max
Story7	21,5	0,0010	0,0019	0,0022	0,0072	0,0071	0,0064	0,0072
Story6	18,5	0,0014	0,0028	0,0032	0,0107	0,0104	0,0093	0,0107
Story5	15,5	0,0019	0,0037	0,0043	0,0145	0,0139	0,0124	0,0145
Story4	12,5	0,0022	0,0045	0,0053	0,0176	0,0165	0,0151	0,0176
Story3	9,5	0,0024	0,0049	0,0057	0,0190	0,0176	0,0165	0,0190
Story2	6,5	0,0022	0,0048	0,0053	0,0176	0,0162	0,0158	0,0176
Story1	3,5	0,0012	0,0027	0,0029	0,0097	0,0088	0,0091	0,0097

3.3.7. Input seismic energy in the structure.

The structure dissipate the input energy in different ways by elastic deformation, pontecial energy, inelastic deformation, kinetic energy, global damping, and energy taking by the dampers. In the figures 24, 25, and 26 are shown the distribution of energy in the structure for the analysis TH1,1 in 45 second for the structure without damper, with non-lineal damper, and with lineal dampers .

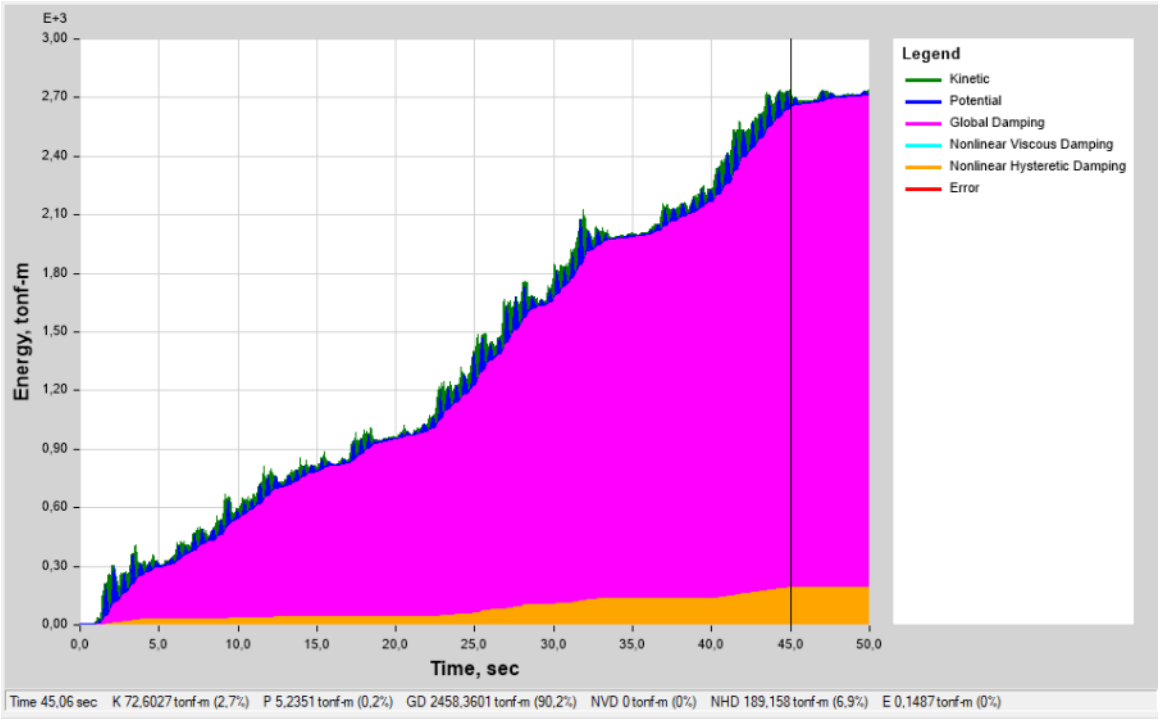

Figure 24. Energy in the structure without dampers.

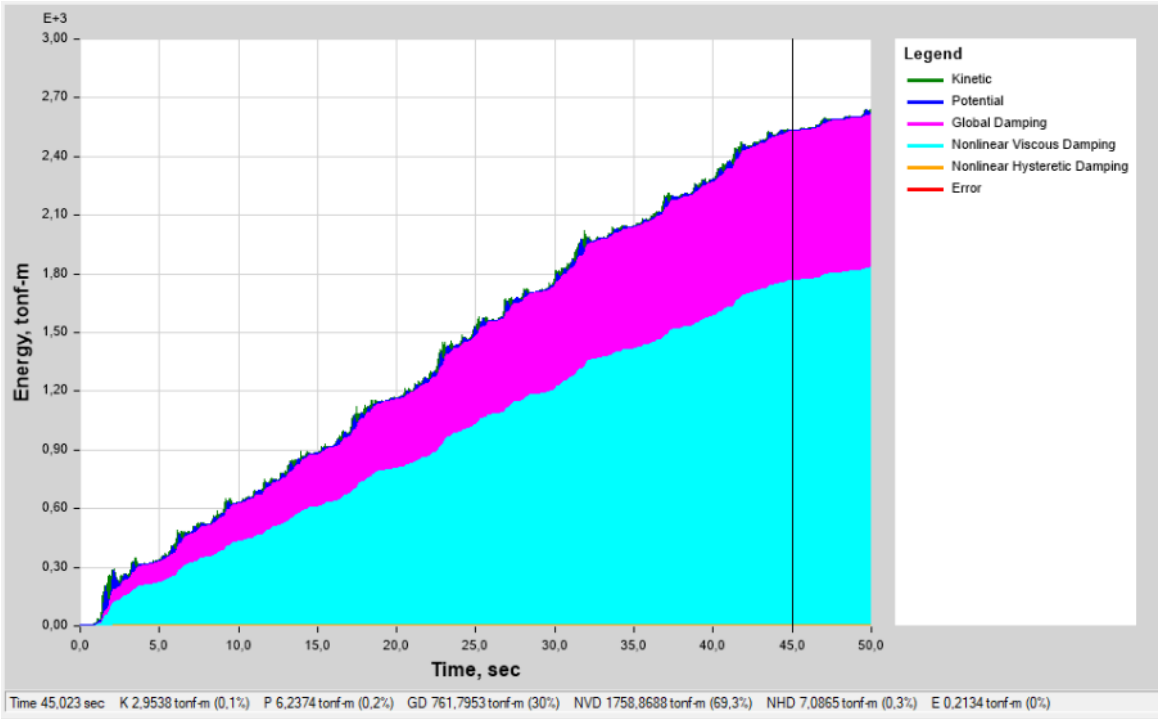

Figure 25. Energy in the structure without nonlinear dampers.

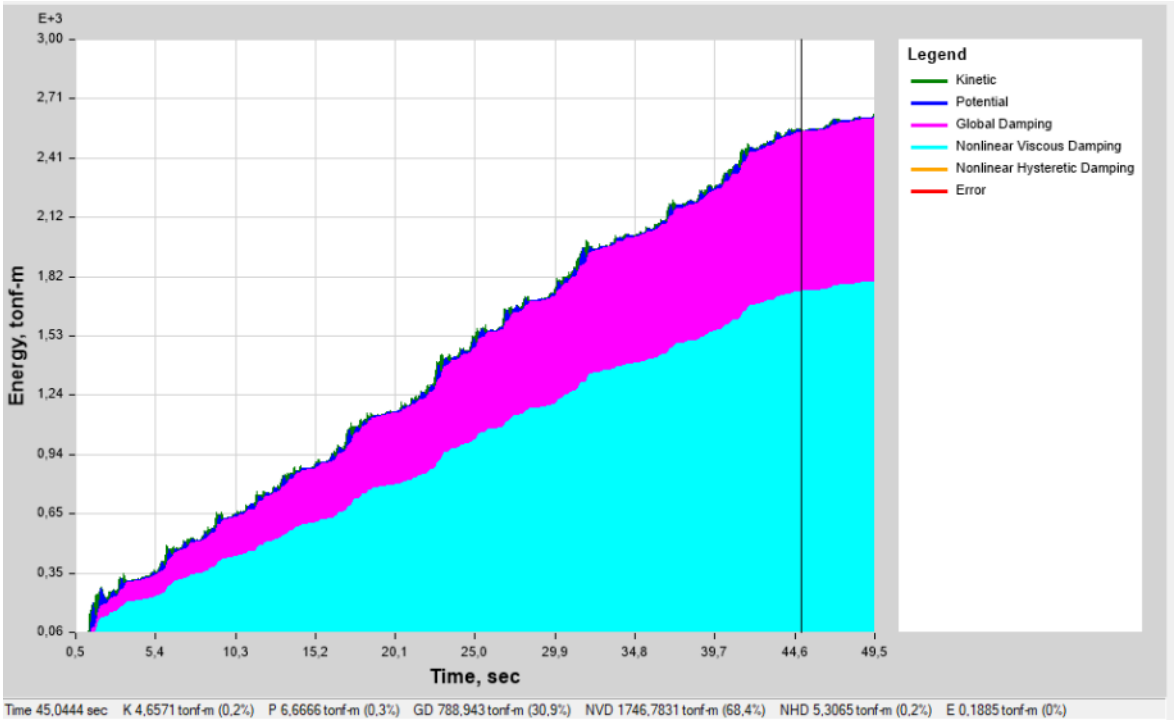

Figure 26. Energy in the structure without lineal dampers.

Table 30.

Energy dissipation of the structure for TH1,1 at 45 seconds for structure with and without dampers.

Energy dissipation	**Normal**	**Nonlinear dampers**	**Lineal dampers**
	%	**%**	**%**
Kinetic	2,7	0,1	0,2
Potential	0,2	0,2	0,3
Global Damping	90,2	30	30,9
Nonlinear Viscous Damping	0	69,3	68,4
Nonlinear Hysteretic Damping	6,9	0,3	0,2
Error	0	0	0
Sum	**100**	**99,9**	**100**

3.3.8. Inelastic behavior of the structure.

In this literal, it will be analysis the develop of the plastic hinges (concentrate nonlinear behavior) for the structure with dampers and without dampers for the case TH1,1 at 45 seconds.

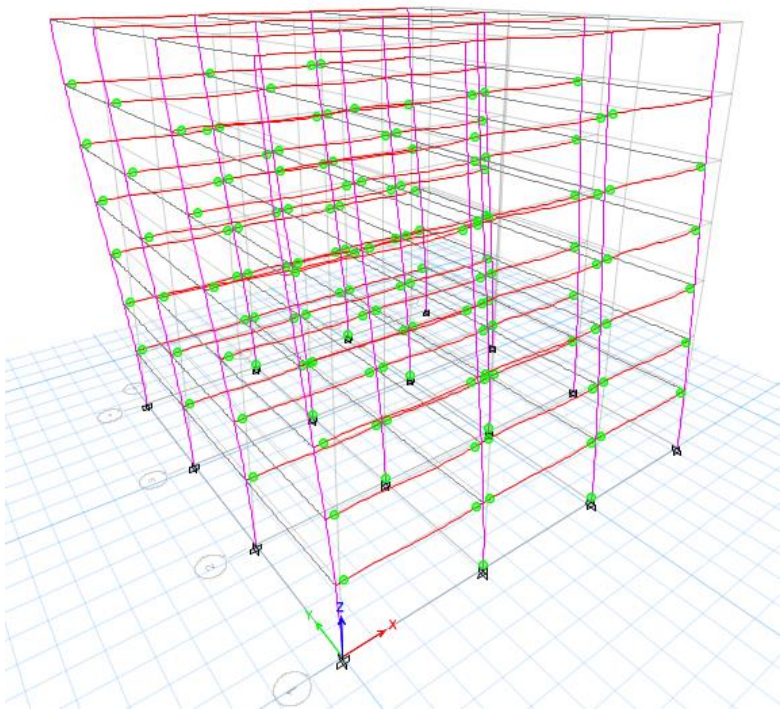

Figure 27. Nonlinear behavior of the structure without dampers.

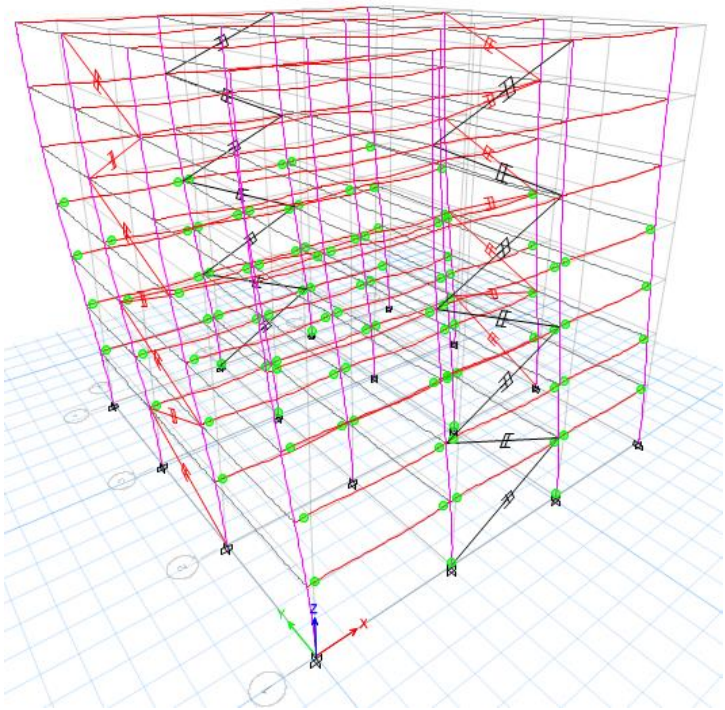

Figure 28. Nonlinear behavior of the structure without nonlinear dampers.

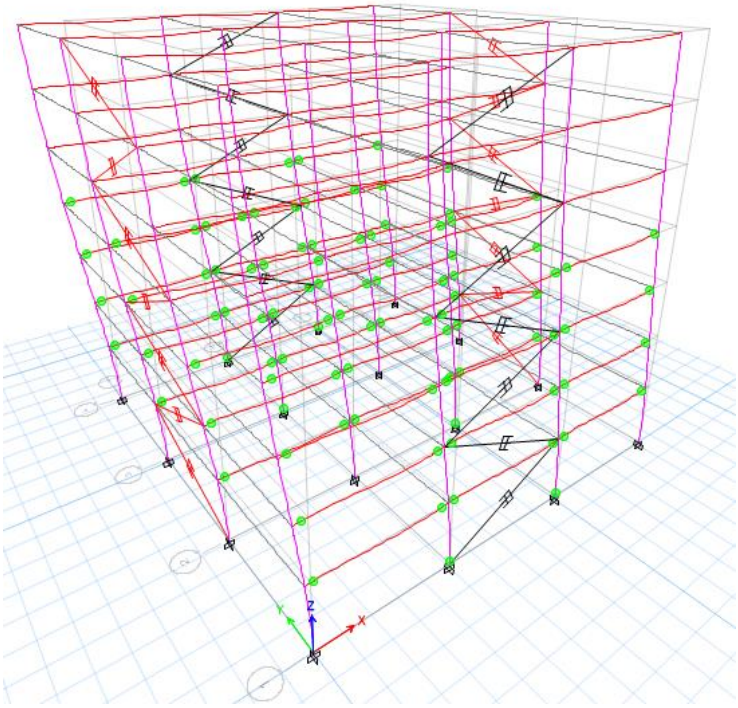

Figure 29. Nonlinear behavior of the structure without linear dampers.

In figure 28 and 29, it shown a reduction in the develop of plastic hinges comparing with figure 27 that is the structure without dampers.

3.3.9. Dampers forces and behavior.

In order to buy the dampers and design the steel brace, it is necessary to know the maximum axial force in the damper of all the time history analysis. In this case, it is shown the axial forces in the linear and nonlinear dampers for the case TH1,1 this process must be repeated for all case and get the maximum value of all cases per damper.

Table 31.

Axial damper forces for TH1,1

Story	Damper	Load Case	Location	Linear	Non linear
				P	P
				tonf	tonf
Story7	K7	TH1.1 Max	I-End	8,6816	13,9343
Story7	K14	TH1.1 Max	I-End	8,6254	13,8907
Story7	K21	TH1.1 Max	I-End	54,6033	60,2641
Story7	K28	TH1.1 Max	I-End	54,5867	60,2242
Story6	K6	TH1.1 Max	I-End	11,615	16,486
Story6	K13	TH1.1 Max	I-End	11,5164	16,6037
Story6	K20	TH1.1 Max	I-End	79,6242	68,8412
Story6	K27	TH1.1 Max	I-End	79,6065	68,8544
Story5	K5	TH1.1 Max	I-End	14,5703	20,5379
Story5	K12	TH1.1 Max	I-End	14,3972	20,2781
Story5	K19	TH1.1 Max	I-End	103,9953	77,4208
Story5	K26	TH1.1 Max	I-End	103,9862	77,3822
Story4	K4	TH1.1 Max	I-End	16,0239	25,257
Story4	K11	TH1.1 Max	I-End	15,9323	24,9958
Story4	K18	TH1.1 Max	I-End	117,1139	83,035
Story4	K25	TH1.1 Max	I-End	117,097	83,012
Story3	K3	TH1.1 Max	I-End	15,9643	26,4887
Story3	K10	TH1.1 Max	I-End	15,8354	26,2822
Story3	K17	TH1.1 Max	I-End	121,2528	85,9504
Story3	K24	TH1.1 Max	I-End	121,2309	85,9176
Story2	K2	TH1.1 Max	I-End	15,096	26,0883
Story2	K9	TH1.1 Max	I-End	14,9435	25,8936
Story2	K16	TH1.1 Max	I-End	114,5928	84,0757
Story2	K23	TH1.1 Max	I-End	114,5854	84,0612
Story1	K1	TH1.1 Max	I-End	10,4274	20,5736
Story1	K8	TH1.1 Max	I-End	10,344	20,2014
Story1	K15	TH1.1 Max	I-End	83,6947	69,8889
Story1	K22	TH1.1 Max	I-End	83,6927	69,8353

In order to know if the damper is working well, the graphic of the hysteresis can be analysis, and the graphic must have an elliptical form. For this case the damper K24 of the three floor that is damper with the maximum axial force is analysis.

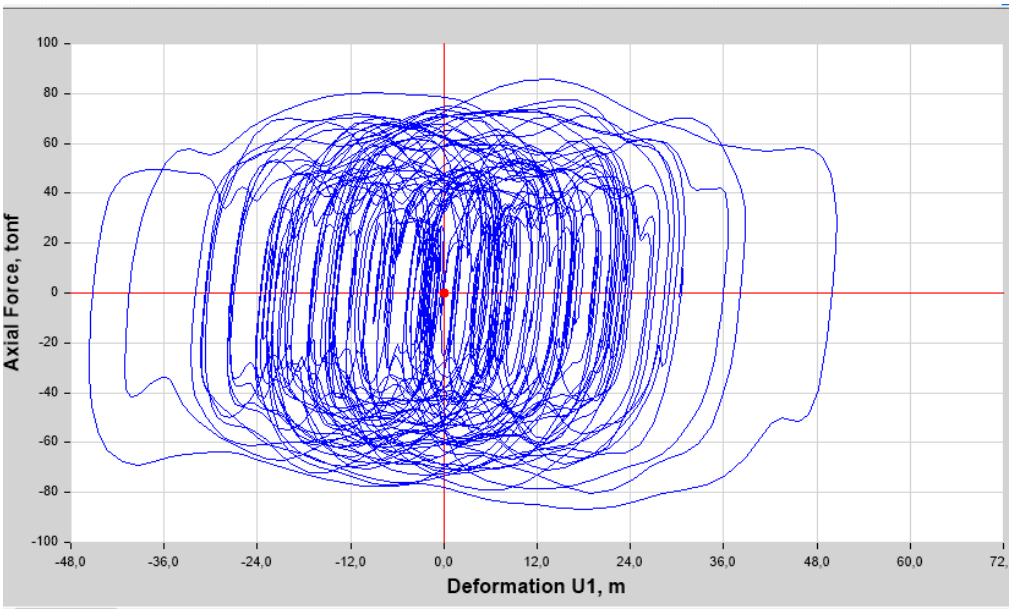

Figure 30. Hysteresis of damper K24 case TH1,1

4. Static nonlinear analysis (Pushover)

4.1. Introduction

The static non-linear analysis known as push-over analysis is a procedure in which a structure is exposed to the gravity seismic loads (vertical loads) and variable increasing lateral load pattern. The growing lateral forces produce the change of the linear behavior to a plastic condition (nonlinear behavior) in the structural elements.

The nonlinear behavior of structural elements can be analyses with fiber distribution, nonlinear finite elements and concentrate plastic behavior. The most common analysis is the concentrate model that uses plastic hinges located in the end or a distance from the extreme of the elements depending of the beam connection, type and composition of the structural element.

The nonlinear behavior of plastic hinges is described by moment-curvature (or rotation) or force-displacement laws. The moment-curvature can be obtained from the American standard FEMA 356 for steel and concrete structural elements. (Almansa, 2018)

The pushover analysis allows to determine the performance of a structure with a specific demand; the performance of the structure is proportional to the geometry, structural system, column-beam connection, and structural element material.

On the other hand, the demand depends of the return period, location of the structure, importance, and seismic hazard. The first step for the pushover analysis is to charge the structure with the gravity load; in this process the structure will suffer the first deformations. After all the gravitational load were applied, the monotonic lateral load is applied gradually.

The structure has an elastic or lineal behavior until the first plastic hinge appears; the plastic hinges can be analysis for bending, shear, and axial force. The lateral continues to increasing, and more plastic hinges appears due to the monotonic load. The analysis remains until that the structure become uneatable and collapse.

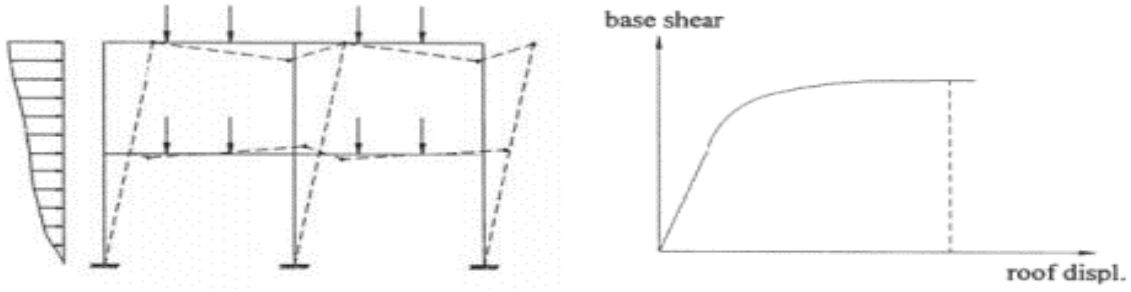

Figure 31. Pushover procedure. Source: (GIANNOPOULOS, 2009)

The relationship between the increasing lateral load (base shear) and structure displacement can be representing in a graphic kwon as capacity curve. A common point to monitor the displacement is located in the roof and near to the center of mass. The capacity curve has a lineal segment that represents the lineal behavior of the structure; the stiffness degradation continues with the developing of the plastic hinges until the collapse point.

The point in which the straight line change to a curve shows the yield displacement; in this point the first plastic hinge occurs. The analysis can be control by force or displacement.

The plastic hinge behavior can be defining with the curve of the figure 11. This figure presents five points labeled A, B, C, D, and E are used to define the force deflection behavior of the hinge. Also, three points labeled IO, LS and CP are used to define the acceptance criteria for the hinge. (IO, LS and CP stand for Immediate Occupancy, Life Safety and Collapse Prevention respectively.)

The values assigned to each of these points vary depending on the type of member as well as many other parameters, and they can be found in the ATC- 40, FEMA-273, and FEMA-356 documents (Federal Emergency Management, 2000)

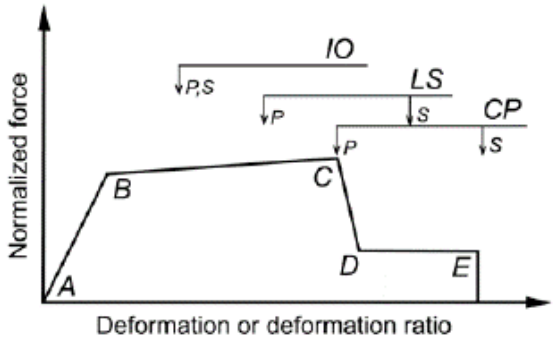

Figure 32. Plastic hinge behavior

4.2. Pushover application

The pushover analysis will be performed in the models of force design, displacement design, and the model with the fluid viscous damper. Furthermore, in the models of displacement and force design the pushover analysis is going to be controlled by displacement and the forces got in the DBDD and BFD. The program ETABS 16 2.0 is used to performer the analysis.

4.2.1. Pushover gravitational load

The non-lineal gravitational load according to the FEMA 356 section 3.2.8, the non-lineal gravitational load is equal to the reactive mas multiplied by 1.1. The Q_D, Q_L, and Q_S are the dead load, twenty-five percent of the live load and the snow load respectively.

$$Q_{NGL} = 1.1\ (Q_D + Q_L + Q_S)$$ Equation 45. (Non-lineal gravitational load)

Table 32.

Non-lineal gravitational load

Distance x (m)	Distance Y (m)	Plant area (m2)	Floors	Dead load DL (Kg/m2)	Live load LL (Kg/m2)	Non-lineal gravitational load (Kg)
21	21	441	7	480	200	1799721

The self-weight of the structure is not taking in count in the table 13, for the program automatic compute that load, and the gravitational load is equal to the three cases. The non-lineal gravitational load is controlled by load in the direction U3 and saved only the final stated.

4.2.2. Pushover lateral load patterns

The regularity of the structure in plant and elevation of the structure carries that more than the seventy-five percent of the participative mass be in the first to mode. This percentage

of mass participative secures that the two first mode are transnationals, and the first mode is the predominant.

According to the FEMA 356, if the response is governed by a single mode of vibration, the lateral distribution will be modal using the first mode technique applying accelerations proportional to the shape of the first mode of the elastic MDOF model or an inverted triangle configuration. The selected loading pattern should produce a deflected shape in the structure similar to that it would undergo in earthquake response. (Dogariu, 2011)

Table 33.

Modal Participating Mass Ratios

Modal Participating Mass Ratios					
Case	**Mode**	**Period**	**UX**	**UY**	**UZ**
		sec			
Modal	1	1,113	0	0,8007	0
Modal	2	1,052	0,8144	0	0
Modal	3	0,852	0	0	0
Modal	4	0,332	0	0,1114	0
Modal	5	0,322	0,1062	0	0
Modal	6	0,257	0	0	0
Modal	7	0,169	0,0423	0	0
Modal	8	0,167	0	0,0465	0
Modal	9	0,132	0	0	0
Modal	10	0,105	0,0211	0	0
Modal	11	0,1	0	0,0235	0
Modal	12	0,079	0	0	0
Modal	13	0,072	0,0104	0	0
Modal	14	0,067	0	0,0116	0
Modal	15	0,053	0,0043	0	0
Modal	16	0,053	0	0	0
Modal	17	0,049	0	0,0048	0
Modal	18	0,044	0,0014	0	0
Modal	19	0,04	0	0,0015	0
Modal	20	0,039	0	0	0
Modal	21	0,032	0	0	0

$F_m = PF_m \, Ø_m S_a w$ Equation 46. (Modal story forces based in the first mode)

$F_x = \frac{W_x \, h_x}{\Sigma_{i=1}^{n} w_i \, h_i} \, V_x$ Equation 47. (Triangular story forces)

Table 34.

Story forces based in triangular and first mode distribution.

	Triangular	1ST Mode
Story	**Fi**	**Fi**
	Ton	**Ton**
7	31,46	29,92
6	27,07	28,21
5	22,68	24,79
4	18,29	19,66
3	13,98	14,53
2	9,56	8,55
1	5,20	3,41
Σ	128,24	129,07

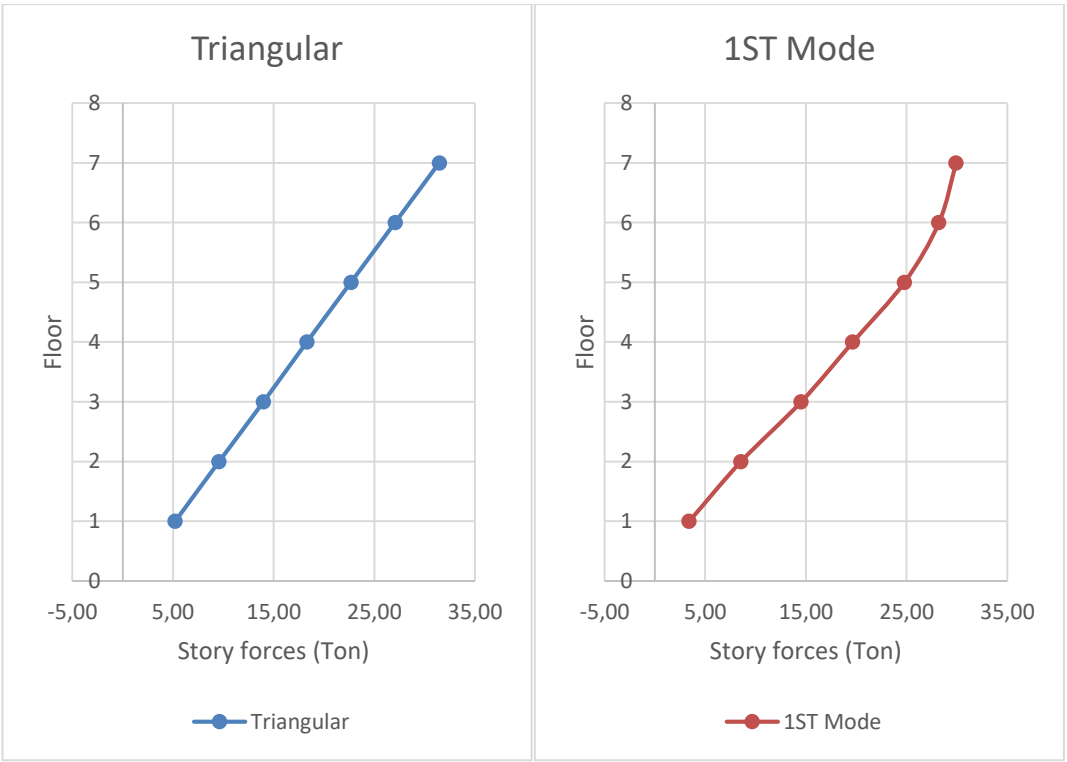

Figure 33. Story forces based in triangular and first mode distribution.

4.2.3. Plastic hinge location

The plastic hinge location in steel structure depends of the type of connection. In this case, the connection used is full restrict moment bolted connection according to the AISC 358-10 type Bolted Flange Plate (BFP) moment connection for special moment frames. In the beams the plastic hinge is located in function of the distance from face of column to nearest row of bolts (S1), spacing of bolt row (S), and number of bolts (N) (AMERICAN INSTITUTE OF STEEL CONSTRUCTION, 2016)

For this structure, the connection is composed of two columns and four rows of bolts of one inches of diameter spacing eight centimeters each row and the first row from the face of the columns.

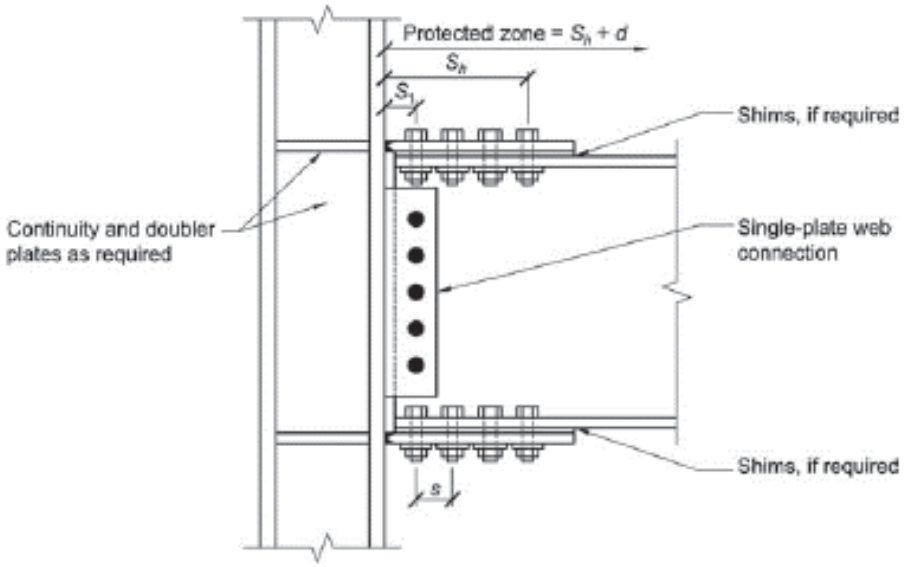

Figure 34. Bolted flange plate moment connection. Source: AISC 358-10

$$S_h = S_1 + S\left(\frac{n}{2} - 1\right)$$ Equation 48. (Plastic hinge location in beams)

$$S_h = 320 \text{ mm}$$

In the case of the columns, the plastic hinge is located a five percent of the element length.

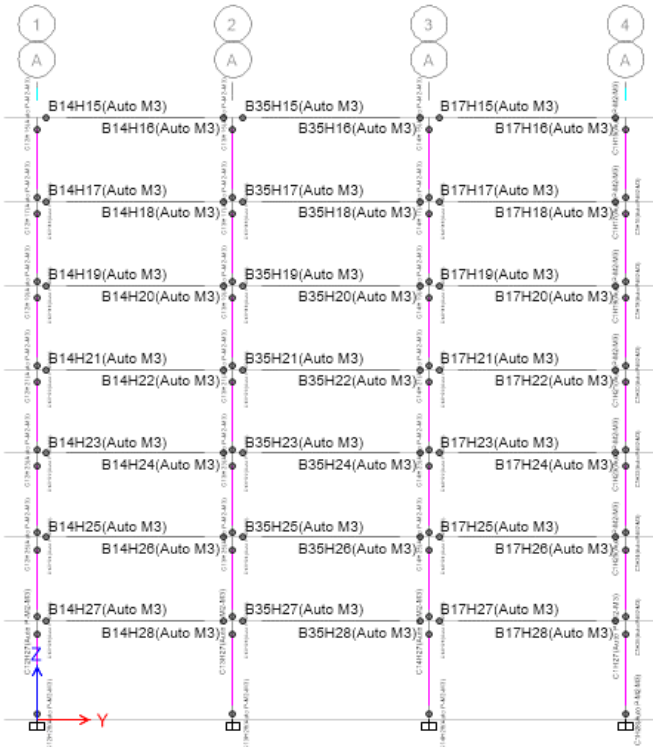

Figure 35. Plastic hinge location in frame.

4.2.4. Pushover results.

The result form the pushover analysis for this case are the capacity curve, performance point, and plastic hinge develops in each direction. The cases analyzed sere the force design and Dbdd design for the triangular, first mode and Dbdd pattern. The plastic hinges are classifying in each increment according they behavior immediate operation (IO), Life safety (Ls) and Collapse prevention (CP). Also the hinges are classifying according the behavior of the hinge with the rotation-force diagram.

Table 35.

Capacity curve DBDD and force design X direction.

Step	DBDD						FORCE					
	DBDD		FIRTS MODE		TRIANGULAR		DBDD		FIRTS MODE		TRIANGULAR	
	Displ	Base Force	Displ	Base Force	Displ	Base Force	Displ	Base Force	Displ	Base Force	Displ	Base Force
	m	Ton	m	Ton	m	Ton	m	Ton	m	Ton	m	Ton
0	0,00	0,00	0,00	0,00	0,00	0,00	0,00	0,00	0,00	0,00	0,00	0,00
1	0,09	349,99	0,09	352,71	0,09	356,35	0,09	329,98	0,09	332,66	0,09	336,12
2	0,17	694,77	0,17	682,50	0,17	694,41	0,17	659,96	0,17	665,32	0,17	672,23
3	0,23	875,25	0,23	864,90	0,23	877,84	0,18	689,20	0,18	677,42	0,18	689,13
4	0,31	980,78	0,31	975,31	0,32	990,74	0,25	893,10	0,24	873,06	0,25	893,98
5	0,41	1049,37	0,40	1038,88	0,41	1055,70	0,34	992,74	0,33	981,29	0,33	993,13
6	0,50	1089,29	0,49	1078,08	0,50	1093,72	0,43	1060,26	0,42	1050,84	0,42	1062,67
7	0,51	1093,28	0,50	1082,78	0,50	1095,38	0,50	1096,50	0,52	1097,97	0,52	1111,26
8	0,37	535,42	0,47	908,20	0,38	576,50	0,54	1113,63	0,53	1103,87	0,53	1116,70
9							0,40	570,99	0,49	915,49	0,49	960,26

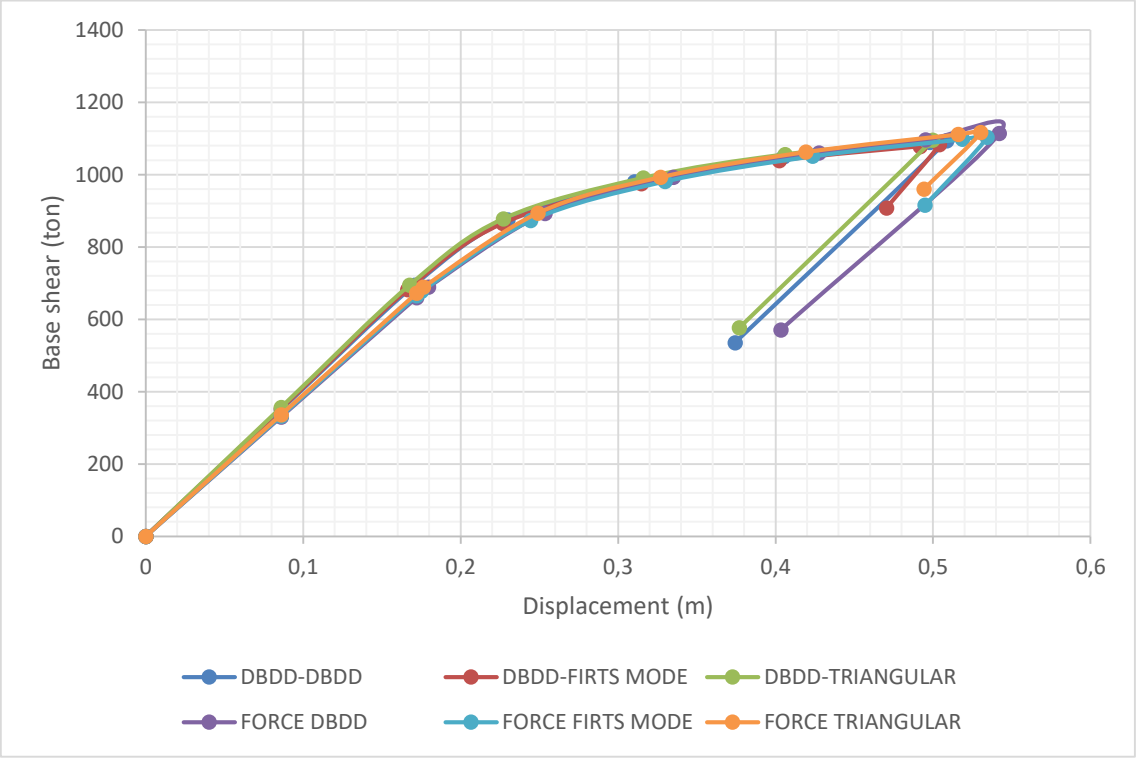

Figure 36. Capacity curve direction X

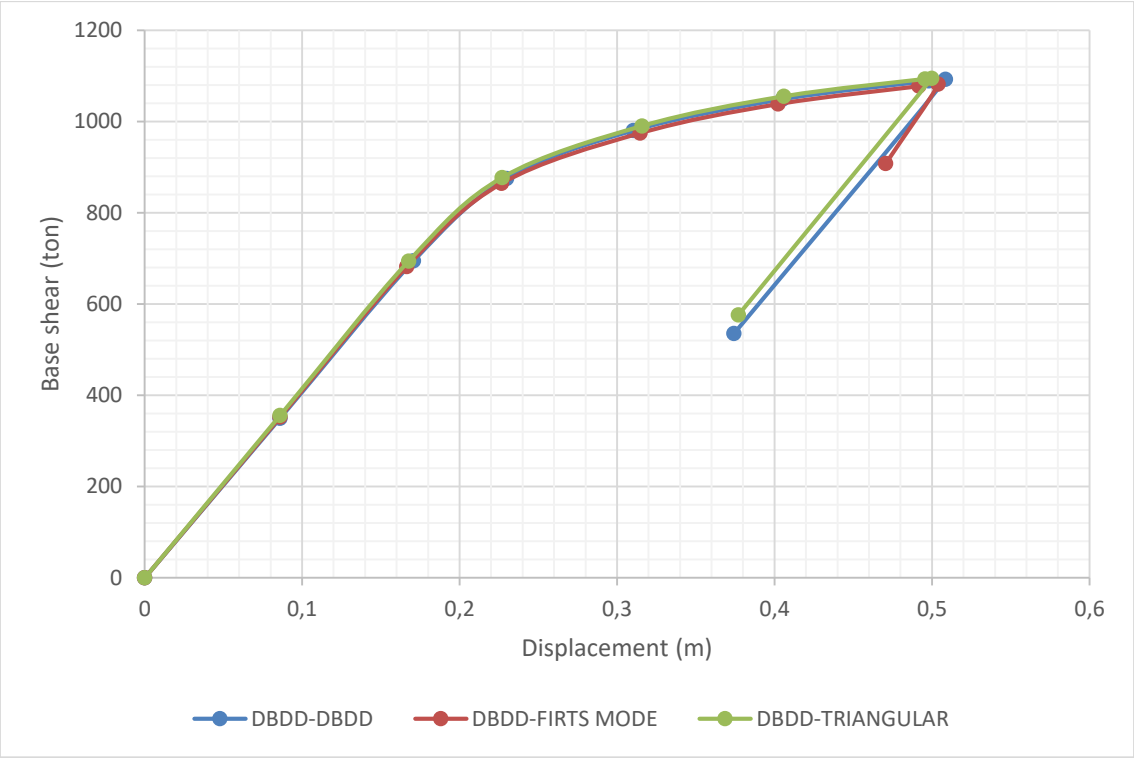

Figure 37. Capacity curve direction X DBDD design

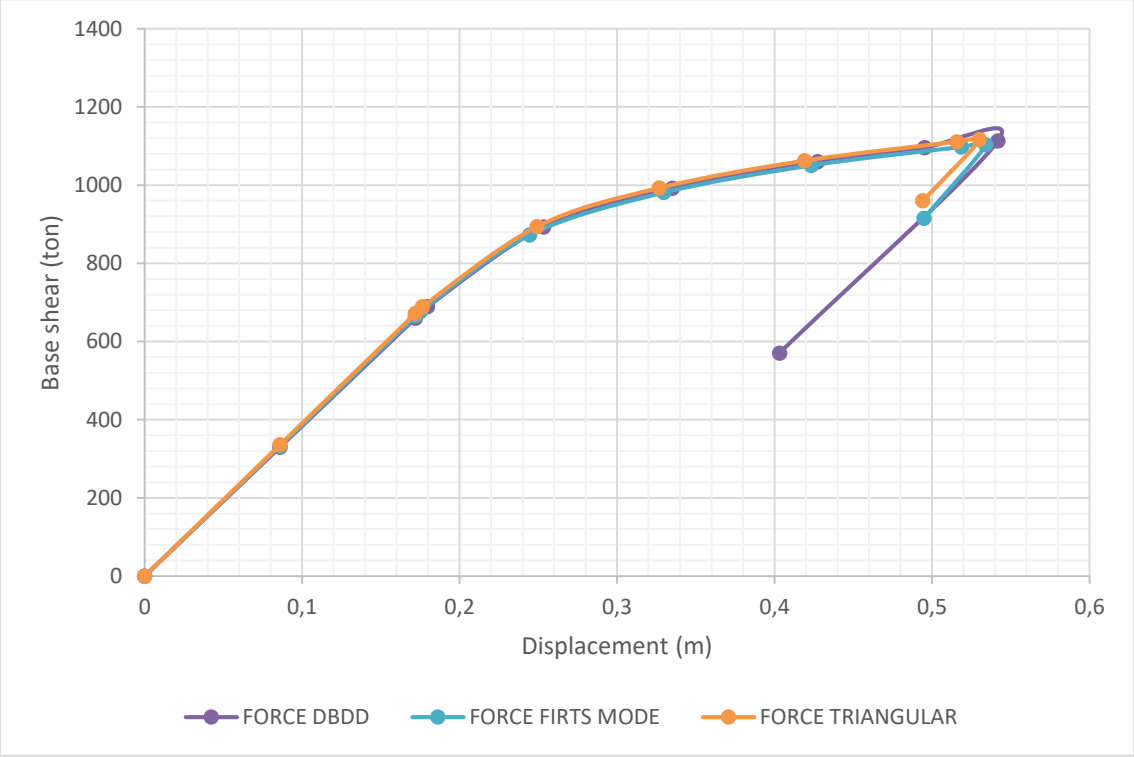

Figure 38. Capacity curve direction X Forces design.

Table 36.

Capacity curve DBDD and force design Y direction.

Step	DBDD						FORCE					
	DBDD		FIRTS MODE		TRIANGULAR		DBDD		FIRTS MODE		TRIANGULAR	
	Displ	Base Force	Displ	Base Force	Displ	Base Force	Displ	Base Force	Displ	Base Force	Displ	Base Force
	m	Ton	m	Ton	m	Ton	m	Ton	m	Ton	m	Ton
0	0,00	0,00	0,00	0,00	0,00	0,00	0,00	0,00	0,00	0,00	0,00	0,00
1	0,09	325,79	0,09	328,47	0,09	331,88	0,09	289,30	0,09	291,91	0,09	294,94
2	0,17	641,25	0,16	630,04	0,17	640,99	0,17	578,60	0,17	583,82	0,17	589,88
3	0,22	801,30	0,22	788,32	0,22	804,55	0,18	612,17	0,18	602,18	0,18	612,46
4	0,32	917,79	0,31	902,80	0,31	921,16	0,24	767,29	0,24	753,89	0,24	767,17
5	0,41	986,15	0,40	971,15	0,41	989,46	0,33	871,65	0,33	866,27	0,32	876,76
6	0,51	1029,45	0,54	1033,74	0,53	1042,34	0,42	938,90	0,41	934,21	0,42	951,72
7	0,57	1050,94	0,56	1040,50	0,55	1053,80	0,51	990,84	0,50	984,15	0,52	1003,61
8	0,42	502,54	0,42	499,52	0,42	520,03	0,61	1024,27	0,59	1017,77	0,61	1035,94
9							0,63	1032,25	0,62	1026,44	0,61	1037,80
10							0,47	482,86	0,46	477,17	0,54	772,68

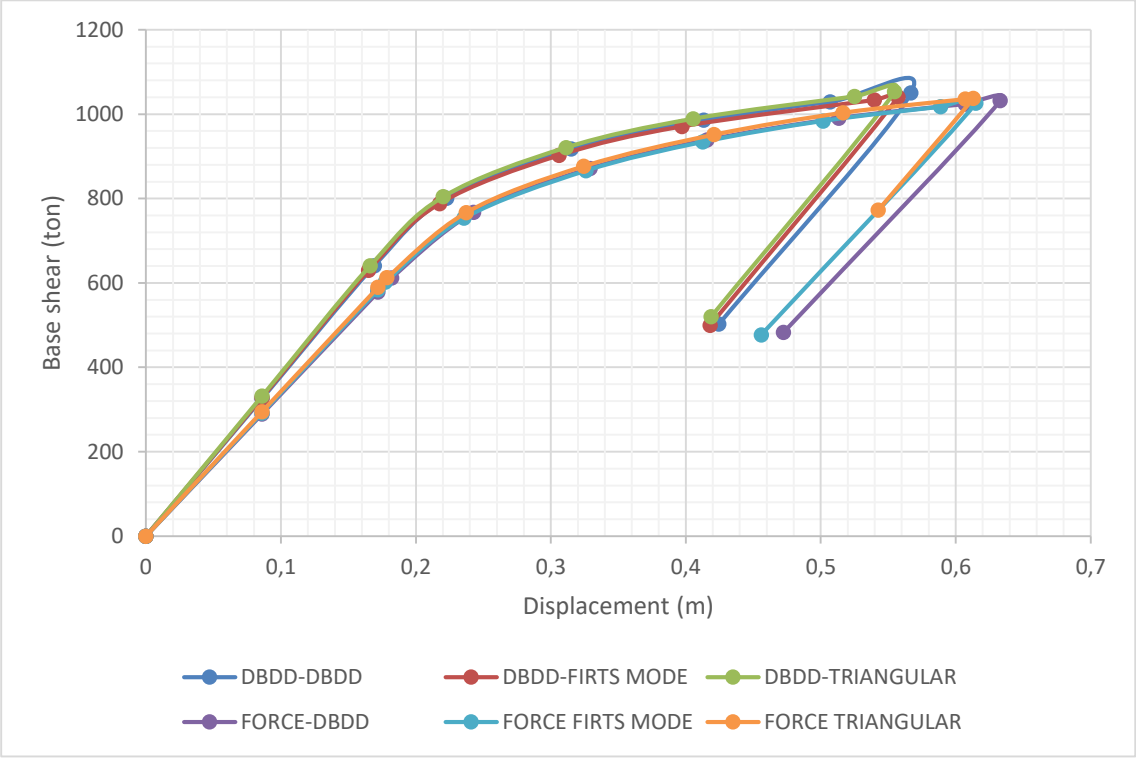

Figure 39. Capacity curve direction Y

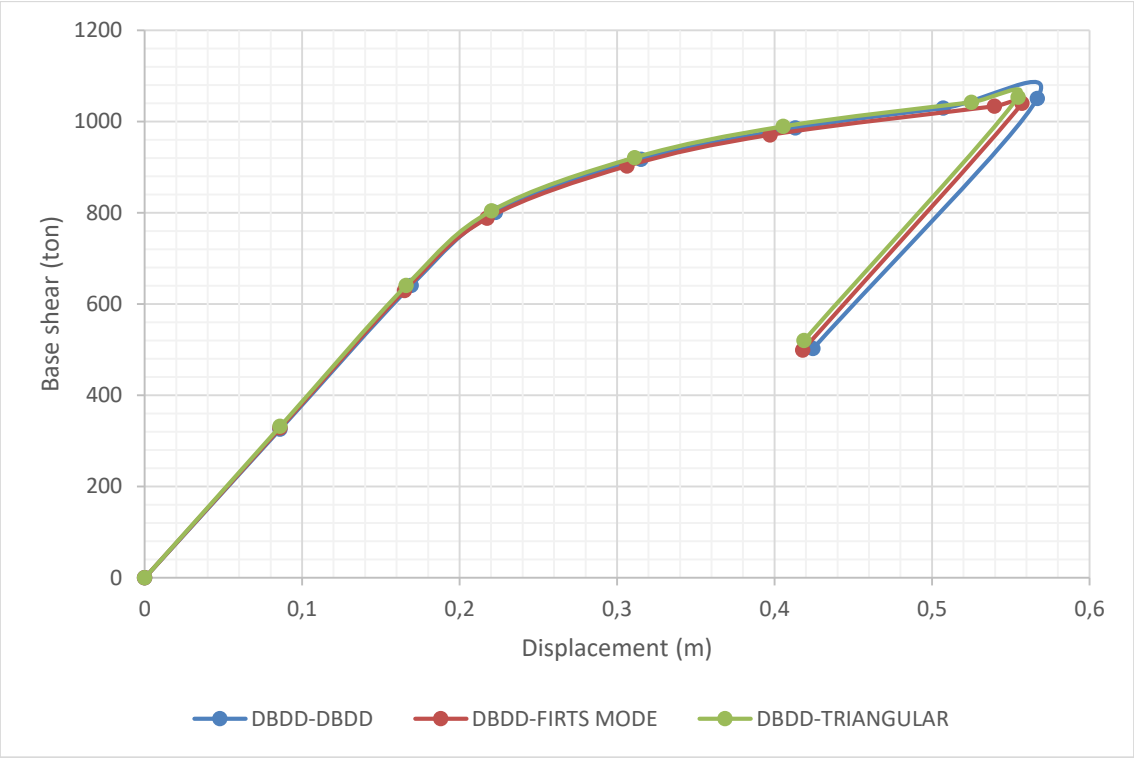

Figure 40. Capacity curve direction Y DBDD design

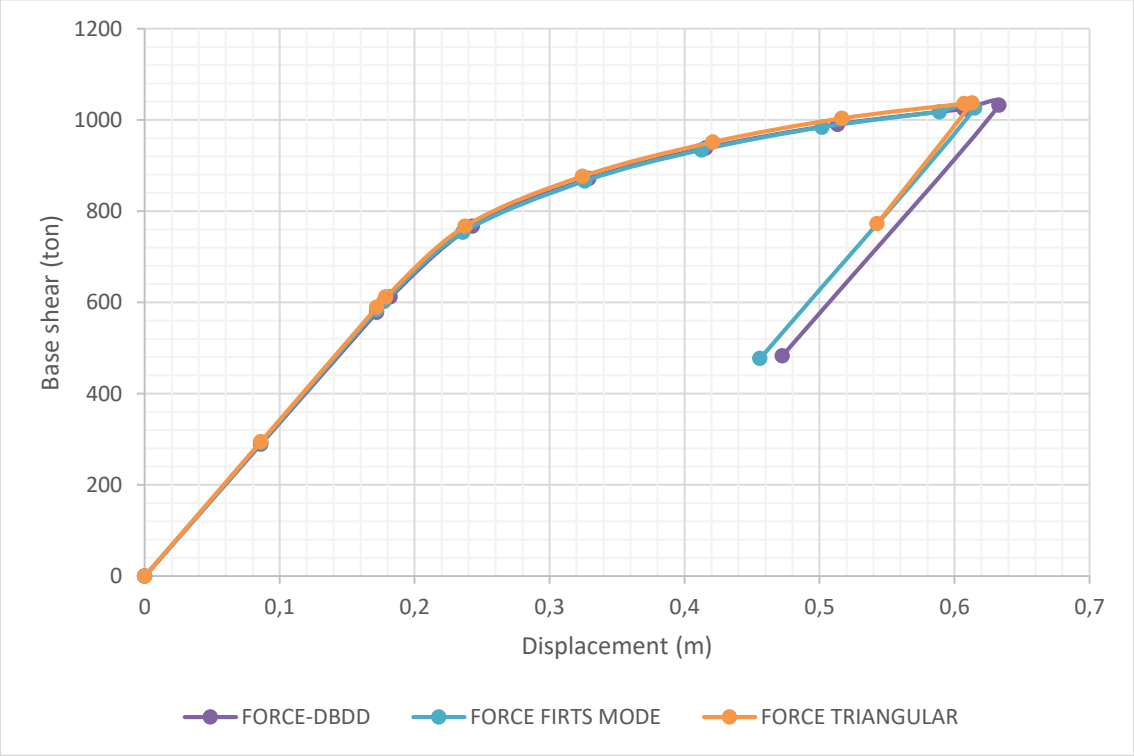

Figure 41. Capacity curve direction Y DBDD design

The table number 36 shows a summary of the performance points, ductility and damping ration of the DBDD and forces design for the three load patterns. The graphic of which were obtained these parameters can be find in the annex.

Table 37.

Result parameters from Pushover X direction.

	DBDD			FORCE		
	DBDD	**FIRTS MODE**	**TRIANGULAR**	**DBDD**	**FIRTS MODE**	**TRIANGULAR**
SHEAR (TON)	874,175	841,672	850,332	821,529	821,105	826,578
DISPLACEMENT (m)	0,221	0,219	0,218	0,227	0,226	0,225
Sa (g)	0,604	0,598	0,604	0,591	0,589	0,593
Sd (m)	0,17	0,171	0,169	0,174	0,175	0,174
Ductility ratio	1,302	1,325	1,311	1,275	1,299	1,285
Damping ratio	0,055	0,055	0,055	0,055	0,055	0,055
Global dritf	0,0102791	0,0101860	0,0101395	0,0105581	0,0105116	0,0104651
Performance	Live safe	Live safe	Live safe	Live safe	Live safe	Live safe

Table 38.

Result parameters from Pushover Y direction.

	DBDD			FORCE		
	DBDD	**FIRTS MODE**	**TRIANGULAR**	**DBDD**	**FIRTS MODE**	**TRIANGULAR**
SHEAR (TON)	807,399	798,275	810,724	764,015	758,35	769,167
DISPLACEMENT (m)	0,228	0,225	0,225	0,242	0,239	0,239
Sa (g)	0,583	0,574	0,583	0,559	0,553	0,561
Sd (m)	0,175	0,175	0,174	0,184	0,184	0,183
Ductility ratio	1,339	1,351	1,349	1,336	1,347	1,341
Damping ratio	0,055	0,055	0,055	0,055	0,055	0,055
Global dritf	0,0106047	0,0104651	0,0104651	0,0112558	0,0111163	0,0111163
Performance	Live safe	Live safe	Live safe	Live safe	Live safe	Live safe

5. Study case

The analysis of pushover will be performed in a real building in which the performance point, and capacity curve of the building with and without shear wall. Also, it will be use fluid viscous to reach the target drift instead of the shear walls. For the implementation of the dampers, a nonlinear dynamic analysis will be performed which will determine the maximum drift without shear wall.

Study description.

5.1. The building (Santana Lofts) has 20 floors for a residential used, and the three first floor are destined to parking zone; the approximate dimensions on plan are 80.00 m x 40.00 m. The building height is 73.60 m. The substructure is formed by a slab elastic foundation on piles.

Figure 42. Architectonical 3D view study case. Source: http://pronobis.com.ec/index.php/proyectos/nuevos-proyectos/santana-lofts-guayaquil

Figure 43. Architectonical plant residential use study case. Source: http://pronobis.com.ec/index.php/proyectos/nuevos-proyectos/santana-lofts-guayaquil.

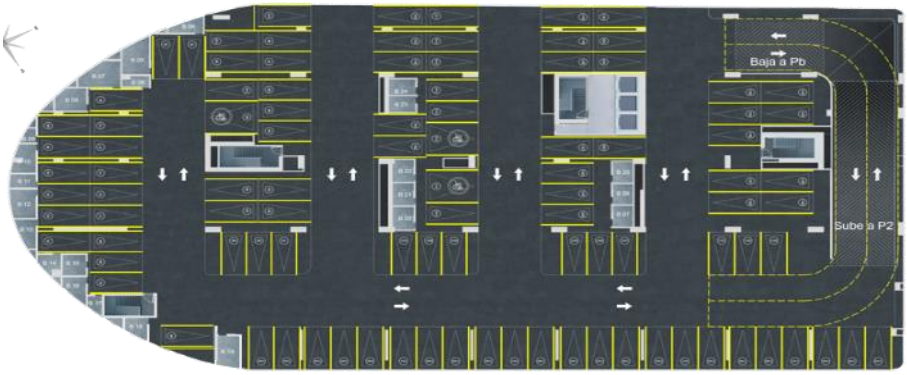

Figure 44. Architectonical plant parking use study case. Source: http://pronobis.com.ec/index.php/proyectos/nuevos-proyectos/santana-lofts-guayaquil.

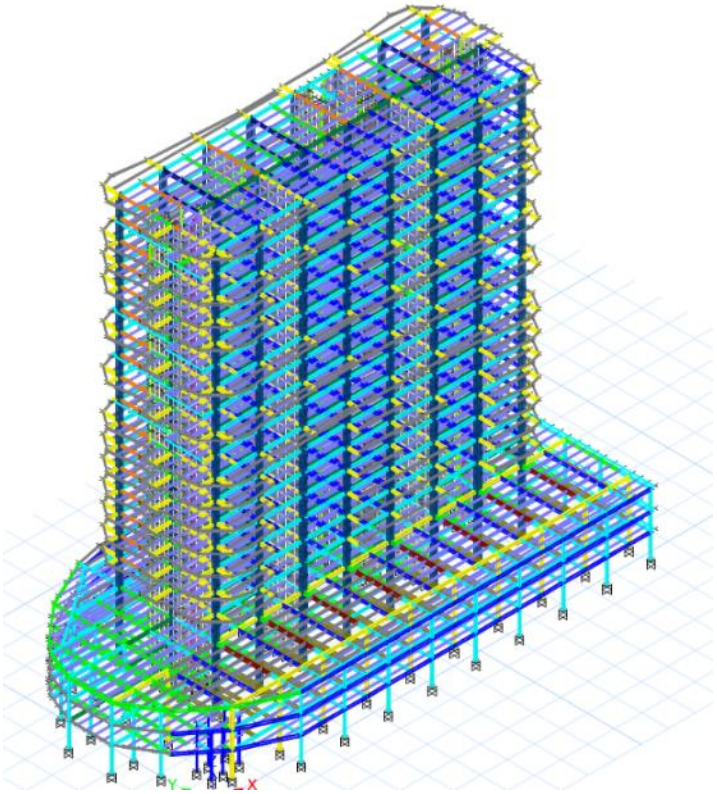

Figure 45.Structural 3D view study case.

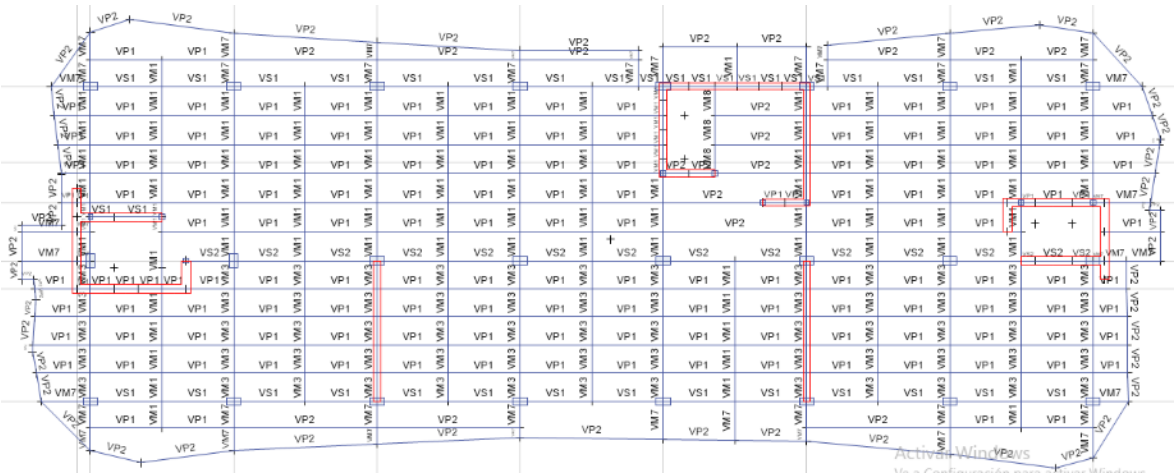

Figure 46. Structural plan view study case.

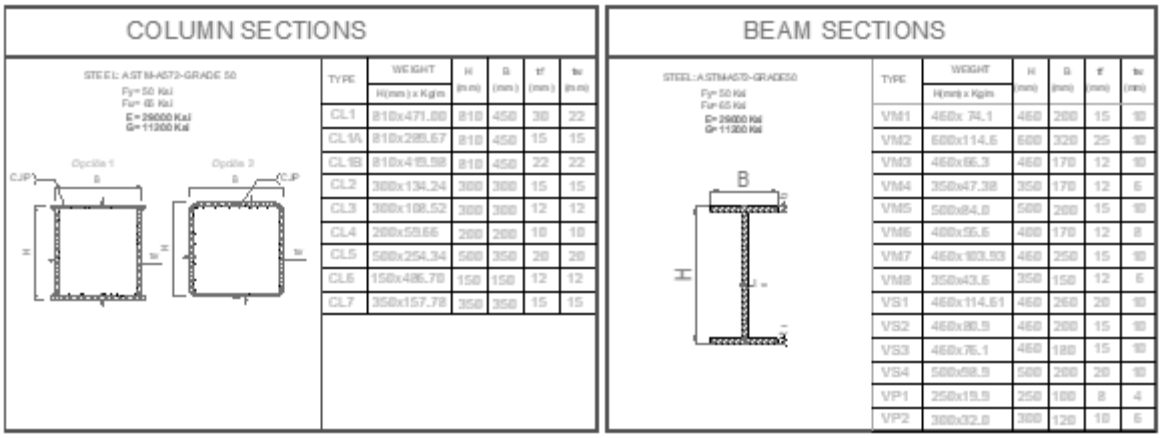

Figure 47. Structural element sections study case.

Materials:

- Columns are built up composite members classified as concrete filled HSS columns which are composed of A572 grade 50 steel and 420Mpa concrete.
- Principal beams (built up) ASTM A572 G50 steel type I.
- Secondary beams (built up) ASTM A572 G50 steel type I.
- Shear walls of thickness of 0.5m with 420Mpa concrete.
- Moment and shear plates, ASTM A572 G50 and A36.
- Bolts ASTM A193 B7 or SAE-1018
- Steel deck steel Grade 90.
- Shear connectors ASTM A-706 Grade 60, Fy = 420MPa.
- Reinforce steel. ASTM A-706 Grade 60, Fy = 420MPa
- Concrete at 28 days of shear walls and for filling tubes; Minimum 42 MPa.

Seismic parameter:

- **Location:** Guayaquil (Coast); Ecuador.
- **Seismic zone:** V. **Characterization of seismic hazard:** High
- **Factor according the site of implantation of the structure:** Z=0.4; η=1.8
- **Soil type:** E;

  r =1.5

  Fa=1.00

  Fd=1.60

  Fs=1.90
- **Structure importance:** Residential I=1
- **Plan and elevation factor:** $\Phi_P = 1$, $\Phi_E = 0.9$
- **Response reduction factor:** R=8
- **Period =** 2.24 seg

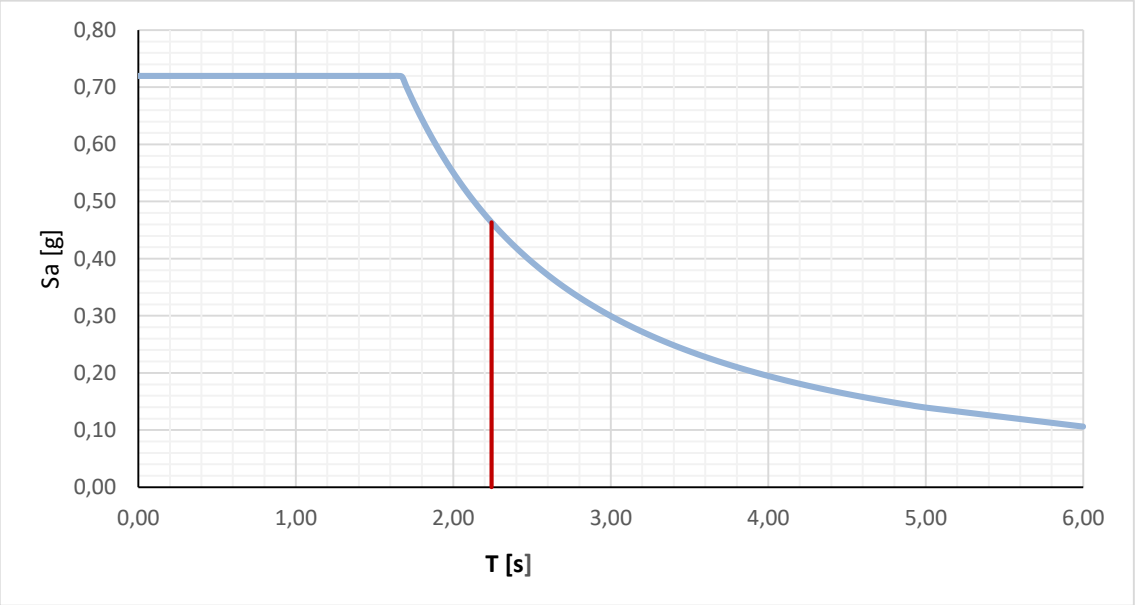

T_o	0,3	T_c	1,67	T_L	3,84

Figure 48. Design acceleration spectra.

5.1.1. Gravitational loads.

The gravitational loads were taking form the NEC 2015. The self-weight of the structural elements is not computed in the next tables because the program ETABS 2016 computed it automatically

Table 39.

Study case live load.

Residential live load	200,00	Kg/m^2
Inaccessible roof.	100,00	Kg/m^2
Light parking.	200,00	Kg/m^2
Gym, public areas.	480,00	Kg/m^2
Pool.	1000	Kg/m^2

Table 40.

Total dead load in story floors.

Steel deck 0.75mm + steel welded mesh R283 + 7cm concrete. Total height =120mm	210,00	Kg/m^2
Gypsum walls.	70,00	Kg/m^2
Floor finishes.	50,00	Kg/m^2
Gypsum roof and installations.	10,00	Kg/m^2
Total dead load=	**340,00**	**Kg/m^2**

Table 41.

Total dead load in communal areas.

Steel deck 0.75mm + steel welded mesh R283 + 7cm concrete. Total height =120mm	210,00	Kg/m2
Gypsum walls.	80,00	Kg/m^2
Floor finishes.	100,00	Kg/m^2
Gypsum roof and installations.	10,00	Kg/m^2
Total dead load=	**400,00**	**Kg/m^2**

Table 42.

Total dead load in parking.

Steel deck 0.75mm + steel welded mesh R283 + 7cm concrete. Total height =120mm	210,00	Kg/m^2
Gypsum walls.	60,00	Kg/m^2
Floor finishes.	40,00	Kg/m^2
Gypsum roof and installations.	10,00	Kg/m^2
Total dead load=	**320,00**	**Kg/m^2**

Pushover structure with shear walls

5.2. 5.2.1. Lateral Load Patterns

In FEMA 356 (Section 2.4.2.1), the use of NSPs must be supplemented with a linear dynamic analysis if any SRSS story shear from a response-spectrum analysis including modes representing 90% of the mass exceeds 130% of the corresponding story shear from a first mode response-spectrum analysis. In FEMA 273 (Section 3.3.3.2.C) a lateral load pattern proportional to the story inertia forces consistent with the story shear distribution calculated by combination of modal responses using (1) Response Spectrum Analysis of the building including a sufficient number of modes to capture 90% of the total mass, and (2) the appropriate ground motion spectrum.

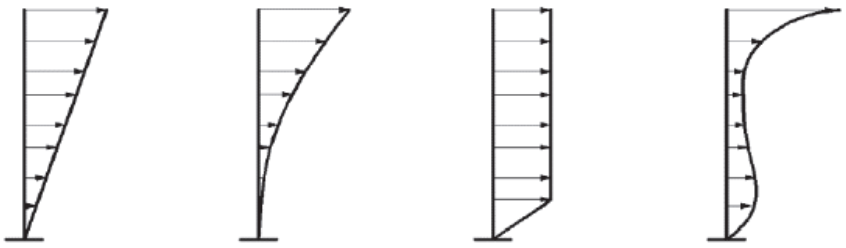

Figure 49. Triangular, first mode, Uniform and SRSS lateral load pattern for pushover.

For the study case “Santana Building” it was performed a modal response analysis taking the first eleven modes that reaches more than 90% of the mass participation in each direction.

Table 43.

Modal mass participation study case.

Case	Mode	Period sec	UX	UY	UZ	Sum UX	Sum UY	Sum UZ
Modal	1	2.066	0.2526	0.0027	0	0.2526	0.0027	0
Modal	2	1.997	0.0778	0.4505	0	0.3304	0.4532	0
Modal	3	1.525	0.2364	0.1095	0	0.5668	0.5627	0
Modal	4	0.442	0.0951	0.0004	0	0.6619	0.5631	0
Modal	5	0.405	0.019	0.1587	0	0.6809	0.7218	0
Modal	6	0.329	0.0941	0.0436	0	0.775	0.7654	0
Modal	7	0.203	0.0419	0.0035	0	0.8169	0.7689	0
Modal	8	0.174	0.0298	0.0781	0	0.8467	0.847	0
Modal	9	0.146	0.0409	0.036	0	0.8876	0.883	0
Modal	10	0.124	0.0187	0.0006	0	0.9063	0.8836	0
Modal	11	0.105	0.0194	0.0352	0	0.9258	0.9188	0

Table 44.

SRSS lateral load for the X and Y direction.

		X AXIS	Y AXIS
Story	**Nivel**	**Story shear (SRSS)**	**Story shear (SRSS)**
		Ton	**Ton**
20	73,6	142,003	141,784
19	70	122,492	119,430
18	66,4	127,251	121,641
17	62,8	100,126	93,680
16	59,2	88,709	81,928
15	55,6	69,833	64,229
14	52	76,379	70,753
13	48,4	58,309	54,409
12	44,8	64,540	60,807
11	41,2	49,406	46,701
10	37,6	54,682	51,900
9	34	46,746	44,460
8	30,4	42,860	41,015
7	26,8	38,314	37,045
6	23,2	34,011	33,279
5	19,6	29,397	29,066
4	16	25,917	25,723
3	11,4	57,405	59,606
2	7,8	27,393	27,566
1	4,6	14,180	14,313

5.2.2. Non-lineal behavior of the structural elements.

For the analysis non-lineal behavior analysis of the elements was used a model of concentrate plasticity by the location of plastic hinge in the principal elements.

5.2.3. Beam.

The beam plastic hinges were located a length from the face of the column (Sh=0) equal to zero according the AISC 358-16 section 8.7 due to the precalificated connection used that is welded unreinforced flange-welded web (WUF-W) moment connection.

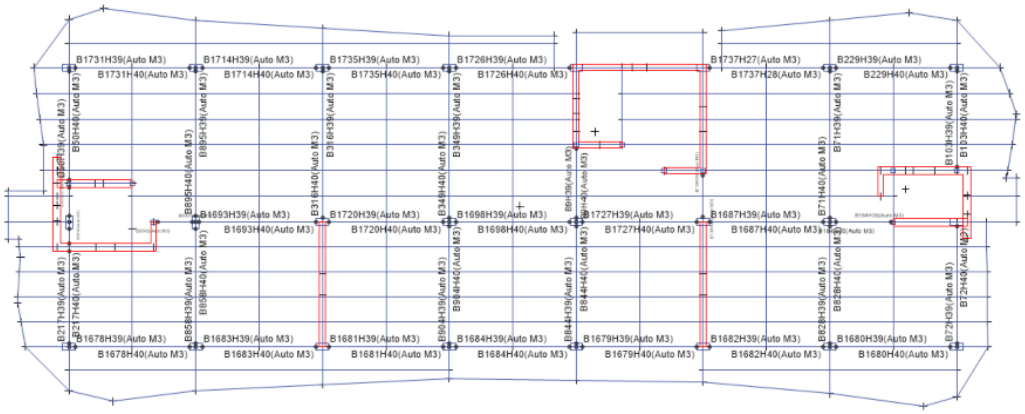

Figure 50.Beam plastic hinge location in plan.

5.2.4. Columns.

The column plastic hinges are located in 0.05 and 0.95 of the element length. The locations of the plastic hinges were based in studies and researches that display that plastic hinges are produced in a length equal to the shortest dimension of the column; this length is around of five percent of the length.

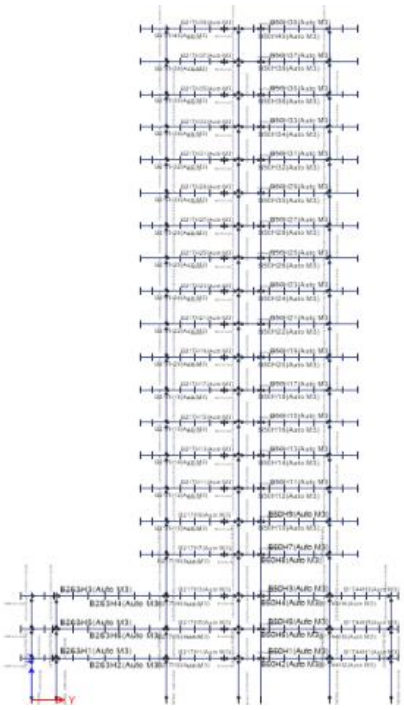

Figure 51,Columns plastic hinge location in plan.

5.2.5. Shear walls

To simulated the inelastic behavior, the shear walls were model as a layer model with the reinforcement steel and thickness of each one. The non-lineal behavior was performed in the longitudinal steel, in the concrete with forces applied in and out of plane. In the case of the forces applied out of the plane the wall transverse section was reduce in twenty-five percent taking account the cracking.

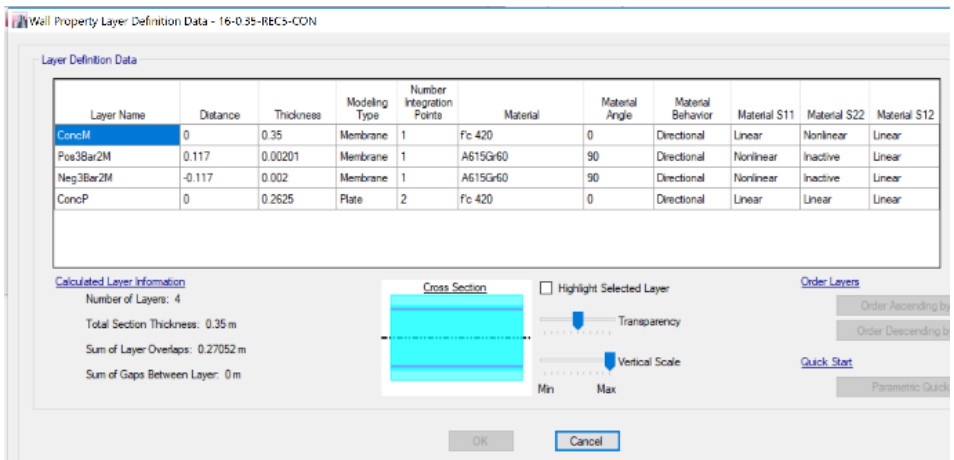

Figure 52. Layered model of shear walls.

5.2.6. Applied loads.

5.2.7. Non-lineal gravitational load.

According to the FEMA 356 section 3.2.8, the non-lineal gravitational load is equal to 1.1 that multiply the dead load, reactive live load in this case equal to 25% of the total live load and the snow load.

$$Q_{CGN} = 1.1\ (Q_D + Q_L + Q_S)$$

The non-lineal gravitational load is controlled by load in the direction U3 and saved only the final stated.

5.2.8. Push X.

The pushover load in the direction X is applied with the FX load patron defined obtained with the SRSS combination, and it started to be applied after the total application of the non-lineal gravitational load. The load is controlled by displacement, and the maximum displacement is in the range of 2 to 4 percent of the height of the building ensuring the live safety analysis until the collapse.

5.2.9. Push Y.

The pushover load in the direction Y is applied with the FY load patron defined obtained with the SRSS combination, and it started to be applied after the total application of the non-lineal gravitational load. The load is controlled by displacement, and the maximum displacement is in the range of 2 to 4 percent of the height of the building ensuring the live safety analysis until the collapse.

5.2.10. Result pushover X direction.

5.2.11. Capacity curve and plastic hinge develop.

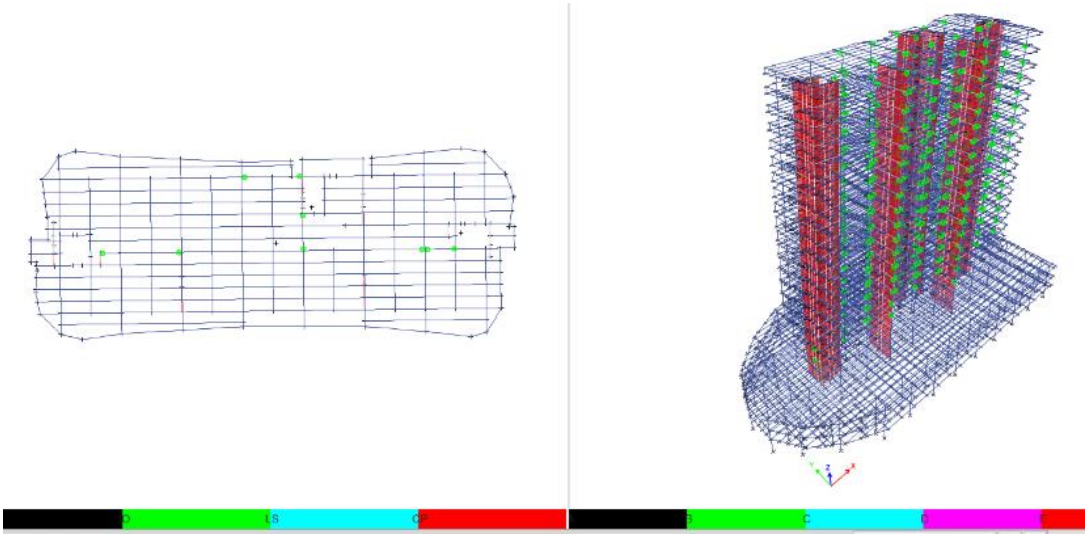

Figure 53.Plastic hinges develop in X direction.

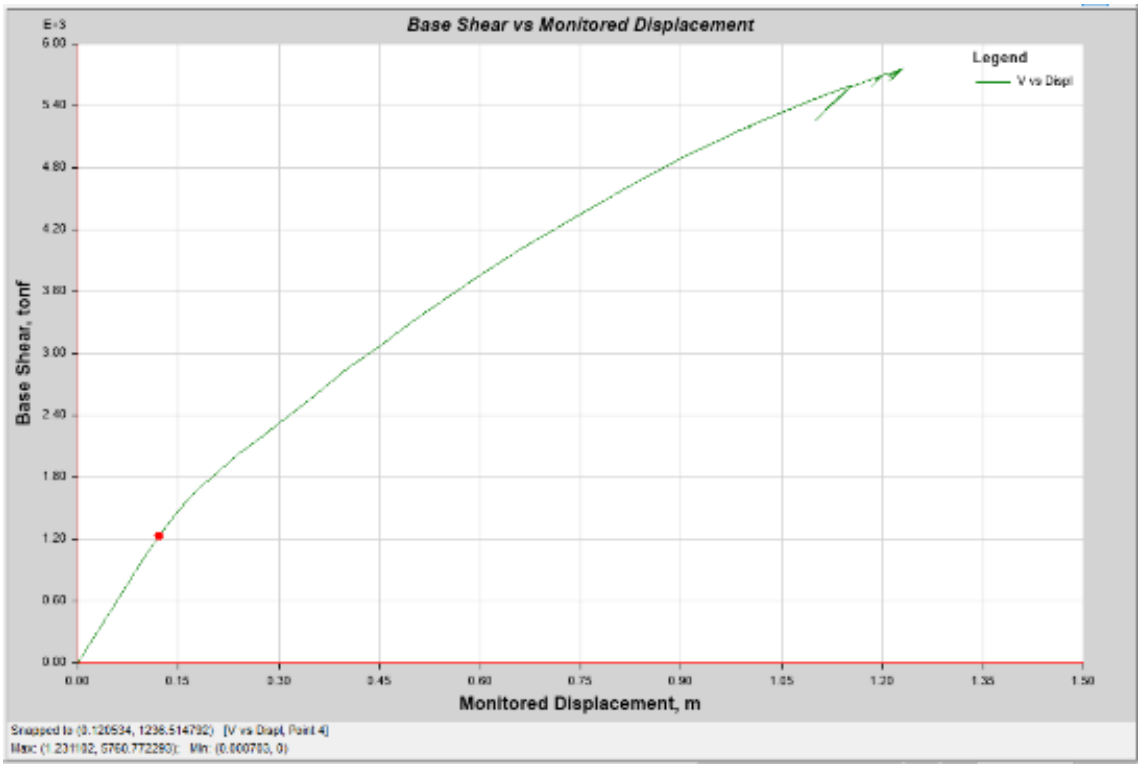

Figure 54. Capacity curve in X direction.

Table 45.

Capacity curve data and plastic hinge develop X direction.

Step	Monitored Displ	Base Force	A-B	B-C	C-D	D-E	>E	A-IO	IO-LS	LS-CP	>CP	Total
	m	tonf										
0	0.001	0.000	2848	0	0	0	0	2848	0	0	0	2848
1	0.031	312.645	2848	0	0	0	0	2848	0	0	0	2848
2	0.061	625.293	2848	0	0	0	0	2848	0	0	0	2848
3	0.091	936.726	2848	0	0	0	0	2848	0	0	0	2848
4	0.121	1236.515	2848	0	0	0	0	2848	0	0	0	2848
5	0.150	1487.121	2848	0	0	0	0	2848	0	0	0	2848
6	0.180	1687.464	2848	0	0	0	0	2848	0	0	0	2848
7	0.210	1858.493	2848	0	0	0	0	2848	0	0	0	2848
8	0.240	2026.779	2848	0	0	0	0	2848	0	0	0	2848
9	0.270	2176.343	2848	0	0	0	0	2848	0	0	0	2848
10	0.300	2327.142	2848	0	0	0	0	2848	0	0	0	2848
11	0.330	2478.405	2848	0	0	0	0	2848	0	0	0	2848
12	0.345	2551.240	2848	0	0	0	0	2848	0	0	0	2848
13	0.375	2709.717	2848	0	0	0	0	2848	0	0	0	2848
14	0.403	2859.700	2847	1	0	0	0	2848	0	0	0	2848
15	0.449	3065.779	2834	14	0	0	0	2848	0	0	0	2848
16	0.487	3254.467	2830	18	0	0	0	2848	0	0	0	2848
17	0.522	3412.857	2809	39	0	0	0	2848	0	0	0	2848
18	0.559	3578.287	2798	50	0	0	0	2848	0	0	0	2848
19	0.595	3736.922	2784	64	0	0	0	2835	13	0	0	2848
20	0.627	3872.909	2767	81	0	0	0	2833	15	0	0	2848
21	0.661	4012.572	2747	101	0	0	0	2829	19	0	0	2848
22	0.692	4134.824	2724	124	0	0	0	2818	30	0	0	2848
23	0.729	4274.566	2711	137	0	0	0	2817	31	0	0	2848
24	0.764	4406.294	2697	151	0	0	0	2812	36	0	0	2848
25	0.801	4541.343	2680	168	0	0	0	2797	51	0	0	2848
26	0.838	4675.797	2658	190	0	0	0	2793	55	0	0	2848
27	0.872	4792.061	2641	207	0	0	0	2785	63	0	0	2848
28	0.908	4916.542	2623	225	0	0	0	2771	77	0	0	2848
29	0.951	5052.629	2566	282	0	0	0	2760	88	0	0	2848
30	0.986	5157.037	2535	313	0	0	0	2739	109	0	0	2848
31	1.005	5212.347	2525	323	0	0	0	2736	112	0	0	2848
32	1.001	5186.669	2525	323	0	0	0	2736	112	0	0	2848
33	1.005	5212.689	2525	323	0	0	0	2736	112	0	0	2848
34	1.045	5323.922	2480	368	0	0	0	2731	117	0	0	2848
35	1.082	5423.198	2433	415	0	0	0	2713	134	0	1	2848
36	1.116	5508.824	2400	448	0	0	0	2700	147	0	1	2848
37	1.154	5601.091	2366	482	0	0	0	2693	153	0	2	2848
38	1.101	5253.557	2366	482	0	0	0	2693	153	0	2	2848
39	1.131	5461.361	2366	482	0	0	0	2693	153	0	2	2848
40	1.153	5582.965	2366	482	0	0	0	2693	153	0	2	2848
41	1.153	5585.163	2366	482	0	0	0	2692	154	0	2	2848

42	1.186	5663.680	2325	523	0	0	0	2688	158	0	2	2848
43	1.199	5693.339	2302	546	0	0	0	2685	161	0	2	2848
44	1.184	5593.311	2302	546	0	0	0	2685	161	0	2	2848
45	1.199	5690.406	2302	546	0	0	0	2685	161	0	2	2848
46	1.199	5691.829	2302	546	0	0	0	2684	162	0	2	2848
47	1.217	5732.432	2282	566	0	0	0	2684	162	0	2	2848
48	1.210	5681.965	2282	566	0	0	0	2684	162	0	2	2848
49	1.216	5720.434	2282	566	0	0	0	2684	162	0	2	2848
50	1.217	5727.379	2282	566	0	0	0	2684	162	0	2	2848
51	1.225	5744.388	2275	573	0	0	0	2681	165	0	2	2848
52	1.209	5644.780	2275	573	0	0	0	2681	165	0	2	2848
53	1.224	5742.597	2275	573	0	0	0	2681	165	0	2	2848
54	1.225	5742.991	2275	573	0	0	0	2681	165	0	2	2848
55	1.230	5756.102	2268	580	0	0	0	2681	165	0	2	2848
56	1.215	5657.166	2268	580	0	0	0	2681	165	0	2	2848
57	1.216	5659.865	2268	580	0	0	0	2681	165	0	2	2848
58	1.217	5669.296	2268	580	0	0	0	2681	165	0	2	2848
59	1.230	5757.110	2268	580	0	0	0	2681	165	0	2	2848
60	1.231	5760.772	2268	580	0	0	0	2681	165	0	2	2848

The analysis of the figure 43, figure 44 and table 46, it shown that there is a correct mechanism of strong column weak beam; the majority of the plastic hinges remains in the elastic zone (A-B zone in the structural behavior of the element and in the classification of the ASCE 7 in immediate occupancy) the after finishing the seismic event. On the hand, 580 plastics hinges enter to a plastic behavior (B-C zone) which 165 are between immediate occupancy and life safety. Finally, only two plastic hinges have a plastic behavior beyond the collapse prevention; these plastic hinges are located in a beam. From the bilinear model, the yield displacement and yield shear were obtained, and they are equal to 0.1966m ad 2002.03 ton.

5.2.12. Performance point.

The demand used was compute according to the NEC 2015. The performance point was found with the single demand with the ADRS capacity-demand diagram.

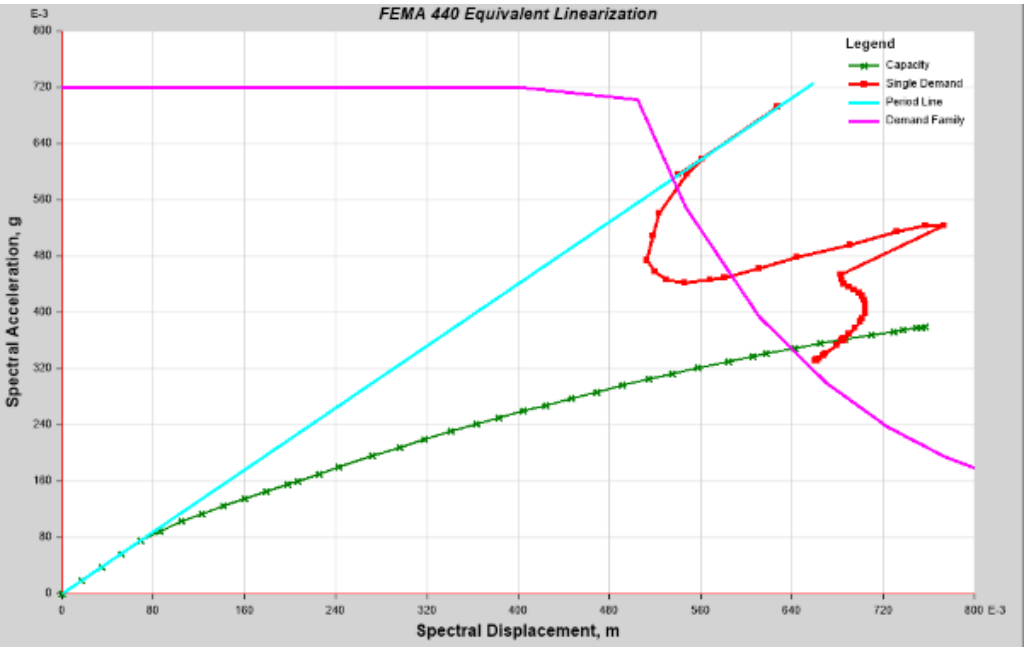

Figure 55. Performance point study case X direction.

Table 46.

Performance point study case X direction.

Shear	5503,898	**ton**
Displacement	1,113	**m**
Sa	0,3617	**g**
Sd	0,685	**m**

Establishing the performance point, the performance of the structure can be determined according to the study of VISION 2000.

The expected performance shares the values of Vision 2000 for the basic objectives, as shown below:

Performance Objective	Drift
Fully operational	$d/H_o < 0.002$
Operational	$d/H_o < 0.005$
Life Safe	$d/H_o < 0.015$

Figure 56. Structure performance by VISON 2000.

$$\Delta = \frac{\mathrm{d}}{\mathrm{H}_o} = \frac{1.11}{73.6} = 0.015081 \text{ Live safe}$$

5.2.13. Result pushover Y direction.

5.2.14. Capacity curve and plastic hinge develop.

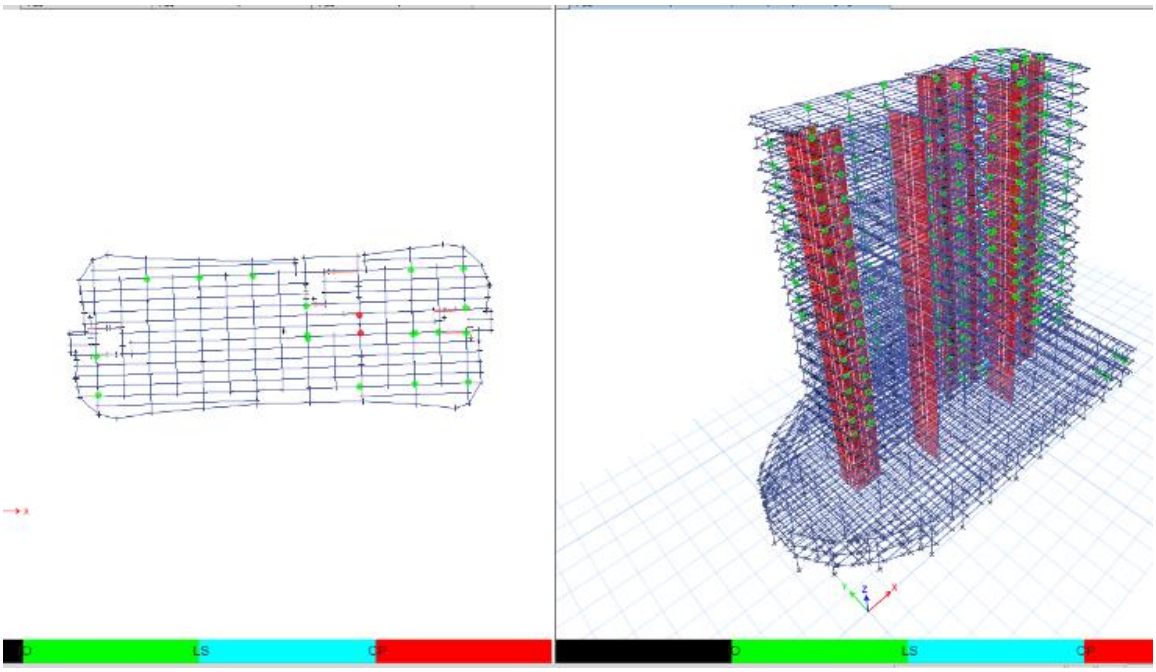

Figure 57. Plastic hinges develop in Y direction.

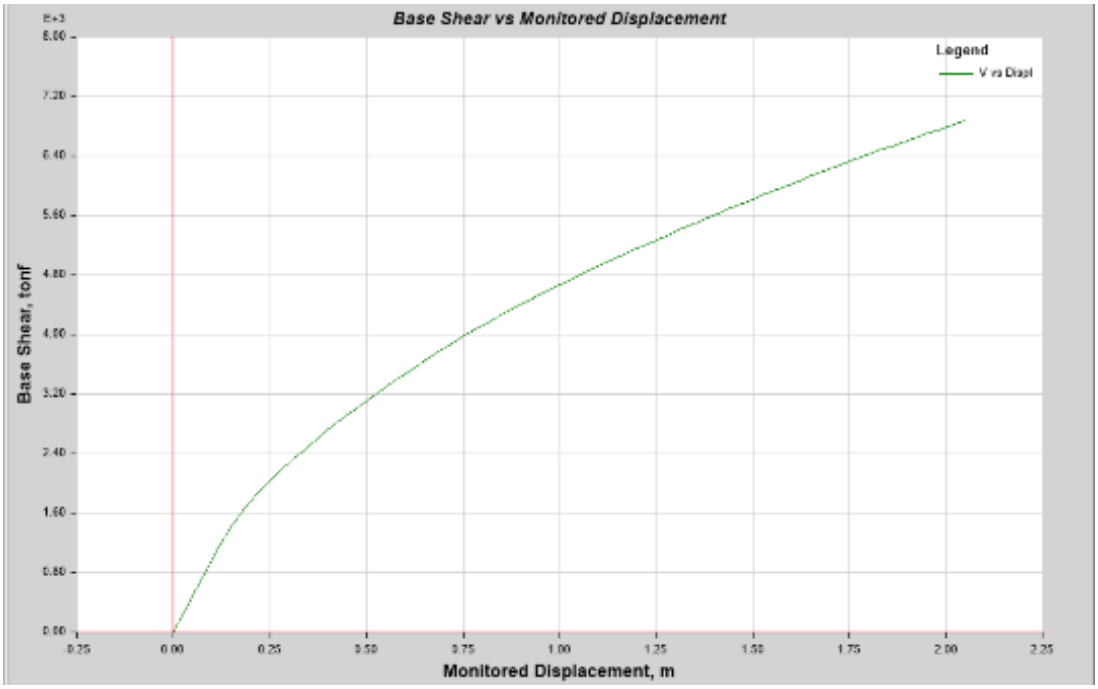

Figure 58. Capacity curve in Y direction.

Table 47.

Capacity curve data and plastic hinge develop Y direction.

Step	Monitored Displ	Base Force	A-B	B-C	C-D	D-E	>E	A-IO	IO-LS	LS-CP	>CP	Total
	M	Tonf										
0	-0.000051	0	2848	0	0	0	0	2848	0	0	0	2848
1	0.029949	295.2156	2848	0	0	0	0	2848	0	0	0	2848
2	0.059949	590.4298	2848	0	0	0	0	2848	0	0	0	2848
3	0.089942	884.8517	2848	0	0	0	0	2848	0	0	0	2848
4	0.119818	1169.103	2848	0	0	0	0	2848	0	0	0	2848
5	0.146043	1400.0084	2847	1	0	0	0	2848	0	0	0	2848
6	0.183186	1656.5447	2835	13	0	0	0	2848	0	0	0	2848
7	0.216627	1855.2999	2819	29	0	0	0	2847	1	0	0	2848
8	0.248446	2023.521	2815	33	0	0	0	2835	13	0	0	2848
9	0.279885	2181.2532	2813	35	0	0	0	2820	28	0	0	2848
10	0.30986	2322.8479	2813	35	0	0	0	2817	31	0	0	2848
11	0.34434	2479.5164	2802	46	0	0	0	2815	33	0	0	2848
12	0.381976	2642.7278	2797	51	0	0	0	2813	35	0	0	2848
13	0.426518	2831.2217	2795	53	0	0	0	2813	35	0	0	2848
14	0.462352	2972.4175	2783	65	0	0	0	2812	36	0	0	2848
15	0.512461	3159.5098	2779	69	0	0	0	2810	38	0	0	2848
16	0.548349	3290.4542	2777	71	0	0	0	2800	48	0	0	2848
17	0.583276	3416.8533	2770	78	0	0	0	2797	51	0	0	2848
18	0.618819	3541.8092	2758	90	0	0	0	2795	53	0	0	2848
19	0.651017	3651.505	2750	98	0	0	0	2789	59	0	0	2848
20	0.683867	3761.8689	2746	96	5	1	0	2783	64	1	0	2848
21	0.718893	3875.7731	2735	98	3	12	0	2781	55	12	0	2848
22	0.757678	3996.4426	2730	92	0	26	0	2778	44	26	0	2848
23	0.790574	4096.6823	2714	106	1	19	8	2777	44	21	6	2848
24	0.82425	4196.127	2688	131	0	10	19	2776	43	14	15	2848
25	0.861522	4301.6978	2666	152	0	5	25	2776	42	5	25	2848
26	0.900915	4409.5329	2640	177	0	4	27	2776	41	4	27	2848
27	0.931553	4491.4349	2626	190	0	3	29	2772	44	3	29	2848
28	0.970107	4592.9093	2600	216	0	2	30	2769	47	2	30	2848
29	1.001082	4672.7985	2590	225	0	3	30	2762	53	3	30	2848
30	1.03337	4754.3044	2581	233	1	2	31	2760	55	2	31	2848
31	1.078738	4866.6428	2565	249	0	2	32	2758	56	2	32	2848
32	1.115816	4956.0529	2551	263	0	2	32	2751	63	2	32	2848
33	1.153638	5047.1833	2535	279	0	1	33	2745	69	1	33	2848
34	1.188667	5130.6842	2517	297	0	0	34	2738	76	1	33	2848
35	1.223053	5211.1081	2508	306	0	0	34	2735	79	0	34	2848
36	1.26178	5300.4452	2494	319	0	1	34	2719	94	1	34	2848
37	1.291794	5368.6914	2482	331	0	1	34	2713	100	1	34	2848
38	1.321798	5436.1958	2473	339	0	2	34	2705	107	2	34	2848
39	1.351804	5503.0753	2461	351	0	2	34	2697	115	2	34	2848
40	1.381806	5568.8881	2453	359	0	2	34	2688	124	2	34	2848
41	1.411814	5633.6751	2445	367	0	2	34	2669	143	2	34	2848

42	1.441815	5697.9182	2431	381	0	2	34	2657	155	2	34	2848
43	1.471824	5761.8093	2413	399	0	1	35	2647	165	1	35	2848
44	1.501829	5824.7588	2395	417	0	1	35	2635	177	1	35	2848
45	1.531827	5887.2853	2377	435	0	0	36	2619	193	0	36	2848
46	1.56182	5949.3569	2364	448	0	0	36	2602	210	0	36	2848
47	1.591827	6010.6074	2354	458	0	0	36	2591	221	0	36	2848
48	1.621843	6071.1791	2348	464	0	0	36	2580	232	0	36	2848
49	1.651851	6131.5409	2342	470	0	0	36	2572	240	0	36	2848
50	1.681867	6191.2428	2329	483	0	0	36	2568	244	0	36	2848
51	1.711869	6250.2015	2314	497	0	1	36	2565	246	1	36	2848
52	1.741869	6308.668	2308	503	0	1	36	2562	249	1	36	2848
53	1.771873	6366.5891	2298	512	1	1	36	2555	256	1	36	2848
54	1.801875	6423.9202	2279	531	0	2	36	2546	264	2	36	2848
55	1.83188	6480.2392	2264	546	0	2	36	2536	274	2	36	2848
56	1.86188	6536.3172	2257	553	0	2	36	2531	279	2	36	2848
57	1.891888	6591.6306	2248	562	0	2	36	2523	287	2	36	2848
58	1.921895	6646.8032	2242	568	0	2	36	2516	294	2	36	2848
59	1.951893	6701.4266	2237	573	0	2	36	2509	301	2	36	2848
60	1.981902	6755.7692	2228	582	0	2	36	2496	314	2	36	2848
61	2.011904	6809.8828	2220	590	0	1	37	2486	324	1	37	2848
62	2.041901	6864.334	2214	590	6	1	37	2474	336	1	37	2848
63	2.047273	6874.2681	2211	592	7	1	37	2473	336	2	37	2848

The analysis of the figure 47, figure 48 and table 45, it shown that there is a correct mechanism of strong column weak beam; the majority of the plastic hinges remains in the elastic zone (A-B zone in the structural behavior of the element and in the classification of the ASCE 7 in immediate occupancy) the after finishing the seismic event. On the hand, 592 plastics hinges enter to a plastic behavior (B-C zone) which 336 are between immediate occupancy and life safety. Finally, 37 plastic hinges have a plastic behavior beyond Collapse Prevention; these plastic hinges are located in a beam.

From the bilinear model, the yield displacement and yield shear were obtained, and they are equal to 0.2211m ad 2140.513 ton.

5.2.15. Performance point.

The demand used was compute according to the NEC 2015. The performance point was found with the single demand with the ADRS capacity-demand diagram.

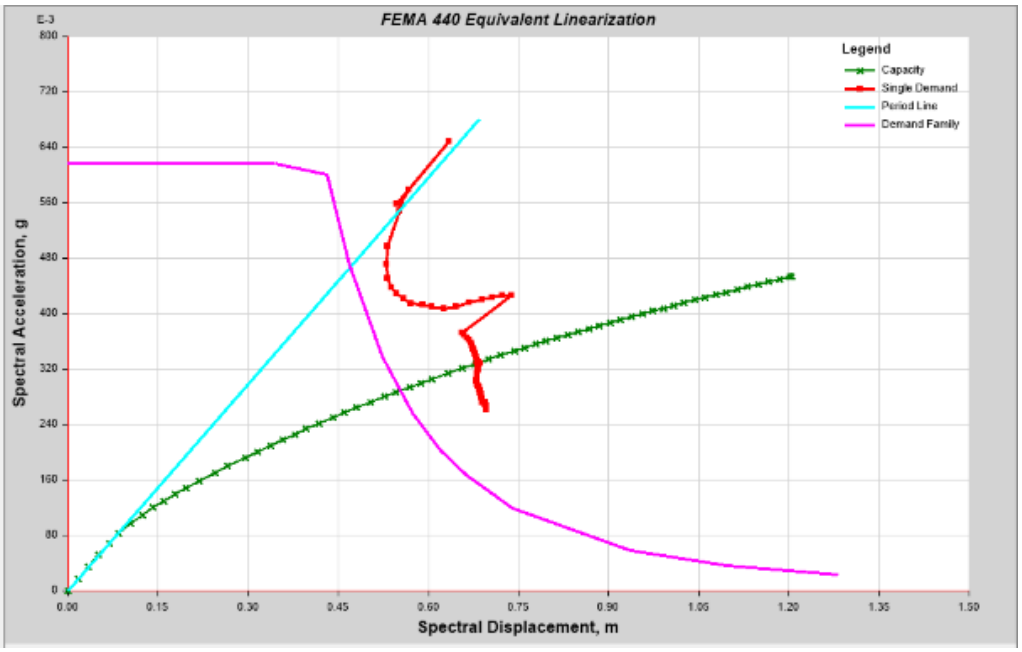

Figure 59. Performance point study case X direction.

Table 48.

Performance point study case X direction.

Shear	5064.589	**ton**
Displacement	1,161	**m**
Sa	0,329	**g**
Sd	0,683	**m**

Establishing the performance point, the performance of the structure can be determined according to the study of VISION 2000.

The expected performance shares the values of Vision 2000 for the basic objectives, as shown below:

Performance Objective	Drift
Fully operational	$d/H_o < 0.002$
Operational	$d/H_o < 0.005$
Life Safe	$d/H_o < 0.015$

Figure 60. Structure performance by VISON 2000.

$$\Delta = \frac{\mathrm{d}}{\mathrm{H}_o} = \frac{1.16}{73.6} = 0.0157 \text{ Live safe}$$

Pushover structure without shear walls

5.3.1. Result pushover X direction.

5.3. 5.3.2. Capacity curve and plastic hinge develop.

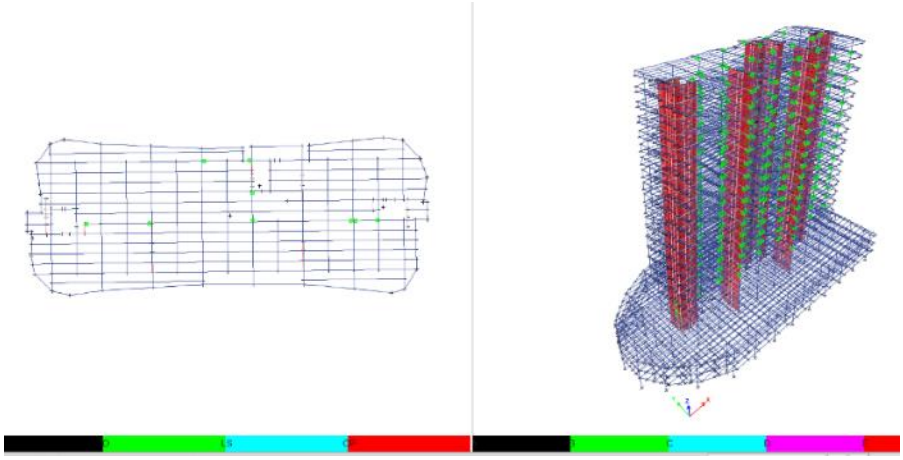

Figure 61. Plastic hinges develop in X direction.

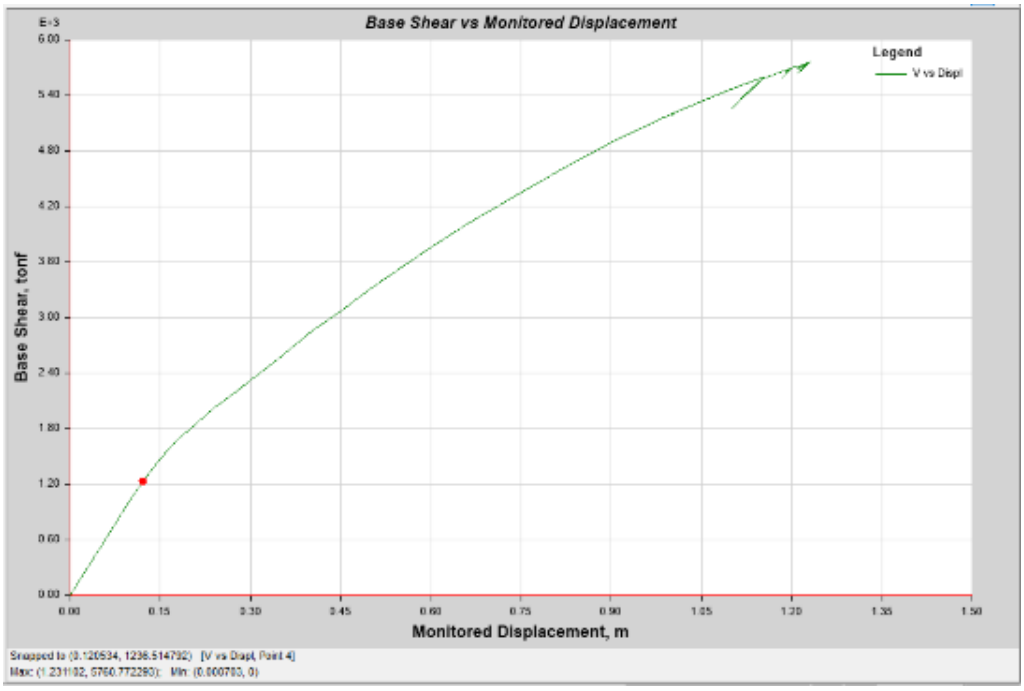

Figure 62. Capacity curve in X direction.

Table 49.

Capacity curve data and plastic hinge develop X direction.

Step	Monitored Displ	Base Force	A-B	B-C	C-D	D-E	>E	A-IO	IO-LS	LS-CP	>CP	Total
	m	tonf										
0	0.001	0.000	2848	0	0	0	0	2848	0	0	0	2848
1	0.031	312.645	2848	0	0	0	0	2848	0	0	0	2848
2	0.061	625.293	2848	0	0	0	0	2848	0	0	0	2848
3	0.091	936.726	2848	0	0	0	0	2848	0	0	0	2848
4	0.121	1236.515	2848	0	0	0	0	2848	0	0	0	2848
5	0.150	1487.121	2848	0	0	0	0	2848	0	0	0	2848
6	0.180	1687.464	2848	0	0	0	0	2848	0	0	0	2848
7	0.210	1858.493	2848	0	0	0	0	2848	0	0	0	2848
8	0.240	2026.779	2848	0	0	0	0	2848	0	0	0	2848
9	0.270	2176.343	2848	0	0	0	0	2848	0	0	0	2848
10	0.300	2327.142	2848	0	0	0	0	2848	0	0	0	2848
11	0.330	2478.405	2848	0	0	0	0	2848	0	0	0	2848
12	0.345	2551.240	2848	0	0	0	0	2848	0	0	0	2848
13	0.375	2709.717	2848	0	0	0	0	2848	0	0	0	2848
14	0.403	2859.700	2847	1	0	0	0	2848	0	0	0	2848
15	0.449	3065.779	2834	14	0	0	0	2848	0	0	0	2848
16	0.487	3254.467	2830	18	0	0	0	2848	0	0	0	2848
17	0.522	3412.857	2809	39	0	0	0	2848	0	0	0	2848
18	0.559	3578.287	2798	50	0	0	0	2848	0	0	0	2848
19	0.595	3736.922	2784	64	0	0	0	2835	13	0	0	2848
20	0.627	3872.909	2767	81	0	0	0	2833	15	0	0	2848
21	0.661	4012.572	2747	101	0	0	0	2829	19	0	0	2848
22	0.692	4134.824	2724	124	0	0	0	2818	30	0	0	2848
23	0.729	4274.566	2711	137	0	0	0	2817	31	0	0	2848
24	0.764	4406.294	2697	151	0	0	0	2812	36	0	0	2848
25	0.801	4541.343	2680	168	0	0	0	2797	51	0	0	2848
26	0.838	4675.797	2658	190	0	0	0	2793	55	0	0	2848
27	0.872	4792.061	2641	207	0	0	0	2785	63	0	0	2848
28	0.908	4916.542	2623	225	0	0	0	2771	77	0	0	2848
29	0.951	5052.629	2566	282	0	0	0	2760	88	0	0	2848
30	0.986	5157.037	2535	313	0	0	0	2739	109	0	0	2848
31	1.005	5212.347	2525	323	0	0	0	2736	112	0	0	2848
32	1.001	5186.669	2525	323	0	0	0	2736	112	0	0	2848
33	1.005	5212.689	2525	323	0	0	0	2736	112	0	0	2848
34	1.045	5323.922	2480	368	0	0	0	2731	117	0	0	2848
35	1.082	5423.198	2433	415	0	0	0	2713	134	0	1	2848
36	1.116	5508.824	2400	448	0	0	0	2700	147	0	1	2848
37	1.154	5601.091	2366	482	0	0	0	2693	153	0	2	2848
38	1.101	5253.557	2366	482	0	0	0	2693	153	0	2	2848
39	1.131	5461.361	2366	482	0	0	0	2693	153	0	2	2848
40	1.153	5582.965	2366	482	0	0	0	2693	153	0	2	2848
41	1.153	5585.163	2366	482	0	0	0	2692	154	0	2	2848

42	1.186	5663.680	2325	523	0	0	0	2688	158	0	2	2848
43	1.199	5693.339	2302	546	0	0	0	2685	161	0	2	2848
44	1.184	5593.311	2302	546	0	0	0	2685	161	0	2	2848
45	1.199	5690.406	2302	546	0	0	0	2685	161	0	2	2848
46	1.199	5691.829	2302	546	0	0	0	2684	162	0	2	2848
47	1.217	5732.432	2282	566	0	0	0	2684	162	0	2	2848
48	1.210	5681.965	2282	566	0	0	0	2684	162	0	2	2848
49	1.216	5720.434	2282	566	0	0	0	2684	162	0	2	2848
50	1.217	5727.379	2282	566	0	0	0	2684	162	0	2	2848
51	1.225	5744.388	2275	573	0	0	0	2681	165	0	2	2848
52	1.209	5644.780	2275	573	0	0	0	2681	165	0	2	2848
53	1.224	5742.597	2275	573	0	0	0	2681	165	0	2	2848
54	1.225	5742.991	2275	573	0	0	0	2681	165	0	2	2848
55	1.230	5756.102	2268	580	0	0	0	2681	165	0	2	2848
56	1.215	5657.166	2268	580	0	0	0	2681	165	0	2	2848
57	1.216	5659.865	2268	580	0	0	0	2681	165	0	2	2848
58	1.217	5669.296	2268	580	0	0	0	2681	165	0	2	2848
59	1.230	5757.110	2268	580	0	0	0	2681	165	0	2	2848
60	1.231	5760.772	2268	580	0	0	0	2681	165	0	2	2848

The analysis of the figure 43, figure 44, and table 50 it shown that there is a correct mechanism of strong column weak beam; the majority of the plastic hinges remains in the elastic zone (A-B zone in the structural behavior of the element and in the classification of the ASCE 7 in immediate occupancy) the after finishing the seismic event. On the hand, 580 plastics hinges enter to a plastic behavior (B-C zone) which 165 are between immediate occupancy and life safety. Finally, only two plastic hinges have a plastic behavior beyond the collapse prevention; these plastic hinges are located in a beam. From the bilinear model, the yield displacement and yield shear were obtained, and they are equal to 0.1966m ad 2002.03 ton.

5.3.3. Performance point.

The demand used was compute according to the NEC 2015. The performance point was found with the single demand with the ADRS capacity-demand diagram.

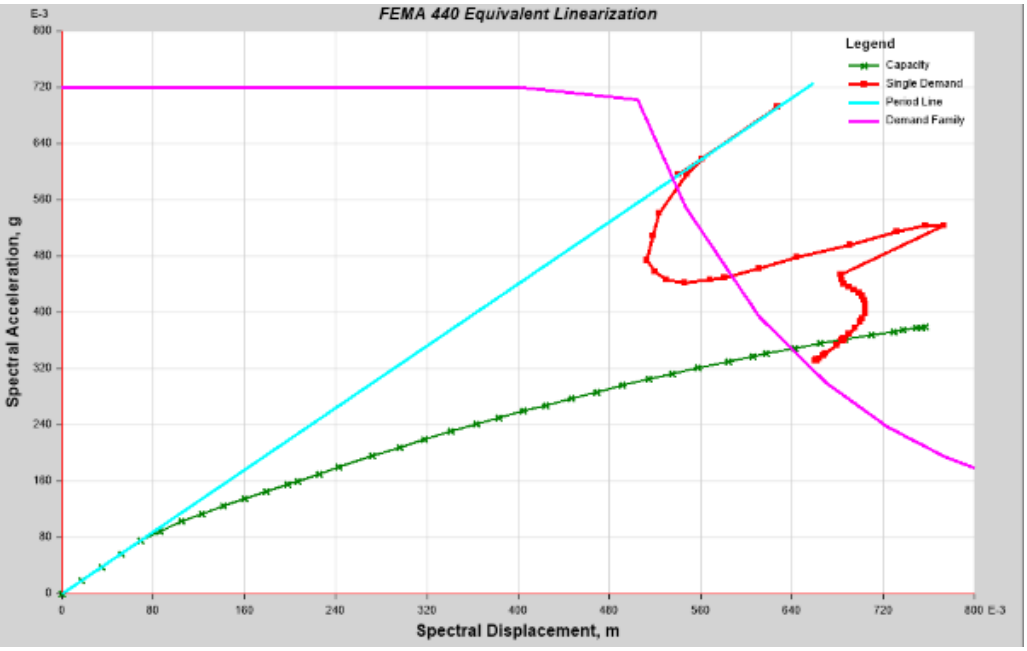

Figure 63. Performance point study case X direction.

Table 50.

Performance point study case X direction.

Shear	5503,898	**ton**
Displacement	1,113	**m**
Sa	0,3617	**g**
Sd	0,685	**m**

Establishing the performance point, the performance of the structure can be determined according to the study of VISION 2000.

The expected performance shares the values of Vision 2000 for the basic objectives, as shown below:

Performance Objective	Drift
Fully operational	$d/H_o < 0.002$
Operational	$d/H_o < 0.005$
Life Safe	$d/H_o < 0.015$

Figure 64. Structure performance by VISON 2000.

$$\Delta = \frac{\mathrm{d}}{\mathrm{H}_o} = \frac{1.11}{73.6} = 0.015081 \text{ Live safe}$$

5.3.4. Result pushover Y direction.

5.3.5. Capacity curve and plastic hinge develop.

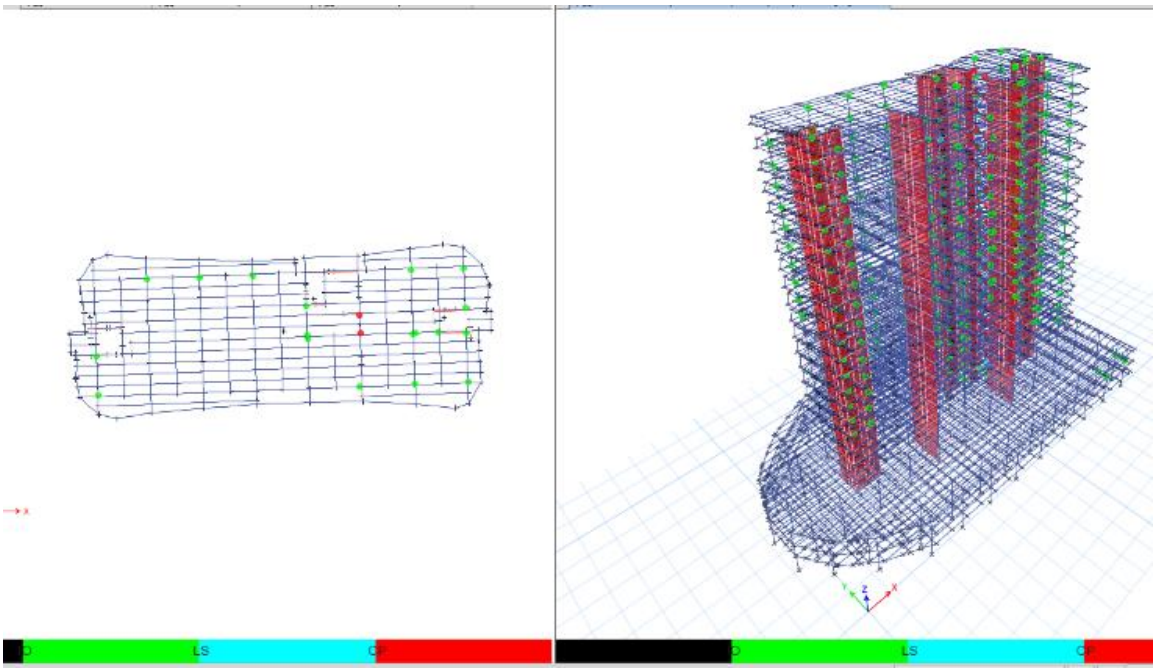

Figure 65. Plastic hinges develop in Y direction.

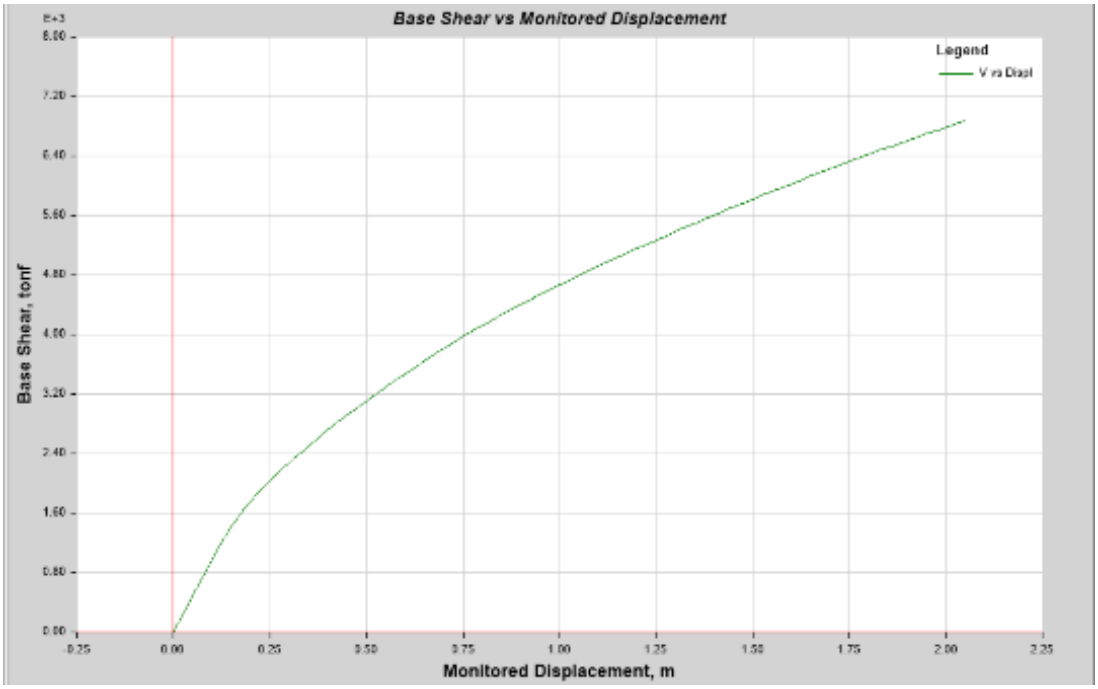

Figure 66. Capacity curve in Y direction.

Table 51.

. Capacity curve data and plastic hinge develop Y direction.

Step	Monitored Displ	Base Force	A-B	B-C	C-D	D-E	>E	A-IO	IO-LS	LS-CP	>CP	Total
	M	Tonf										
0	-0.000051	0	2848	0	0	0	0	2848	0	0	0	2848
1	0.029949	295.2156	2848	0	0	0	0	2848	0	0	0	2848
2	0.059949	590.4298	2848	0	0	0	0	2848	0	0	0	2848
3	0.089942	884.8517	2848	0	0	0	0	2848	0	0	0	2848
4	0.119818	1169.103	2848	0	0	0	0	2848	0	0	0	2848
5	0.146043	1400.0084	2847	1	0	0	0	2848	0	0	0	2848
6	0.183186	1656.5447	2835	13	0	0	0	2848	0	0	0	2848
7	0.216627	1855.2999	2819	29	0	0	0	2847	1	0	0	2848
8	0.248446	2023.521	2815	33	0	0	0	2835	13	0	0	2848
9	0.279885	2181.2532	2813	35	0	0	0	2820	28	0	0	2848
10	0.30986	2322.8479	2813	35	0	0	0	2817	31	0	0	2848
11	0.34434	2479.5164	2802	46	0	0	0	2815	33	0	0	2848
12	0.381976	2642.7278	2797	51	0	0	0	2813	35	0	0	2848
13	0.426518	2831.2217	2795	53	0	0	0	2813	35	0	0	2848
14	0.462352	2972.4175	2783	65	0	0	0	2812	36	0	0	2848
15	0.512461	3159.5098	2779	69	0	0	0	2810	38	0	0	2848
16	0.548349	3290.4542	2777	71	0	0	0	2800	48	0	0	2848
17	0.583276	3416.8533	2770	78	0	0	0	2797	51	0	0	2848
18	0.618819	3541.8092	2758	90	0	0	0	2795	53	0	0	2848
19	0.651017	3651.505	2750	98	0	0	0	2789	59	0	0	2848
20	0.683867	3761.8689	2746	96	5	1	0	2783	64	1	0	2848
21	0.718893	3875.7731	2735	98	3	12	0	2781	55	12	0	2848
22	0.757678	3996.4426	2730	92	0	26	0	2778	44	26	0	2848
23	0.790574	4096.6823	2714	106	1	19	8	2777	44	21	6	2848
24	0.82425	4196.127	2688	131	0	10	19	2776	43	14	15	2848
25	0.861522	4301.6978	2666	152	0	5	25	2776	42	5	25	2848
26	0.900915	4409.5329	2640	177	0	4	27	2776	41	4	27	2848
27	0.931553	4491.4349	2626	190	0	3	29	2772	44	3	29	2848
28	0.970107	4592.9093	2600	216	0	2	30	2769	47	2	30	2848
29	1.001082	4672.7985	2590	225	0	3	30	2762	53	3	30	2848
30	1.03337	4754.3044	2581	233	1	2	31	2760	55	2	31	2848
31	1.078738	4866.6428	2565	249	0	2	32	2758	56	2	32	2848
32	1.115816	4956.0529	2551	263	0	2	32	2751	63	2	32	2848
33	1.153638	5047.1833	2535	279	0	1	33	2745	69	1	33	2848
34	1.188667	5130.6842	2517	297	0	0	34	2738	76	1	33	2848
35	1.223053	5211.1081	2508	306	0	0	34	2735	79	0	34	2848
36	1.26178	5300.4452	2494	319	0	1	34	2719	94	1	34	2848
37	1.291794	5368.6914	2482	331	0	1	34	2713	100	1	34	2848
38	1.321798	5436.1958	2473	339	0	2	34	2705	107	2	34	2848
39	1.351804	5503.0753	2461	351	0	2	34	2697	115	2	34	2848
40	1.381806	5568.8881	2453	359	0	2	34	2688	124	2	34	2848
41	1.411814	5633.6751	2445	367	0	2	34	2669	143	2	34	2848

42	1.441815	5697.9182	2431	381	0	2	34	2657	155	2	34	2848
43	1.471824	5761.8093	2413	399	0	1	35	2647	165	1	35	2848
44	1.501829	5824.7588	2395	417	0	1	35	2635	177	1	35	2848
45	1.531827	5887.2853	2377	435	0	0	36	2619	193	0	36	2848
46	1.56182	5949.3569	2364	448	0	0	36	2602	210	0	36	2848
47	1.591827	6010.6074	2354	458	0	0	36	2591	221	0	36	2848
48	1.621843	6071.1791	2348	464	0	0	36	2580	232	0	36	2848
49	1.651851	6131.5409	2342	470	0	0	36	2572	240	0	36	2848
50	1.681867	6191.2428	2329	483	0	0	36	2568	244	0	36	2848
51	1.711869	6250.2015	2314	497	0	1	36	2565	246	1	36	2848
52	1.741869	6308.668	2308	503	0	1	36	2562	249	1	36	2848
53	1.771873	6366.5891	2298	512	1	1	36	2555	256	1	36	2848
54	1.801875	6423.9202	2279	531	0	2	36	2546	264	2	36	2848
55	1.83188	6480.2392	2264	546	0	2	36	2536	274	2	36	2848
56	1.86188	6536.3172	2257	553	0	2	36	2531	279	2	36	2848
57	1.891888	6591.6306	2248	562	0	2	36	2523	287	2	36	2848
58	1.921895	6646.8032	2242	568	0	2	36	2516	294	2	36	2848
59	1.951893	6701.4266	2237	573	0	2	36	2509	301	2	36	2848
60	1.981902	6755.7692	2228	582	0	2	36	2496	314	2	36	2848
61	2.011904	6809.8828	2220	590	0	1	37	2486	324	1	37	2848
62	2.041901	6864.334	2214	590	6	1	37	2474	336	1	37	2848
63	2.047273	6874.2681	2211	592	7	1	37	2473	336	2	37	2848

The analysis of the figure 47, figure 48 and table 45, it shown that there is a correct mechanism of strong column weak beam; the majority of the plastic hinges remains in the elastic zone (A-B zone in the structural behavior of the element and in the classification of the ASCE 7 in immediate occupancy) the after finishing the seismic event. On the hand, 592 plastics hinges enter to a plastic behavior (B-C zone) which 336 are between immediate occupancy and life safety. Finally, 37 plastic hinges have a plastic behavior beyond Collapse Prevention; these plastic hinges are located in a beam.

From the bilinear model, the yield displacement and yield shear were obtained, and they are equal to 0.2211m ad 2140.513 ton.

5.3.6. Performance point.

The demand used was compute according to the NEC 2015. The performance point was found with the single demand with the ADRS capacity-demand diagram.

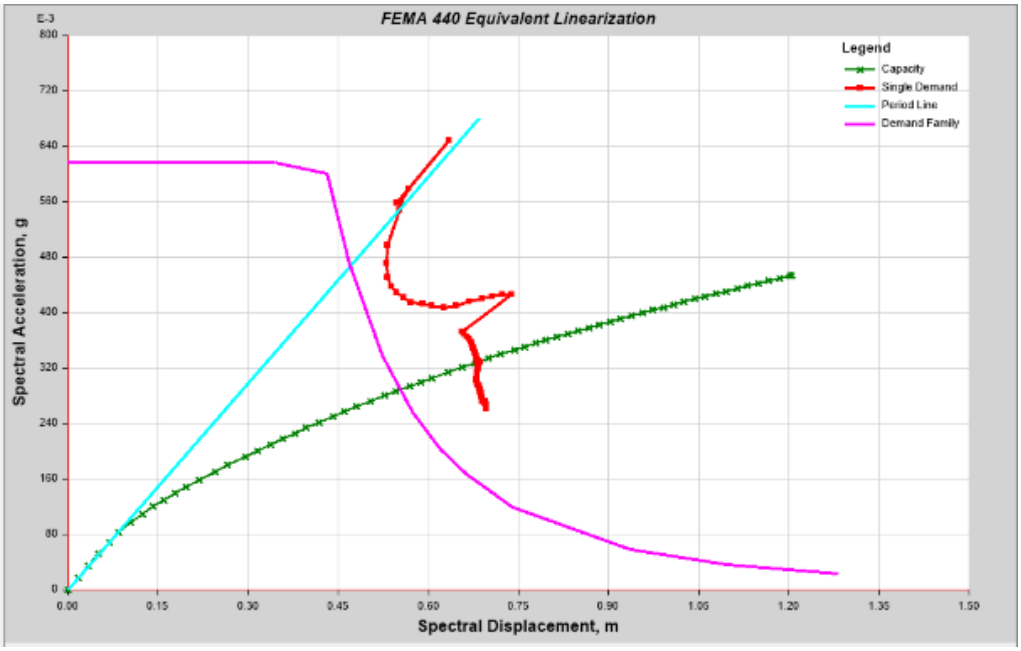

Figure 67. Performance point study case X direction.

Table 52.

Performance point study case X direction.

Shear	5064.589	**ton**
Displacement	1,161	**m**
Sa	0,329	**g**
Sd	0,683	**m**

Establishing the performance point, the performance of the structure can be determined according to the study of VISION 2000.

The expected performance shares the values of Vision 2000 for the basic objectives, as shown below:

Performance Objective	Drift
Fully operational	$d/H_o < 0.002$
Operational	$d/H_o < 0.005$
Life Safe	$d/H_o < 0.015$

Figure 68. Structure performance by VISON 2000.

$$\Delta = \frac{\mathrm{d}}{\mathrm{H}_o} = \frac{1.16}{73.6} = 0.0157 \text{ Live safe}$$

5.4. FVDs implementation

The FVDs will be implemented in the structure without shear walls in which the maximum drift exceeds the target drift established in the Ecuadorian code NEC. In this structure the target drift in lower than the maximum drift of the code. The target drift for this structure is 0.015.

5.4.1. Non-lineal time history analysis without dampers.

According with the geological, geotechnical, and the soil type were generating three synthetic accelerogram. Three accelerogram is the minimum of the registers establish in the North American and Equadorian code.

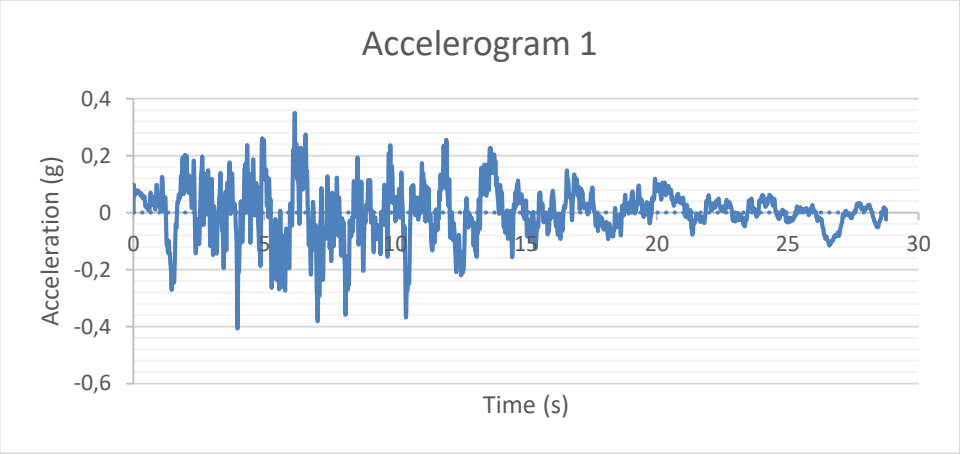

Figure 69. Artificial accelerogram 1 of the study case.

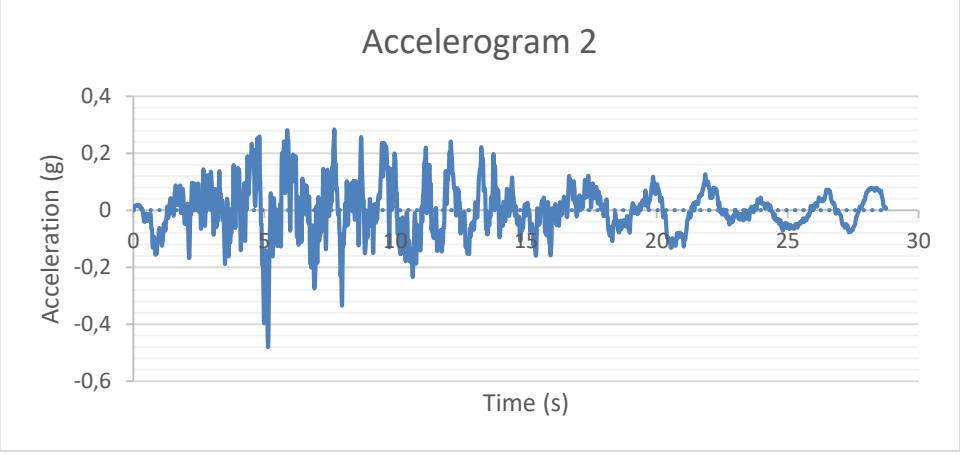

Figure 70. Artificial accelerogram 2 of the study case.

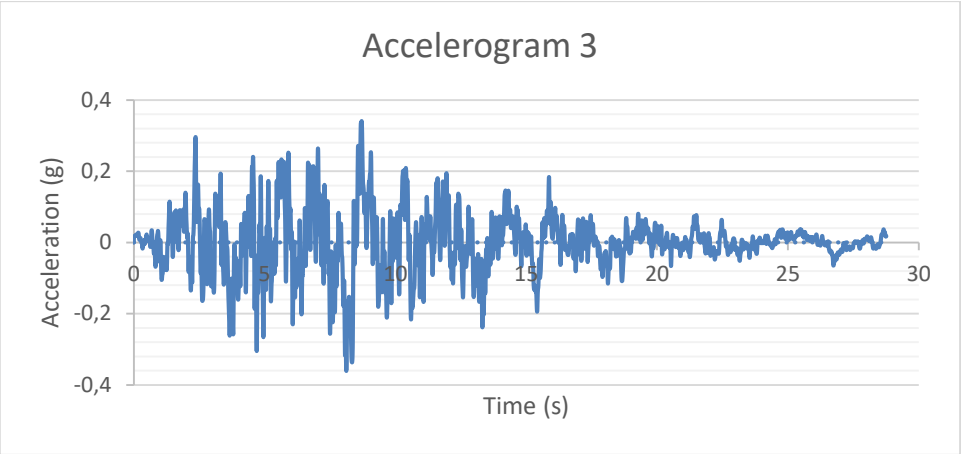

Figure 71. Artificial accelerogram 3 of the study case.

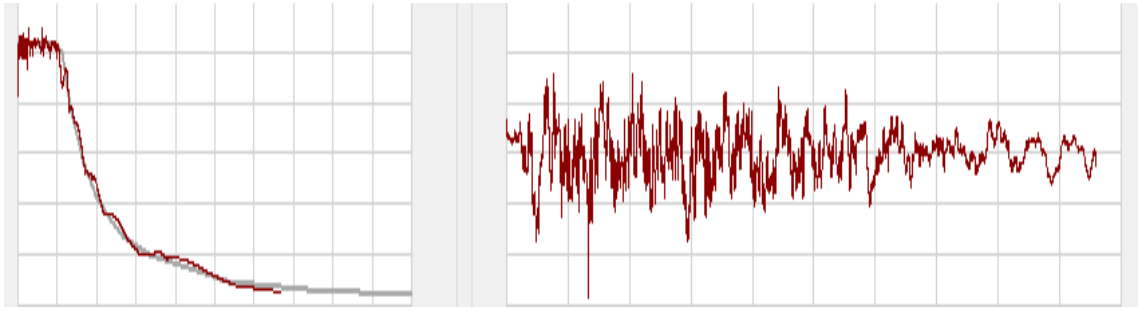

Figure 72. Matching accelerogram 1 with response spectra study case.

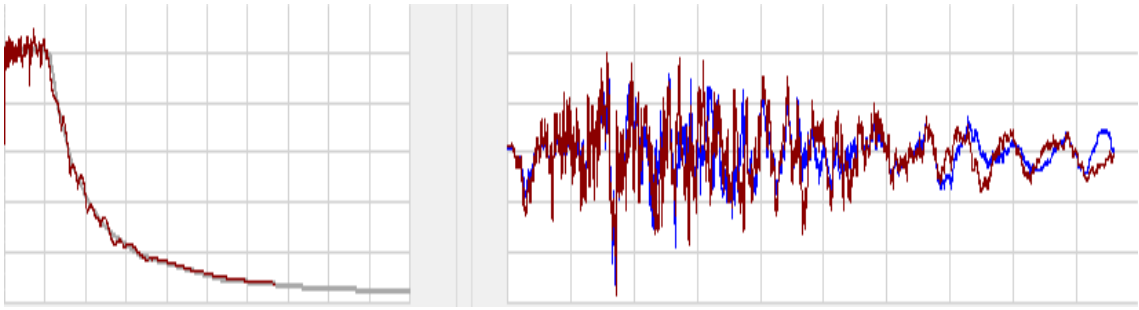

Figure 73. Matching accelerogram 2 with response spectra study case.

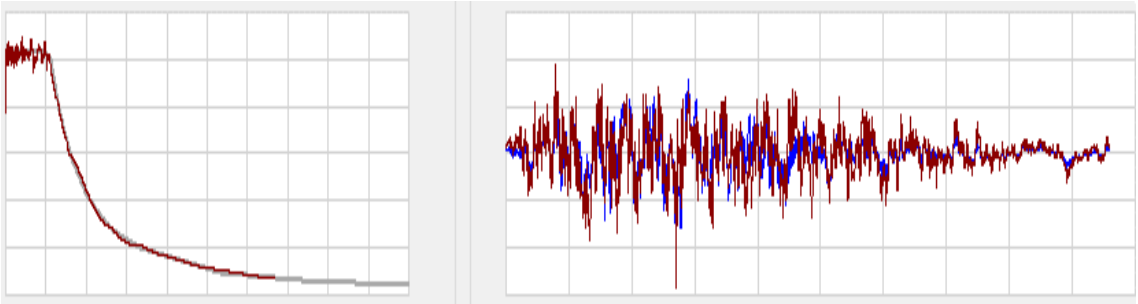

Figure 74. Matching accelerogram 3 with response spectra study case.

Obtaining the artificial accelegrams, they were matching with the elastic spectra. In order to load case for the time history analysis with components X and Y, the accelerograms were combining taking the hundred percent for one direction and thirty percent in the perpendicular direction.

Table 53.

Maximum and minimum drifts X direction of the study case.

Story	THSISMO 1A		THSISMO 1B		THSISMO 2A		THSISMO 2B		THSISMO 3A		THSISMO 3B	
	max	min	max	min	max	min	max	min	max	min	max	min
20	0,0068	0,0081	0,0025	0,0020	0,0039	0,0042	0,0025	0,0028	0,0072	0,0085	0,0014	0,0015
19	0,0096	0,0114	0,0035	0,0026	0,0054	0,0057	0,0034	0,0037	0,0100	0,0120	0,0018	0,0021
18	0,0128	0,0146	0,0045	0,0033	0,0071	0,0076	0,0046	0,0045	0,0131	0,0134	0,0024	0,0027
17	0,0156	0,0164	0,0056	0,0040	0,0088	0,0093	0,0056	0,0049	0,0163	0,0108	0,0029	0,0033
16	0,0181	0,0168	0,0066	0,0046	0,0105	0,0111	0,0064	0,0051	0,0189	0,0123	0,0035	0,0038
15	0,0201	0,0152	0,0070	0,0052	0,0123	0,0127	0,0070	0,0025	0,0202	0,0140	0,0041	0,0044
14	0,0209	0,0080	0,0071	0,0057	0,0135	0,0138	0,0071	0,0019	0,0208	0,0155	0,0045	0,0048
13	0,0215	0,0074	0,0070	0,0052	0,0149	0,0148	0,0070	0,0028	0,0213	0,0071	0,0050	0,0051
12	0,0222	0,0095	0,0071	0,0030	0,0164	0,0151	0,0071	0,0037	0,0225	0,0081	0,0054	0,0053
11	0,0226	0,0123	0,0073	0,0028	0,0178	0,0142	0,0074	0,0039	0,0208	0,0114	0,0058	0,0050
10	0,0231	0,0149	0,0051	0,0033	0,0192	0,0139	0,0078	0,0042	0,0158	0,0144	0,0062	0,0048
9	0,0207	0,0168	0,0055	0,0043	0,0205	0,0151	0,0047	0,0051	0,0142	0,0104	0,0066	0,0052
8	0,0148	0,0173	0,0038	0,0052	0,0214	0,0166	0,0050	0,0058	0,0114	0,0118	0,0069	0,0057
7	0,0164	0,0164	0,0043	0,0055	0,0222	0,0181	0,0055	0,0063	0,0129	0,0138	0,0072	0,0058
6	0,0172	0,0177	0,0051	0,0066	0,0226	0,0195	0,0058	0,0067	0,0155	0,0171	0,0074	0,0059
5	0,0178	0,0185	0,0060	0,0076	0,0218	0,0194	0,0061	0,0068	0,0181	0,0203	0,0070	0,0062
4	0,0216	0,0221	0,0063	0,0099	0,0231	0,0225	0,0075	0,0069	0,0238	0,0272	0,0069	0,0075
3	0,0150	0,0139	0,0061	0,0068	0,0133	0,0144	0,0051	0,0048	0,0177	0,0200	0,0041	0,0052
2	0,0115	0,0098	0,0050	0,0051	0,0088	0,0105	0,0038	0,0035	0,0140	0,0159	0,0035	0,0038
1	0,0099	0,0078	0,0049	0,0043	0,0087	0,0086	0,0033	0,0031	0,0123	0,0139	0,0037	0,0034

Table 54.

Absolute maximum drifts X direction study case.

Story	Elevation m	THSISMO 1A	THSISMO 1B	THSISMO 2A	THSISMO 2B	THSISMO 3A	THSISMO 3B	MAX
20	73,6	0,0081	0,0081	0,0025	0,0039	0,0042	0,0042	0,0085
19	70	0,0114	0,0114	0,0035	0,0054	0,0057	0,0057	0,0120
18	66,4	0,0146	0,0146	0,0045	0,0071	0,0076	0,0076	0,0146
17	62,8	0,0164	0,0164	0,0056	0,0088	0,0093	0,0093	0,0164
16	59,2	0,0181	0,0168	0,0066	0,0105	0,0111	0,0111	0,0189
15	55,6	0,0201	0,0152	0,0070	0,0123	0,0127	0,0127	0,0202
14	52	0,0209	0,0080	0,0071	0,0135	0,0138	0,0138	0,0209
13	48,4	0,0215	0,0074	0,0070	0,0149	0,0149	0,0148	0,0215
12	44,8	0,0222	0,0095	0,0071	0,0164	0,0164	0,0151	0,0225
11	41,2	0,0226	0,0123	0,0073	0,0178	0,0178	0,0142	0,0226
10	37,6	0,0231	0,0149	0,0051	0,0192	0,0192	0,0139	0,0231
9	34	0,0207	0,0168	0,0055	0,0205	0,0205	0,0151	0,0207
8	30,4	0,0173	0,0173	0,0052	0,0214	0,0214	0,0166	0,0214
7	26,8	0,0164	0,0164	0,0055	0,0222	0,0222	0,0181	0,0222
6	23,2	0,0177	0,0177	0,0066	0,0226	0,0226	0,0195	0,0226
5	19,6	0,0185	0,0185	0,0076	0,0218	0,0218	0,0194	0,0218
4	16	0,0221	0,0221	0,0099	0,0231	0,0231	0,0225	0,0272
3	11,4	0,0150	0,0139	0,0068	0,0133	0,0144	0,0144	0,0200
2	7,8	0,0115	0,0098	0,0051	0,0088	0,0105	0,0105	0,0159
1	4,6	0,0099	0,0078	0,0049	0,0087	0,0087	0,0086	0,0139

Table 55.

Maximum and minimum drifts Y direction of the study case.

Story	THSISMO 1A		THSISMO 1B		THSISMO 2A		THSISMO 2B		THSISMO 3A		THSISMO 3B	
	max	min	max	min	max	min	max	min	max	min	max	min
20	0,0050	0,0043	0,0160	0,0128	0,0050	0,0031	0,0112	0,0128	0,0032	0,0059	0,0139	0,0092
19	0,0070	0,0027	0,0214	0,0165	0,0070	0,0042	0,0132	0,0171	0,0040	0,0081	0,0156	0,0118
18	0,0088	0,0020	0,0274	0,0197	0,0091	0,0055	0,0148	0,0218	0,0046	0,0104	0,0199	0,0125
17	0,0061	0,0032	0,0320	0,0206	0,0096	0,0068	0,0149	0,0251	0,0026	0,0115	0,0220	0,0077
16	0,0008	0,0045	0,0283	0,0198	0,0078	0,0079	0,0151	0,0244	0,0018	0,0093	0,0045	0,0110
15	0,0014	0,0059	0,0150	0,0192	0,0050	0,0089	0,0140	0,0114	0,0024	0,0040	0,0052	0,0157
14	0,0008	0,0064	0,0100	0,0215	0,0034	0,0093	0,0099	0,0076	0,0031	0,0035	0,0096	0,0195
13	0,0029	0,0051	0,0075	0,0253	0,0038	0,0095	0,0072	0,0081	0,0045	0,0041	0,0138	0,0203
12	0,0048	0,0045	0,0131	0,0292	0,0049	0,0097	0,0076	0,0109	0,0065	0,0058	0,0172	0,0187
11	0,0065	0,0050	0,0190	0,0312	0,0061	0,0095	0,0090	0,0144	0,0088	0,0077	0,0202	0,0196
10	0,0085	0,0064	0,0242	0,0301	0,0070	0,0102	0,0118	0,0175	0,0111	0,0095	0,0240	0,0212
9	0,0103	0,0079	0,0260	0,0216	0,0081	0,0099	0,0149	0,0207	0,0130	0,0113	0,0279	0,0240
8	0,0116	0,0091	0,0197	0,0204	0,0094	0,0099	0,0142	0,0224	0,0141	0,0126	0,0308	0,0258
7	0,0123	0,0102	0,0240	0,0223	0,0109	0,0097	0,0179	0,0241	0,0085	0,0136	0,0325	0,0281
6	0,0103	0,0108	0,0276	0,0243	0,0121	0,0097	0,0222	0,0268	0,0081	0,0145	0,0284	0,0262
5	0,0113	0,0085	0,0305	0,0261	0,0131	0,0102	0,0262	0,0299	0,0093	0,0152	0,0287	0,0192
4	0,0111	0,0078	0,0372	0,0318	0,0131	0,0108	0,0345	0,0359	0,0116	0,0162	0,0295	0,0253
3	0,0065	0,0068	0,0196	0,0161	0,0088	0,0076	0,0205	0,0197	0,0111	0,0099	0,0158	0,0153
2	0,0050	0,0059	0,0153	0,0127	0,0067	0,0068	0,0175	0,0152	0,0090	0,0077	0,0124	0,0132
1	0,0052	0,0058	0,0153	0,0135	0,0061	0,0070	0,0182	0,0148	0,0083	0,0075	0,0124	0,0137

Table 56.

Absolute maximum drifts Y direction study case.

Story	Elevation m	THSISMO 1A	THSISMO 1B	THSISMO 2A	THSISMO 2B	THSISMO 3A	THSISMO 3B	MAX
20	73,6	0,0050	0,0160	0,0160	0,0128	0,0050	0,0112	0,0160
19	70	0,0070	0,0214	0,0214	0,0165	0,0070	0,0132	0,0214
18	66,4	0,0088	0,0274	0,0274	0,0197	0,0091	0,0148	0,0274
17	62,8	0,0061	0,0320	0,0320	0,0206	0,0096	0,0149	0,0320
16	59,2	0,0045	0,0283	0,0283	0,0198	0,0079	0,0151	0,0283
15	55,6	0,0059	0,0150	0,0192	0,0192	0,0089	0,0140	0,0192
14	52	0,0064	0,0100	0,0215	0,0215	0,0093	0,0099	0,0215
13	48,4	0,0051	0,0075	0,0253	0,0253	0,0095	0,0095	0,0253
12	44,8	0,0048	0,0131	0,0292	0,0292	0,0097	0,0097	0,0292
11	41,2	0,0065	0,0190	0,0312	0,0312	0,0095	0,0095	0,0312
10	37,6	0,0085	0,0242	0,0301	0,0301	0,0102	0,0118	0,0301
9	34	0,0103	0,0260	0,0260	0,0216	0,0099	0,0149	0,0279
8	30,4	0,0116	0,0197	0,0204	0,0204	0,0099	0,0142	0,0308
7	26,8	0,0123	0,0240	0,0240	0,0223	0,0109	0,0179	0,0325
6	23,2	0,0108	0,0276	0,0276	0,0243	0,0121	0,0222	0,0284
5	19,6	0,0113	0,0305	0,0305	0,0261	0,0131	0,0262	0,0305
4	16	0,0111	0,0372	0,0372	0,0318	0,0131	0,0345	0,0372
3	11,4	0,0068	0,0196	0,0196	0,0161	0,0088	0,0205	0,0205
2	7,8	0,0059	0,0153	0,0153	0,0127	0,0068	0,0175	0,0175
1	4,6	0,0058	0,0153	0,0153	0,0135	0,0070	0,0182	0,0182

After performing the Time History Fast Non-Lineal Analysis in the structure, the maximum drifts were obtaining. In the X and Y axes, the absolute maximum drifts are equal to 0.0272 and 0.0372 respectively.

In both cases, the maximum drift of the time history analysis is greater than the maximum drift establishes by the owner (0.015) and the obtaining of the static force analysis. The viscous damper will be used to get the target drift.

5.4.2. Linear Viscous Dampers Parameters

In this building different damper configurations and damper coefficients were analyzed. The linear dampers with a location of the dampers in the perimeter of the building showed the best performance; in the next tables, it will be computed the damping coefficient

of this dampers and configuration an in the result section it will be present the results of the other configuration and dampers with different damping.

There were located four damper in each direction per floor will be locates, and the damping coefficient is equal to one. The formula on the FDV damping coefficient is reducing due to the elimination of roof response amplitude term because it has exponential equal to zero such.

$$B = \frac{D_{max}}{D_{target}}$$

$$B = \frac{0.0272}{0.015} = 1.81 \text{ Reduction factor X axes}$$

$$B = \frac{0.0372}{0.20} = 2.48 \text{ Reduction factor Y axes}$$

$$\beta_{eff} = e^{\frac{\left(\frac{0.41\ln(\beta_0)-2.31}{B}\right)+2.31}{0.41}}$$

$$\beta_{eff} = 55.21\% \text{ Factor X axis}$$

$$\beta_{damper} = 55.21 - 5 = 50.21\% \text{ Factor Y axis}$$

$$\beta_{damper} = 30.40 - 5 = 30.40\% \text{ Factor X axis}$$

After it was performed two interactions staring with 50% of effective damping of the dampers, it was found that the optimal damping is equal to 40% in both directions with for dampers in each direction per floor.

T = 4.2 seg (Period of the mode)

$\beta_{mD} = 2.7$ (damping coefficient)

$\alpha = 1$

Table 57.

Parameters necessaries to compute the FVD damping coefficients Y direction study case

NIVEL	φi	φi²	φrj	MASS (Ton)	COSΘ	Σφi²xmi	Σ(φrj)^1+α xcos^1+α Θj
1	0,03163	0,00100	0,03163	188,25635	1,06923	0,18837	0,00114
2	0,06837	0,00467	0,03674	185,15360	1,22266	0,86544	0,00202
3	0,12008	0,01442	0,05171	292,06951	1,17666	4,21124	0,00370
4	0,21153	0,04475	0,09146	82,21859	1,06923	3,67899	0,00956
5	0,29203	0,08528	0,08050	80,54077	1,17666	6,86873	0,00897
6	0,37236	0,13865	0,08033	80,52911	1,17666	11,16572	0,00893
7	0,45003	0,20252	0,07766	79,85960	1,17666	16,17346	0,00835
8	0,52369	0,27425	0,07367	80,36925	1,17666	22,04149	0,00751
9	0,59270	0,35130	0,06901	79,52610	1,17666	27,93726	0,00659
10	0,65639	0,43085	0,06369	87,86131	1,17666	37,85497	0,00562
11	0,71460	0,51066	0,05821	70,26553	1,17666	35,88162	0,00469
12	0,76741	0,58891	0,05280	87,86131	1,17666	51,74282	0,00386
13	0,81481	0,66392	0,04741	70,28855	1,17666	46,66599	0,00311
14	0,85702	0,73448	0,04220	87,42290	1,17666	64,21030	0,00247
15	0,89402	0,79928	0,03700	69,40269	1,17666	55,47192	0,00190
16	0,92535	0,85627	0,03133	79,22550	1,17666	67,83836	0,00136
17	0,95122	0,90483	0,02588	76,59751	1,17666	69,30739	0,00093
18	0,97188	0,94454	0,02065	87,07366	1,17666	82,24490	0,00059
19	0,98776	0,97566	0,01588	69,29756	1,17666	67,61094	0,00035
20	1,00000	1,00000	0,01224	81,27231	1,17666	81,27231	0,00021

$\Gamma = 1.327$

$\lambda = 2^{2+\alpha} \frac{\Gamma^2(1+\frac{\alpha}{2})}{\Gamma(2+\alpha)}$ $\lambda = 3.1415$

$A = \frac{g x \Gamma_i x S_a x T}{4 x \beta_{mD} x \pi^2}$ $A = 0.231\ m$

$\sum C_j = \frac{\beta_H 2\pi A^{1-\alpha} \omega^{2-\alpha} \sum_i m_i \Phi_i^2}{\lambda \sum_j \Phi_{rj}^{1+\alpha} \cos^{1+\alpha} \theta_j}$ $\sum C_j = 11011\ Tn\frac{s}{m}$ (Per floor)

$C_Y = 2753\ Tn\frac{s}{m}$ (In each damper)

T = 3.4 seg (Period of the mode)

$\beta_{mD} = 2.4$ (damping coefficient)

$\alpha = 1$

Table 58.

Parameters necessaries to compute the FVD damping coefficients X direction study case.

NIVEL	ϕi	ϕi^2	ϕrj	MASS (Ton)	COSΘ	$\Sigma \phi i^2 x mi$	$\Sigma(\phi rj)^{1+\alpha} x \cos^{1+\alpha} \Theta j$
1	0,03000655	0,04	0,030	188,256354	1,04836124	0,17	0,00099
2	0,06816898	0,09	0,038	185,153595	1,2067017	0,86	0,00212
3	0,12390036	0,15	0,056	292,069514	1,15904272	4,48	0,00417
4	0,21352550	0,25	0,090	82,218587	1,04836124	3,75	0,00883
5	0,29165550	0,34	0,078	80,540768	1,15904272	6,85	0,00820
6	0,36984259	0,42	0,078	80,529108	1,15904272	11,02	0,00821
7	0,44620554	0,49	0,076	79,859604	1,15904272	15,90	0,00783
8	0,51961934	0,56	0,073	80,369245	1,15904272	21,70	0,00724
9	0,58939638	0,62	0,070	79,526095	1,15904272	27,63	0,00654
10	0,65455454	0,68	0,065	87,861312	1,15904272	37,64	0,00570
11	0,71460921	0,74	0,060	70,265525	1,15904272	35,88	0,00484
12	0,76945361	0,79	0,055	87,861312	1,15904272	52,02	0,00404
13	0,81876938	0,83	0,049	70,288548	1,15904272	47,12	0,00327
14	0,86266715	0,87	0,044	87,422896	1,15904272	65,06	0,00259
15	0,90097097	0,91	0,038	69,402685	1,15904272	56,34	0,00197
16	0,93215935	0,93	0,031	79,225498	1,15904272	68,84	0,00131
17	0,95689808	0,96	0,025	76,59751	1,15904272	70,14	0,00082
18	0,97594241	0,98	0,019	87,073657	1,15904272	82,93	0,00049
19	0,98989225	0,99	0,014	69,297558	1,15904272	67,90	0,00026
20	1,00000000	1,00	0,010	81,272312	1,15904272	81,27	0,00014

$\Gamma = 1.323$

$\lambda = 2^{2+\alpha} \frac{\Gamma^2(1+\frac{\alpha}{2})}{\Gamma(2+\alpha)}$ $\lambda = 3.1415$

$A = \frac{g x \Gamma_i x S_a x T}{4 x \beta_{mD} x \pi^2}$ $A = 0.210\ m$

$\sum C_j = \frac{\beta_H 2\pi A^{1-\alpha} \omega^{2-\alpha} \sum_i m_i \Phi_i^2}{\lambda \sum_j \Phi_{rj}^{1+\alpha} \cos^{1+\alpha} \theta_j}$ $\sum C_j = 14074.422\ Tn\frac{s}{m}$ (Per floor)

$C_X = 3519 Tn \frac{s}{m}$ (In each damper)

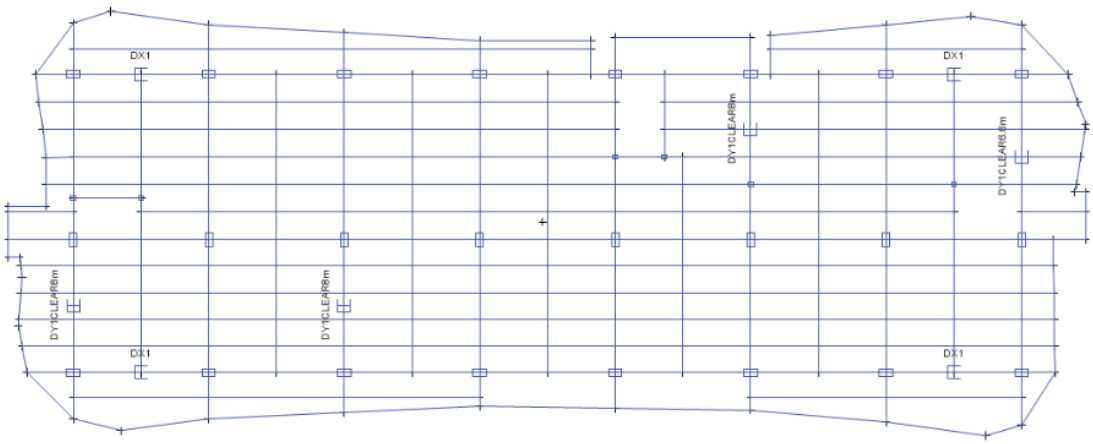

Figure 75. Plan view damper location study case.

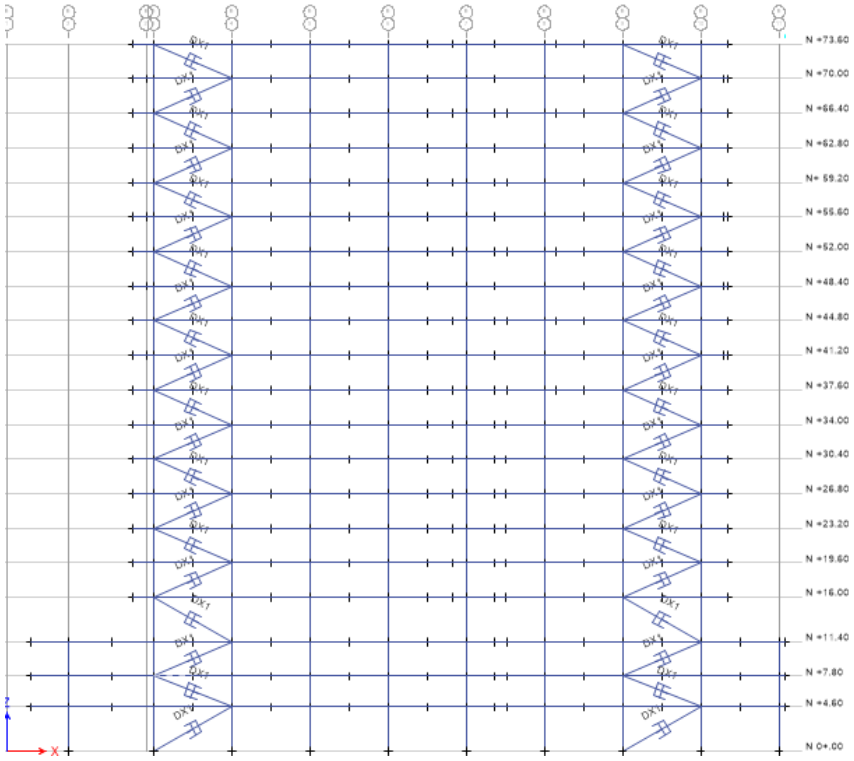

Figure 76. Elevation view B axis of dampers in X direction study case.

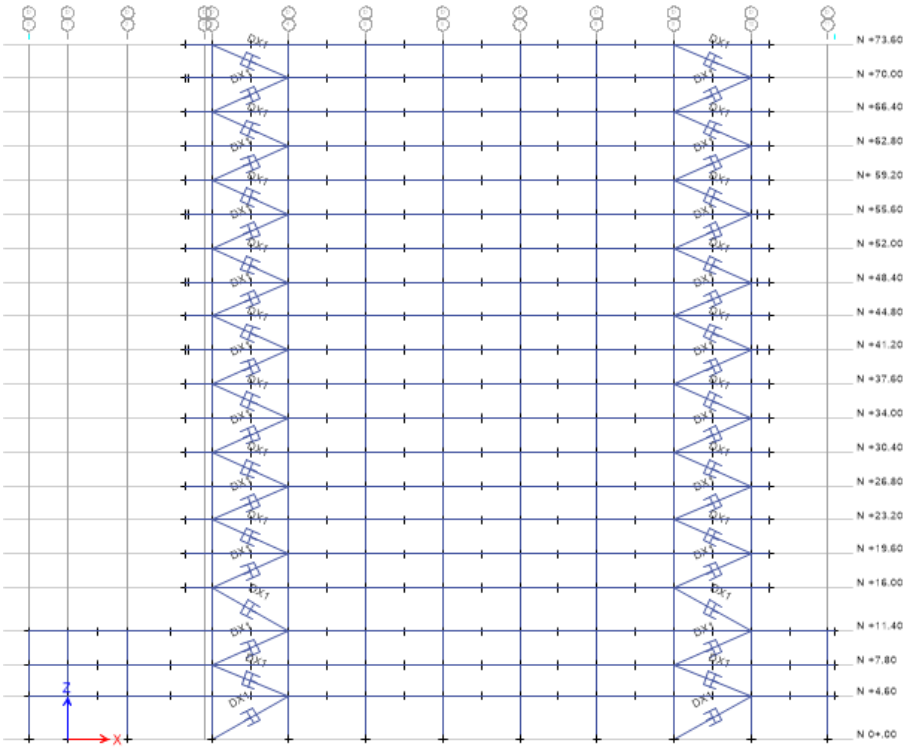

Figure 77. Elevation view D axis of dampers in X direction study case.

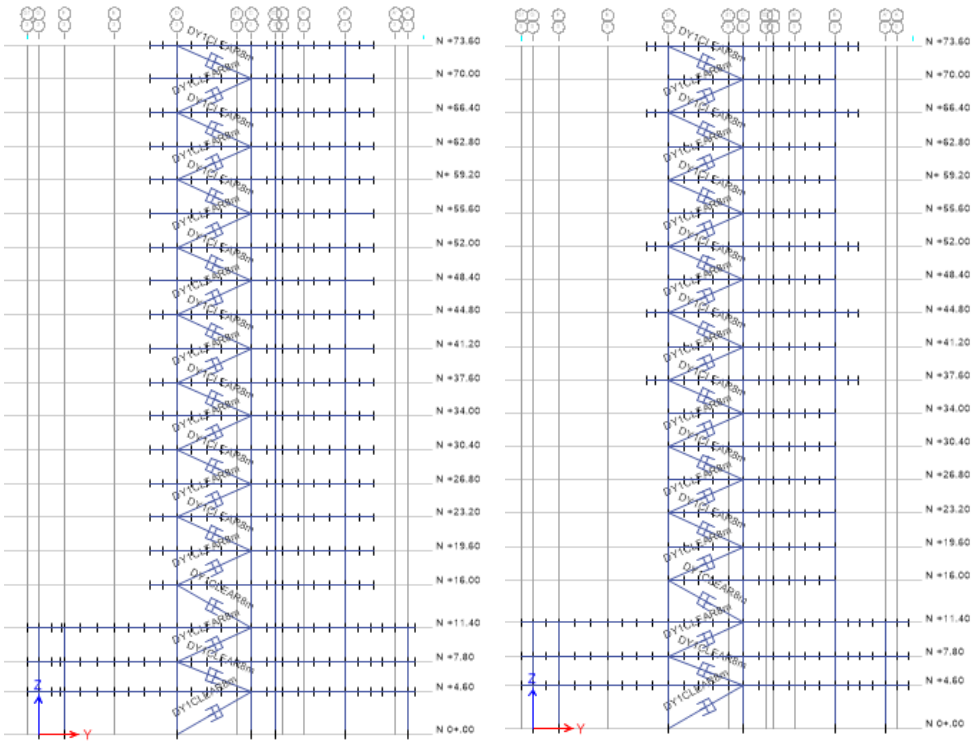

Figure 78. Elevation view 3 and 5 axes of dampers in X direction study case.

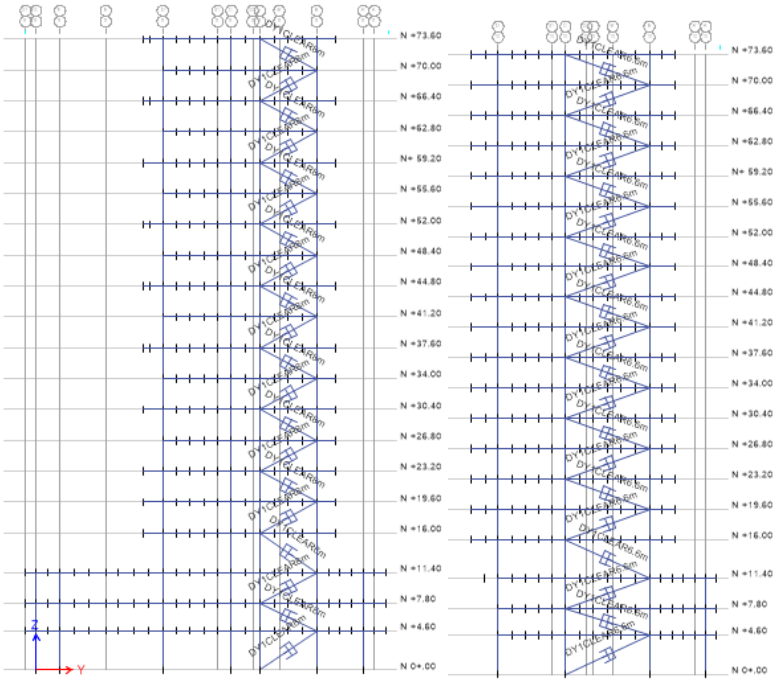

Figure 79. Elevation view 8 and 10 axes of dampers in X direction study case.

5.4.3. Results linear Viscous Dampers

After it was proceeded an interactive process, it was achieved a maximum drift of 0.0148 in THSISMO3A and 0.0152 in THSISMO3A in the directions X and Y respectively. These maximum drifts are lower or equal to the target drift define by the owner (0.015); the reduction of the maximum drifts is around 100% in both directions with the use of linear viscous damper with a damping coefficient equal to 1.

Table 59.

Maximum and minimum drifts Y direction with lineal dampers study case.

Story	THSISMO 1A		THSISMO 1B		THSISMO 2A		THSISMO 2B		THSISMO 3A		THSISMO 3B	
	max	min	max	min	max	min	max	min	max	min	max	min
20	0,0019	0,0014	0,0010	0,0006	0,0014	0,0017	0,0007	0,0006	0,0026	0,0013	0,0005	0,0007
19	0,0025	0,0019	0,0013	0,0007	0,0019	0,0023	0,0009	0,0007	0,0036	0,0017	0,0007	0,0009
18	0,0034	0,0025	0,0017	0,0009	0,0025	0,0031	0,0012	0,0010	0,0048	0,0023	0,0009	0,0012
17	0,0043	0,0030	0,0021	0,0011	0,0032	0,0038	0,0014	0,0012	0,0060	0,0029	0,0011	0,0014
16	0,0052	0,0036	0,0025	0,0014	0,0038	0,0046	0,0017	0,0014	0,0072	0,0035	0,0013	0,0017
15	0,0062	0,0042	0,0029	0,0015	0,0044	0,0054	0,0021	0,0015	0,0084	0,0040	0,0015	0,0019
14	0,0071	0,0047	0,0032	0,0016	0,0050	0,0060	0,0024	0,0017	0,0093	0,0044	0,0017	0,0021
13	0,0080	0,0053	0,0035	0,0017	0,0055	0,0065	0,0026	0,0019	0,0102	0,0047	0,0019	0,0023
12	0,0088	0,0058	0,0038	0,0019	0,0061	0,0071	0,0029	0,0021	0,0111	0,0051	0,0021	0,0024
11	0,0096	0,0063	0,0041	0,0020	0,0066	0,0076	0,0031	0,0023	0,0120	0,0056	0,0022	0,0026
10	0,0103	0,0067	0,0044	0,0021	0,0070	0,0080	0,0033	0,0025	0,0128	0,0060	0,0024	0,0027
9	0,0110	0,0071	0,0047	0,0023	0,0074	0,0085	0,0035	0,0027	0,0136	0,0065	0,0025	0,0029
8	0,0115	0,0074	0,0048	0,0024	0,0077	0,0088	0,0037	0,0028	0,0141	0,0068	0,0026	0,0029
7	0,0120	0,0077	0,0050	0,0025	0,0080	0,0091	0,0039	0,0029	0,0146	0,0071	0,0027	0,0030
6	0,0123	0,0079	0,0050	0,0025	0,0082	0,0092	0,0040	0,0029	0,0148	0,0072	0,0028	0,0030
5	0,0124	0,0079	0,0050	0,0026	0,0083	0,0090	0,0040	0,0030	0,0147	0,0072	0,0028	0,0030
4	0,0116	0,0072	0,0045	0,0023	0,0079	0,0081	0,0038	0,0026	0,0136	0,0066	0,0026	0,0028
3	0,0094	0,0057	0,0033	0,0018	0,0063	0,0061	0,0032	0,0020	0,0106	0,0050	0,0022	0,0021
2	0,0080	0,0048	0,0028	0,0017	0,0053	0,0048	0,0027	0,0017	0,0088	0,0047	0,0018	0,0017
1	0,0049	0,0029	0,0018	0,0011	0,0032	0,0030	0,0016	0,0011	0,0055	0,0031	0,0011	0,0011

Table 60.

Absolute maximum drifts Y direction with lineal dampers study case.

Story	Elevation m	THSISMO 1A	THSISMO 1B	THSISMO 2A	THSISMO 2B	THSISMO 3A	THSISMO 3B	MAX
20	73,6	0,0019	0,0010	0,0017	0,0007	0,0026	0,0007	0,0026
19	70	0,0025	0,0013	0,0023	0,0009	0,0036	0,0009	0,0036
18	66,4	0,0034	0,0017	0,0031	0,0012	0,0048	0,0012	0,0048
17	62,8	0,0043	0,0021	0,0038	0,0014	0,0060	0,0014	0,0060
16	59,2	0,0052	0,0025	0,0046	0,0017	0,0072	0,0017	0,0072
15	55,6	0,0062	0,0029	0,0054	0,0021	0,0084	0,0019	0,0084
14	52	0,0071	0,0032	0,0060	0,0024	0,0093	0,0021	0,0093
13	48,4	0,0080	0,0035	0,0065	0,0026	0,0102	0,0023	0,0102
12	44,8	0,0088	0,0038	0,0071	0,0029	0,0111	0,0024	0,0111
11	41,2	0,0096	0,0041	0,0076	0,0031	0,0120	0,0026	0,0120
10	37,6	0,0103	0,0044	0,0080	0,0033	0,0128	0,0027	0,0128
9	34	0,0110	0,0047	0,0085	0,0035	0,0136	0,0029	0,0136
8	30,4	0,0115	0,0048	0,0088	0,0037	0,0141	0,0029	0,0141
7	26,8	0,0120	0,0050	0,0091	0,0039	0,0146	0,0030	0,0146
6	23,2	0,0123	0,0050	0,0092	0,0040	0,0148	0,0030	0,0148
5	19,6	0,0124	0,0050	0,0090	0,0040	0,0147	0,0030	0,0147
4	16	0,0116	0,0045	0,0081	0,0038	0,0136	0,0028	0,0136
3	11,4	0,0094	0,0033	0,0063	0,0032	0,0106	0,0022	0,0106
2	7,8	0,0080	0,0028	0,0053	0,0027	0,0088	0,0018	0,0088
1	4,6	0,0049	0,0018	0,0032	0,0016	0,0055	0,0011	0,0055

Table 61.

Maximum and minimum drifts X direction with lineal dampers study case.

Story	THSISMO 1A		THSISMO 1B		THSISMO 2A		THSISMO 2B		THSISMO 3A		THSISMO 3B	
	max	min	max	min	max	min	max	min	max	min	max	min
20	0,001	0,0008	0,00245	0,00155	0,00106	0,00078	0,00206	0,00146	0,00083	0,0007	0,00285	0,00151
19	0,00123	0,00089	0,00293	0,00195	0,00116	0,00088	0,00241	0,00182	0,00102	0,00077	0,00346	0,00192
18	0,00157	0,00111	0,00358	0,00248	0,00135	0,00104	0,00288	0,00229	0,00121	0,00093	0,00429	0,00247
17	0,00195	0,00139	0,00429	0,00304	0,00154	0,00136	0,00341	0,00277	0,00135	0,00118	0,00518	0,00306
16	0,00235	0,00171	0,00511	0,00361	0,00174	0,0016	0,00408	0,00321	0,00148	0,00139	0,00618	0,00361
15	0,00275	0,00204	0,00608	0,00429	0,00216	0,00172	0,00489	0,00376	0,00185	0,0018	0,00728	0,00413
14	0,00305	0,00219	0,00691	0,00489	0,00233	0,00182	0,00553	0,00422	0,00195	0,00177	0,00824	0,00468
13	0,00347	0,00241	0,00753	0,00538	0,00258	0,00209	0,00606	0,00483	0,00214	0,00178	0,00899	0,00531
12	0,00378	0,00259	0,0084	0,00598	0,00276	0,00231	0,00673	0,00536	0,0023	0,0019	0,01001	0,00586
11	0,00422	0,00291	0,00898	0,00664	0,00304	0,00262	0,00728	0,00601	0,0025	0,00214	0,01092	0,00651
10	0,00449	0,00316	0,00989	0,00717	0,00335	0,00281	0,00794	0,00654	0,00279	0,00231	0,01182	0,00705
9	0,0049	0,00348	0,01045	0,00792	0,00359	0,00311	0,00861	0,00719	0,00298	0,0026	0,013	0,00769
8	0,00508	0,00368	0,01123	0,00837	0,00391	0,00325	0,00912	0,00759	0,00323	0,00272	0,01362	0,00813
7	0,0054	0,00394	0,01165	0,00895	0,00409	0,00348	0,00968	0,0081	0,00336	0,00296	0,01461	0,00861
6	0,00538	0,00405	0,01198	0,00914	0,00435	0,00347	0,00991	0,00828	0,00352	0,00297	0,01487	0,00881
5	0,00534	0,00401	0,0121	0,00927	0,00454	0,00349	0,01001	0,00834	0,00348	0,003	0,01516	0,00884
4	0,00455	0,00317	0,01063	0,00812	0,00418	0,00321	0,0088	0,00725	0,00315	0,00267	0,01324	0,00763
3	0,00356	0,00188	0,008	0,00599	0,00372	0,00268	0,00637	0,00503	0,00263	0,00284	0,00973	0,00519
2	0,00314	0,00164	0,00624	0,00476	0,00305	0,00218	0,00501	0,00402	0,00212	0,0023	0,00772	0,00417
1	0,00171	0,00114	0,00419	0,00314	0,00194	0,0014	0,00328	0,00268	0,0013	0,00134	0,00509	0,00274

Table 62.

Absolute maximum drifts X direction with lineal dampers study case.

Story	Elevation	THSISMO 1A	THSISMO 1B	THSISMO 2A	THSISMO 2B	THSISMO 3A	THSISMO 3B	MAX
	m							
20	73,6	0,0010	0,0024	0,0011	0,0021	0,0008	0,0028	0,0028
19	70	0,0012	0,0029	0,0012	0,0024	0,0010	0,0035	0,0035
18	66,4	0,0016	0,0036	0,0014	0,0029	0,0012	0,0043	0,0043
17	62,8	0,0020	0,0043	0,0015	0,0034	0,0013	0,0052	0,0052
16	59,2	0,0023	0,0051	0,0017	0,0041	0,0015	0,0062	0,0062
15	55,6	0,0028	0,0061	0,0022	0,0049	0,0018	0,0073	0,0073
14	52	0,0030	0,0069	0,0023	0,0055	0,0020	0,0082	0,0082
13	48,4	0,0035	0,0075	0,0026	0,0061	0,0021	0,0090	0,0090
12	44,8	0,0038	0,0084	0,0028	0,0067	0,0023	0,0100	0,0100
11	41,2	0,0042	0,0090	0,0030	0,0073	0,0025	0,0109	0,0109
10	37,6	0,0045	0,0099	0,0033	0,0079	0,0028	0,0118	0,0118
9	34	0,0049	0,0105	0,0036	0,0086	0,0030	0,0130	0,0130
8	30,4	0,0051	0,0112	0,0039	0,0091	0,0032	0,0136	0,0136
7	26,8	0,0054	0,0116	0,0041	0,0097	0,0034	0,0146	0,0146
6	23,2	0,0054	0,0120	0,0043	0,0099	0,0035	0,0149	0,0149
5	19,6	0,0053	0,0121	0,0045	0,0100	0,0035	0,0152	0,0152
4	16	0,0045	0,0106	0,0042	0,0088	0,0032	0,0132	0,0132
3	11,4	0,0036	0,0080	0,0037	0,0064	0,0028	0,0097	0,0097
2	7,8	0,0031	0,0062	0,0030	0,0050	0,0023	0,0077	0,0077
1	4,6	0,0017	0,0042	0,0019	0,0033	0,0013	0,0051	0,0051

5.4.4. Input seismic energy in the structure.

In the figures 70 and 70 are shown the distribution of energy in the structure for the analysis THSISMO3A in 28.94 second for the structure without damper and with lineal dampers.

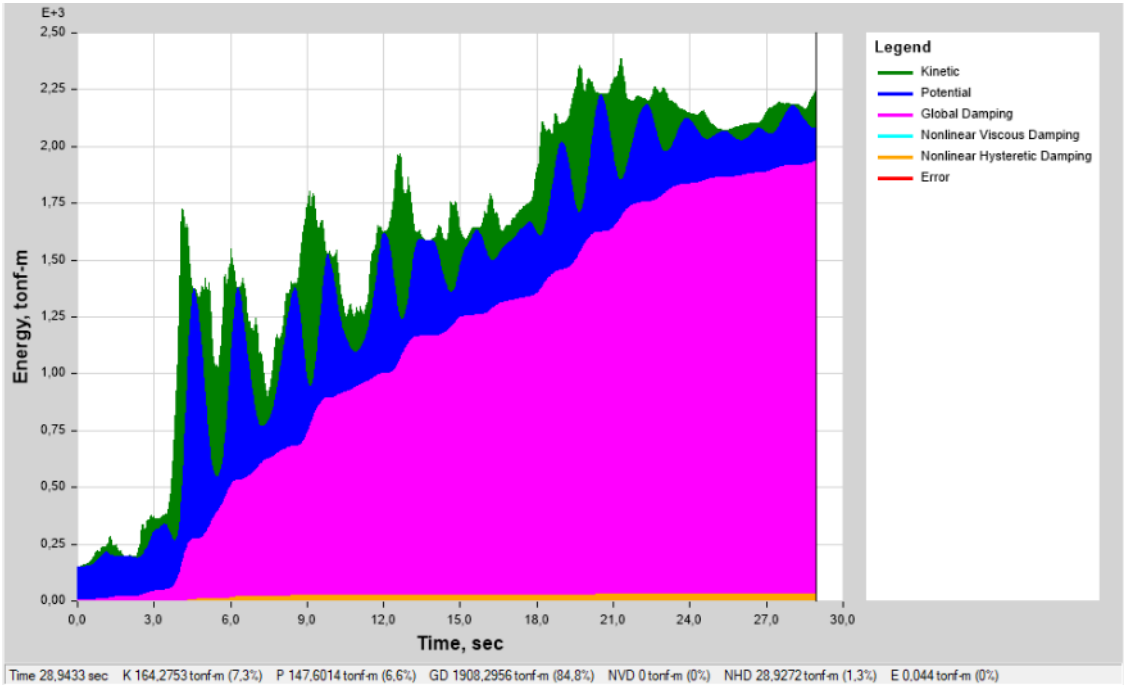

Figure 80. Energy in the structure without dampers study case.

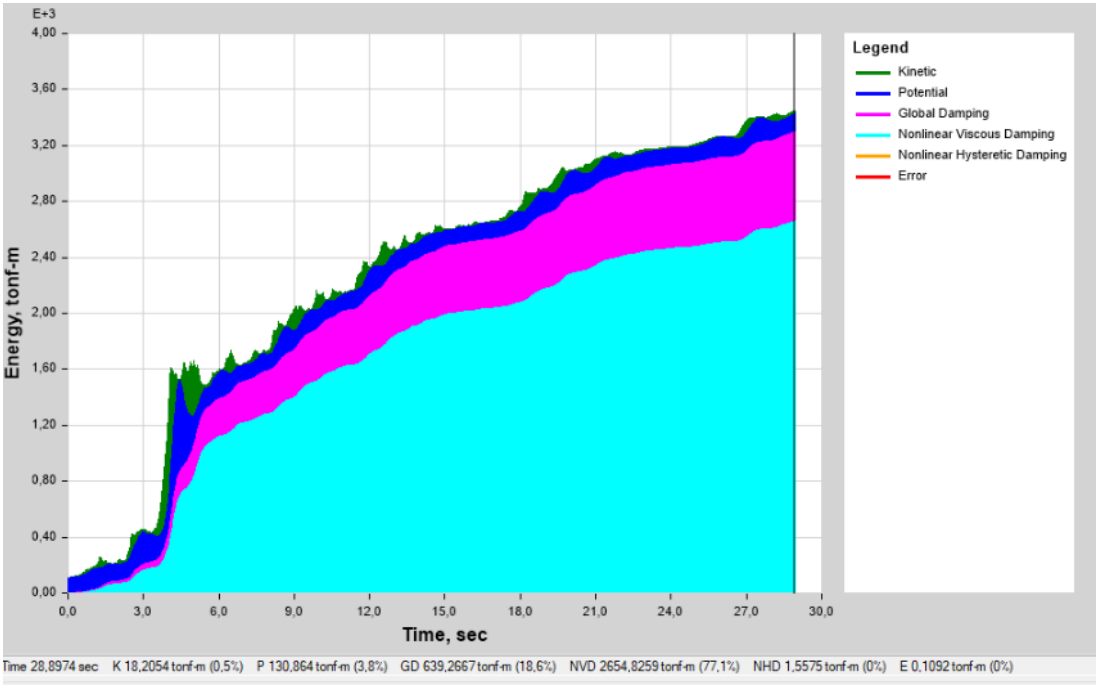

Figure 81. Energy in the structure without linear dampers study case.

Table 63.

Energy dissipation of the structure for THSISMO3,4 at 28,94 seconds for structure with and without dampers study case.

Energy dissipation	Normal	Lineal dampers
	%	%
Kinetic	7,3	0,5
Potential	6,6	3.8
Global Damping	84.8	18.6
Nonlinear Viscous Damping	0	77.1
Nonlinear Hysteretic Damping	1.3	0,0
Error	0	0
Sum	**100**	**100**

5.4.5. Inelastic behavior of the structure.

It will be analysis the develop of the plastic hinges (concentrate nonlinear behavior) for the structure with dampers and without dampers for the cases THSISMO3B at 29 seconds.

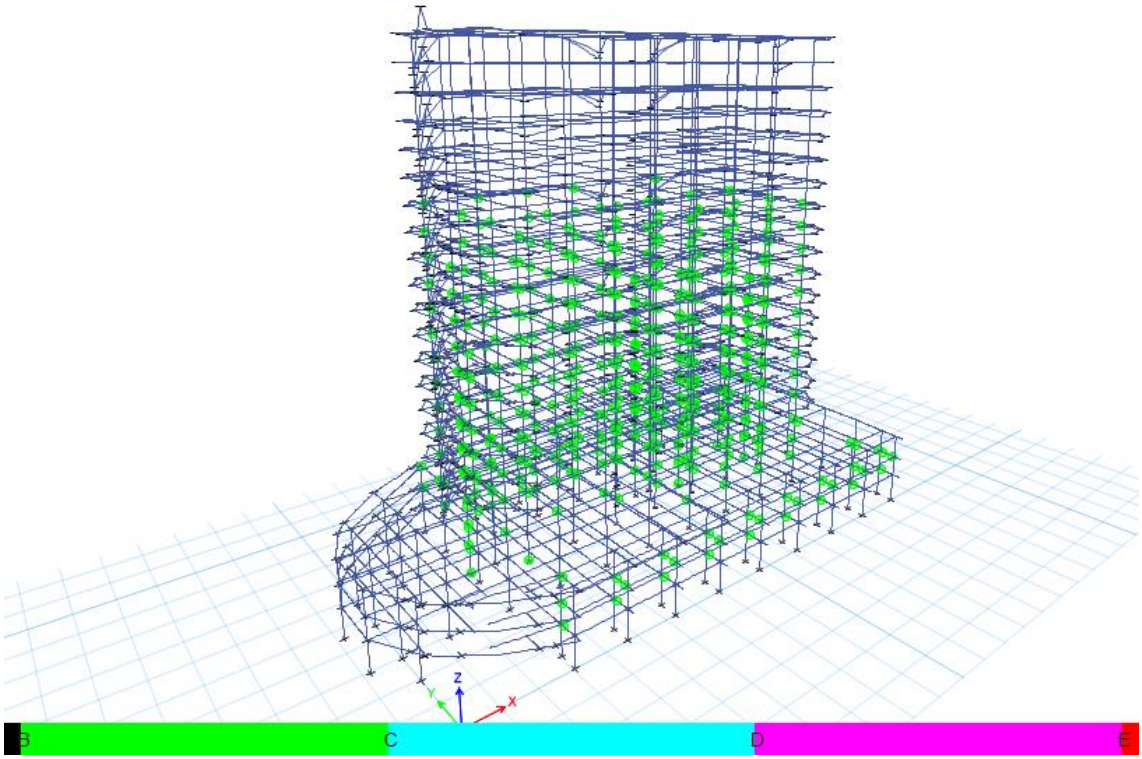

Figure 82. Nonlinear behavior of the structure without dampers.

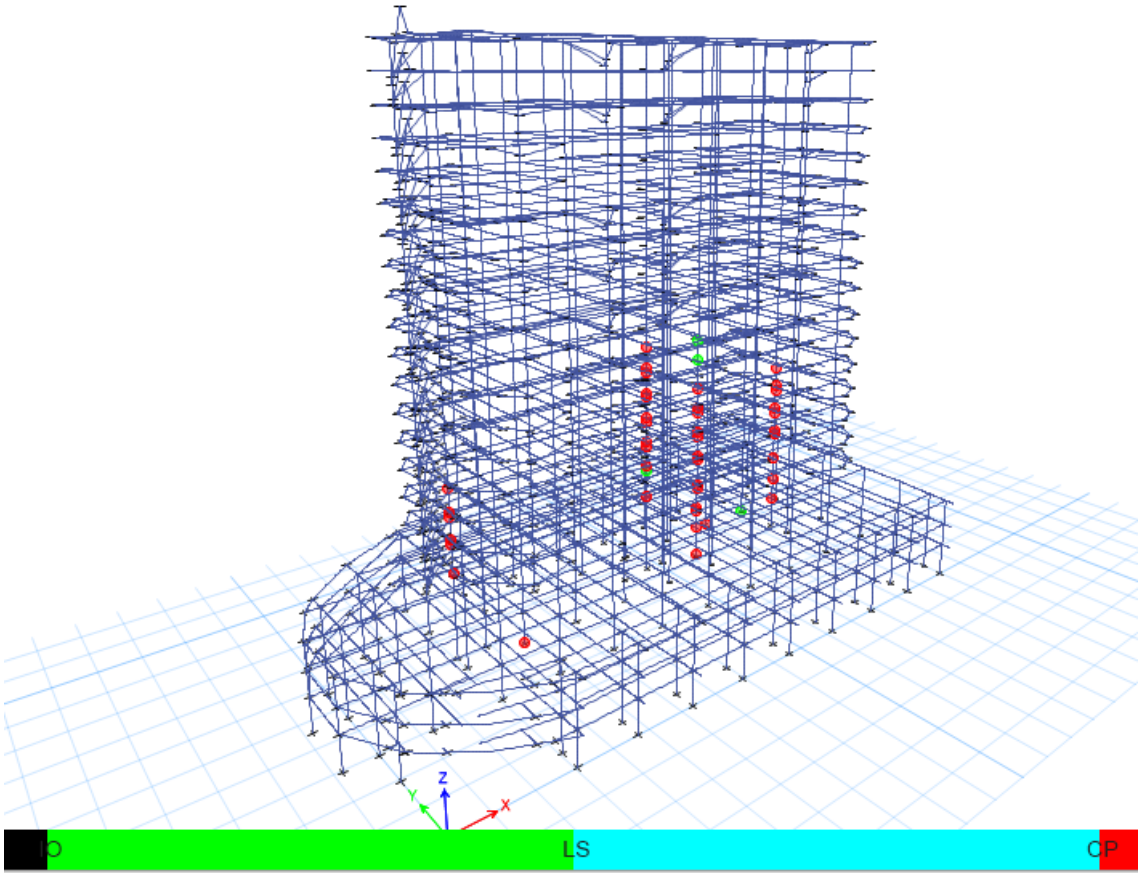

Figure 83. Plastic hinge performance according ASCE42 structure without dampers.

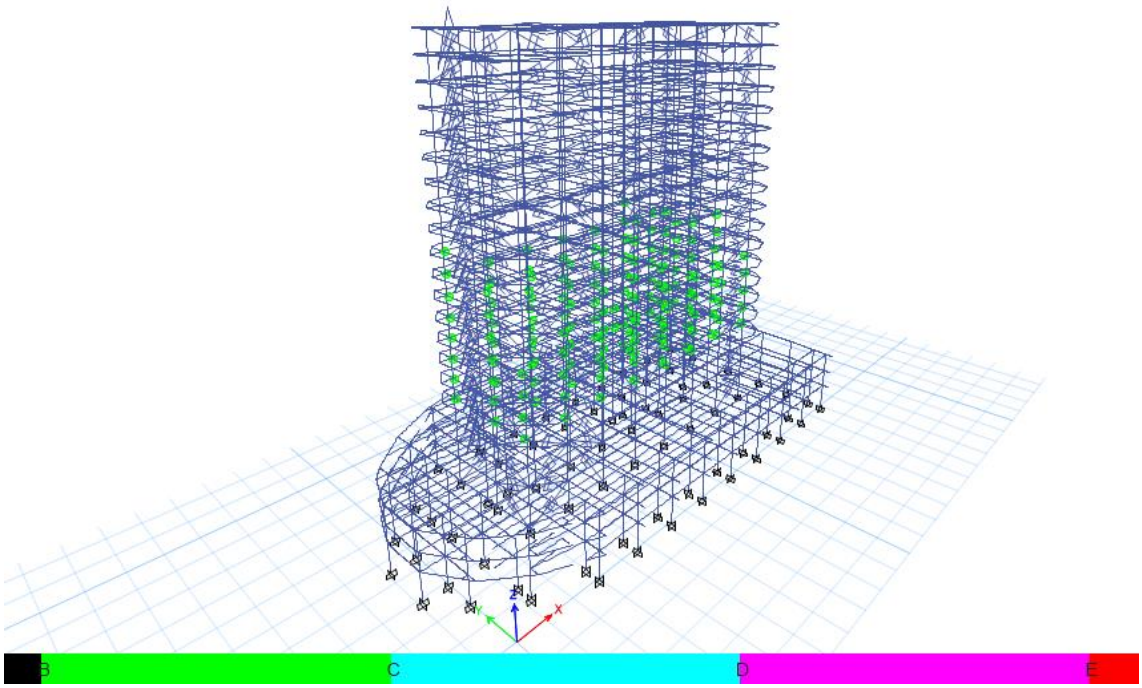

Figure 84. Nonlinear behavior of the structure without linear dampers.

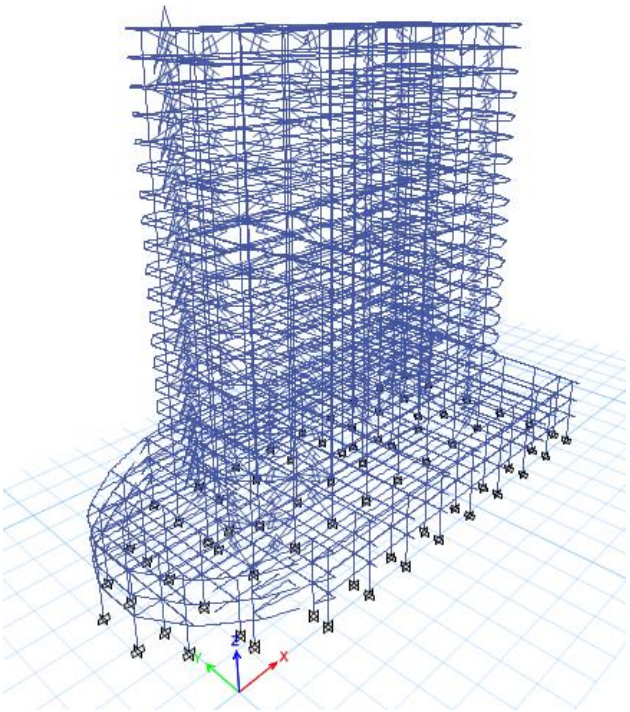

Figure 85. Plastic hinge performance according ASCE42 structure with dampers.

5.4.6. Dampers forces and behavior.

In table 62 it is shown the axial forces in the linear and nonlinear dampers for the case THSISMO3B this process must be repeated for all case and get the maximum value of all cases per damper. The figure 76 shows the non-linear behavior of the damper K145 for the case THSISMO3B that has an approximately elliptical form.

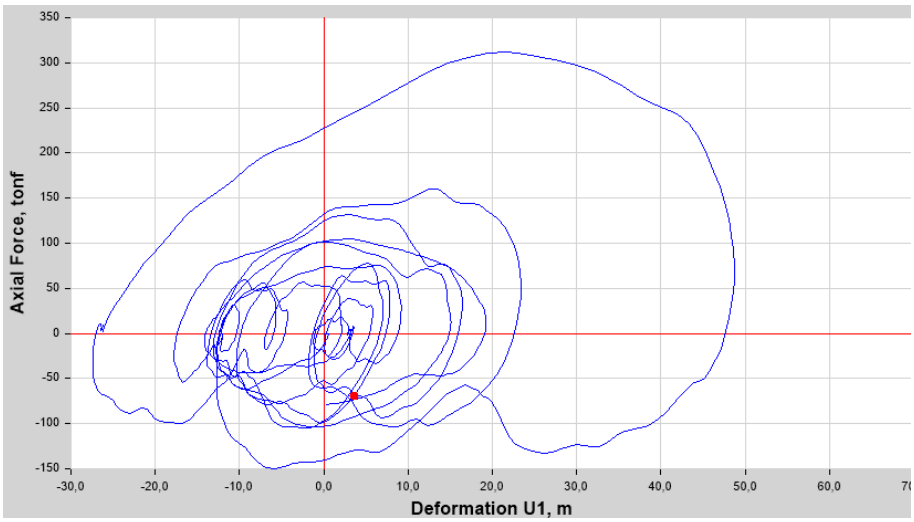

Figure 86. Hysteresis behavior THSISMO3B.

Table 64.

Linear damper force study case for THSISMO3B.

Story	Link	Location	P tonf	Story	Link	Location	P tonf	Story	Link	Location	P tonf
N +73.60	K20	I-End	16,3718	N +48.40	K13	I-End	42,3622	N +23.20	K6	I-End	78,9734
N +73.60	K40	I-End	24,1078	N +48.40	K33	I-End	45,0032	N +23.20	K26	I-End	74,6217
N +73.60	K60	I-End	30,5606	N +48.40	K53	I-End	53,2388	N +23.20	K46	I-End	77,3527
N +73.60	K80	I-End	15,0954	N +48.40	K73	I-End	55,3824	N +23.20	K66	I-End	91,2336
N +73.60	K100	I-End	28,6511	N +48.40	K93	I-End	176,6983	N +23.20	K86	I-End	142,9886
N +73.60	K120	I-End	18,8594	N +48.40	K113	I-End	156,8405	N +23.20	K106	I-End	133,2393
N +73.60	K140	I-End	20,0777	N +48.40	K133	I-End	174,6354	N +23.20	K126	I-End	144,8458
N +73.60	K160	I-End	25,6686	N +48.40	K153	I-End	194,8854	N +23.20	K146	I-End	149,1962
N +70.00	K19	I-End	15,1723	N +44.80	K12	I-End	62,87	N +19.60	K5	I-End	65,7955
N +70.00	K39	I-End	23,9977	N +44.80	K32	I-End	51,5689	N +19.60	K25	I-End	68,6134
N +70.00	K59	I-End	36,2544	N +44.80	K52	I-End	46,3652	N +19.60	K45	I-End	80,2191
N +70.00	K79	I-End	16,7077	N +44.80	K72	I-End	78,9422	N +19.60	K65	I-End	75,0615
N +70.00	K99	I-End	58,3913	N +44.80	K92	I-End	95,7127	N +19.60	K85	I-End	296,6769
N +70.00	K119	I-End	43,3796	N +44.80	K112	I-End	81,5778	N +19.60	K105	I-End	276,8815
N +70.00	K139	I-End	56,0423	N +44.80	K132	I-End	94,3596	N +19.60	K125	I-End	296,5637
N +70.00	K159	I-End	67,0185	N +44.80	K152	I-End	101,3913	N +19.60	K145	I-End	312,1631
N +66.40	K18	I-End	22,8886	N +41.20	K11	I-End	54,2294	N +16.00	K4	I-End	91,9936
N +66.40	K38	I-End	19,8	N +41.20	K31	I-End	55,1491	N +16.00	K24	I-End	90,3198
N +66.40	K58	I-End	24,6128	N +41.20	K51	I-End	56,4933	N +16.00	K44	I-End	103,1454
N +66.40	K78	I-End	31,251	N +41.20	K71	I-End	66,5511	N +16.00	K64	I-End	98,3153
N +66.40	K98	I-End	42,015	N +41.20	K91	I-End	211,7455	N +16.00	K84	I-End	147,7729
N +66.40	K118	I-End	31,521	N +41.20	K111	I-End	196,7189	N +16.00	K104	I-End	144,116
N +66.40	K138	I-End	34,3869	N +41.20	K131	I-End	215,437	N +16.00	K124	I-End	152,1504
N +66.40	K158	I-End	42,7688	N +41.20	K151	I-End	236,7127	N +16.00	K144	I-End	158,5908
N +62.80	K17	I-End	24,9718	N +37.60	K10	I-End	71,9595	N +11.40	K3	I-End	64,2953
N +62.80	K37	I-End	27,0103	N +37.60	K30	I-End	62,1099	N +11.40	K23	I-End	65,7882
N +62.80	K57	I-End	32,1512	N +37.60	K50	I-End	51,8673	N +11.40	K43	I-End	74,8138
N +62.80	K77	I-End	31,4822	N +37.60	K70	I-End	87,1672	N +11.40	K63	I-End	60,6456
N +62.80	K97	I-End	93,2723	N +37.60	K90	I-End	113,2493	N +11.40	K83	I-End	161,9855
N +62.80	K117	I-End	77,6088	N +37.60	K110	I-End	101,1988	N +11.40	K103	I-End	172,1442
N +62.80	K137	I-End	94,6901	N +37.60	K130	I-End	114,4957	N +11.40	K123	I-End	166,8479
N +62.80	K157	I-End	105,7938	N +37.60	K150	I-End	121,2555	N +11.40	K143	I-End	185,5052
N+ 59.20	K16	I-End	38,6145	N +34.00	K9	I-End	61,6971	N +7.80	K2	I-End	55,0636
N+ 59.20	K36	I-End	28,3054	N +34.00	K29	I-End	62,918	N +7.80	K22	I-End	57,0622
N+ 59.20	K56	I-End	37,4502	N +34.00	K49	I-End	64,2387	N +7.80	K42	I-End	74,7944
N+ 59.20	K76	I-End	51,2223	N +34.00	K69	I-End	71,1423	N +7.80	K62	I-End	63,262
N+ 59.20	K96	I-End	63,7601	N +34.00	K89	I-End	254,2404	N +7.80	K82	I-End	64,1689
N+ 59.20	K116	I-End	49,399	N +34.00	K109	I-End	237,2508	N +7.80	K102	I-End	65,1352
N+ 59.20	K136	I-End	53,6609	N +34.00	K129	I-End	255,414	N +7.80	K122	I-End	63,4648
N+ 59.20	K156	I-End	62,1599	N +34.00	K149	I-End	278,6615	N +7.80	K142	I-End	66,8037
N +55.60	K15	I-End	32,9143	N +30.40	K8	I-End	77,0199	N +4.60	K1	I-End	56,1781
N +55.60	K35	I-End	38,1167	N +30.40	K28	I-End	68,1248	N +4.60	K21	I-End	56,601
N +55.60	K55	I-End	48,6403	N +30.40	K48	I-End	59,7099	N +4.60	K41	I-End	73,2284
N +55.60	K75	I-End	50,1362	N +30.40	K68	I-End	91,6571	N +4.60	K61	I-End	64,2007
N +55.60	K95	I-End	137,7514	N +30.40	K88	I-End	130,4881	N +4.60	K81	I-End	95,3364
N +55.60	K115	I-End	114,622	N +30.40	K108	I-End	120,0004	N +4.60	K101	I-End	121,0751
N +55.60	K135	I-End	135,8336	N +30.40	K128	I-End	132,7936	N +4.60	K121	I-End	101,2311
N +55.60	K155	I-End	150,731	N +30.40	K148	I-End	138,6087	N +4.60	K141	I-End	111,6752
N +52.00	K14	I-End	52,9034	N +26.80	K7	I-End	64,7665				
N +52.00	K34	I-End	39,5932	N +26.80	K27	I-End	68,0926				
N +52.00	K54	I-End	44,1082	N +26.80	K47	I-End	66,7257				
N +52.00	K74	I-End	67,283	N +26.80	K67	I-End	75,6542				
N +52.00	K94	I-End	81,9303	N +26.80	K87	I-End	288,1307				
N +52.00	K114	I-End	64,0687	N +26.80	K107	I-End	268,9566				
N +52.00	K134	I-End	75,548	N +26.80	K127	I-End	288,4265				
N +52.00	K154	I-End	81,3812	N +26.80	K147	I-End	308,6873				

5.4.7. Dampers forces and behavior.

The determination of the damping coefficients, positions and numbers of damper is achieved by an iterative process. In this literal are going to be showed some results obtained. The first try was located the dampers in the position where the shear walls were, and only two damper in each direction per floor were located. The results presents are for some demands in some cases the greater demand THSISMO3A and THSISMO3B

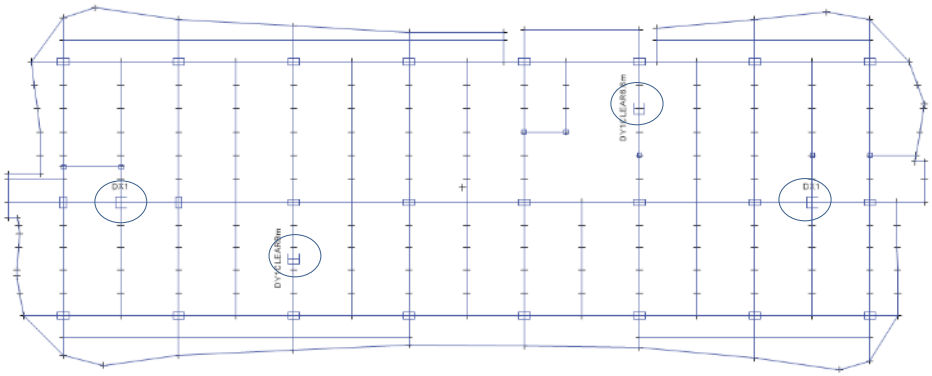

Figure 87. Plan location dampers first iteration study case.

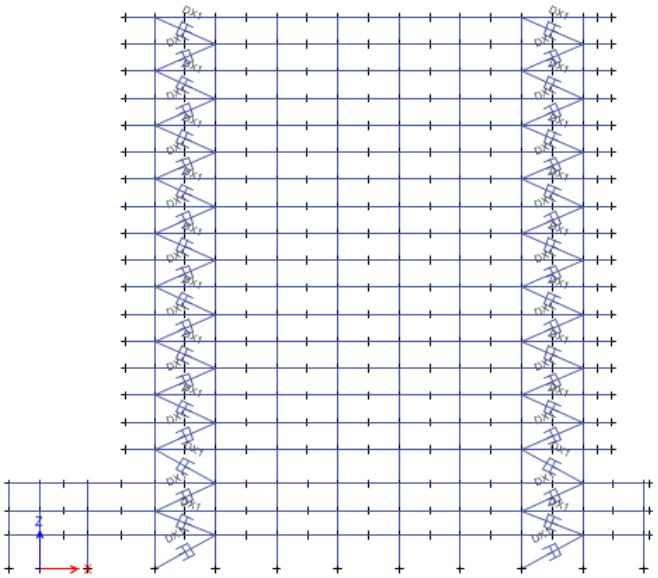

Figure 88. Elevation location and configuration of the dampers first iteration study case.

Table 65.

First iteration result for THSISMO 3A Y THSISMO 3B.

DAMPING 50%				
α	3A		3B	
	Max	Min	Max	Min
0,4	0,019098	0,010799	0,021921	0,016166
0,5	0,018876	0,010509	0,021117	0,015109
0,6	0,018279	0,009901	0,020693	0,01421
0,7	0,018072	0,009748	0,020288	0,013394
0,8	0,01751	0,009188	0,019792	0,012646
0,9	0,017349	0,009149	0,019345	0,012147
1	0,01681	0,008374	0,018448	0,011083

The second iteration were using the linear dampers that had the better results with the same location in plan of the first iteration.

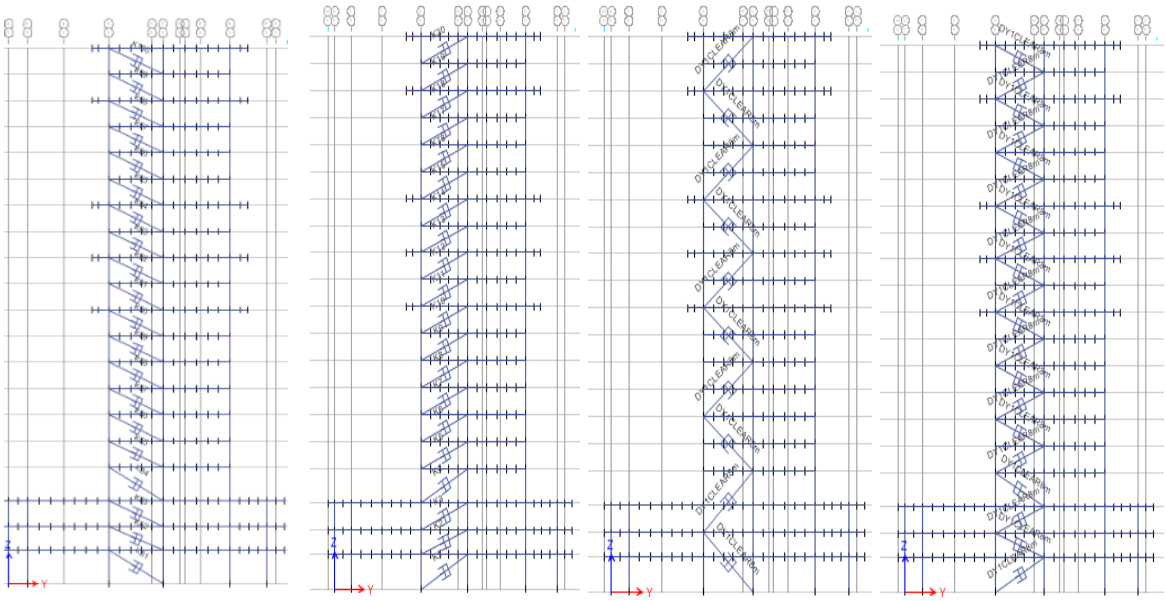

Figure 89. Elevation axes 5 iteration 2

Table 66.

Second iteration result for THSISMO 3A and THSISMO 3B.

DAMPING 50%					
α	3A		3B		Observation
	Max	Min	Max	Min	
1	0,01681	0,008374	0,018448	0,011083	Two diagonal connected to the panel
1	0,018184	0,010874	0,019019	0,012335	One diagonal connected to the panel
1	0,01783	0,0107	0,022014	0,011998	Diagonal connected left to right
1	0,017545	0,0107	0,018263	0,011998	Two floors connected

6. Conclusions

Conclusions of chapter 2.

6.1.

- The direct displacement based design has more accurate approached to the real behavior of the structure due to the use of the secant stiffness that take in count the degradation of the original stiffness in the elastic range product of the appeared of the plastic hinges and the incursion in the non-linear.
- The equation of the yield drift steel frames (Equation 49) for steel frame established by Presley in 2007; it does not consider the contribution of the columns being a simplification that introduce an error. The equation formulated by Reyes Garcia in the master thesis Development of a displacement based design method for steel frame-RC in 2007 is more accurate that contemplate the nonlinear behavior of the column.

$$\theta_y = \frac{\emptyset_{yb}\, L_b + 0.9\emptyset_{yc}\, L_c}{6}$$

Where $Ø_{yb\ and}\ Ø_{yc}$ are the yield curvature of the beam and column; L_b and L_c are the lengths.

- The final structure obtained from the DDBD presents a greater ductility with the less quantity of material (2.54%) than the structure obtained from the force method for the same maximum drift. In the case of chapter one the difference in quantity is low due to de regularity and size of structure, but in real cases with bigger structures the economical saving will be substantial.

6.2.

- Although the base shear considering in the DDBD is greater 17.8% of the structure in chapter one than the obtained with force method, the structure obtained lighter due to the displacement profile based in the fundamental mode that uses the DDBD.

Conclusions of chapter 3.

- The Fluid viscous dampers (FVDs) are one of the best seismic protection systems because the functioning of them is out of phase with respect of the seismic response of the building. In the point of maximum displacement and null velocity where the

structure has the grates stress the damper do not work, but in the point of maximum velocity and null displacement (rest point) the dampers produces their maximum forces and the stress in the building due to the seismic event are cero.

- The use of the dampers does not affect the mode periods in the structure because these kind of damper are velocity dependents. Also, the stiffness of the structure remains equal but the mass participation can change. The FVDs can be used not only to decrease the drift but also to correct the torsion in the structure.
- The diagonal configuration for the FVDs represents on one best configuration due to the use of one steel profile per damper producing economic saving, reduce the horizontal and vertical displacement in the structure and can be used to connected two floors if the project needed.
- The implementation of this seismic protection system reduce the formation of plastic hinges in the structure, and these protection system reduces the acting forces in the developed plastic hinge maintaining the majority in the zone of immediate occupation.
- The majority of the input energy in the building by the seismic is dissipated by the dampers in form of work and heat, and the energy taking by the plastic deformation is almost null.
- The fast nonlinear analysis (time history analysis) is the best option in the analysis of the structures with concentrate elements with nonlinear behavior due to the saving of time, modal analysis, and the use of Ritz vectors.
- The bolted connection secures the develop of the maximum capacity of the structure due to the capacity design of it. The capacity design of the connection ensure that the beam develop all the plastic capacity.

6.3.

Conclusions of chapter 4.

- Before to performance a nonlinear static analysis (pushover), it must be performed a modal analysis to determine the load patter to use; similarly, it have to be analysis the type of connection used or to be used to compute the plastic hinge location using the American Code ANSI/AISC 358-16.

- The analysis pushover allows to verify the mechanist of the structure. In the case of the DDBD and force model, it was confirmed that is correct mechanism strong column weak beam is present in both.
- In both model the performance is in the range of life safe analyzing the global drift by the parameters of VISION 2000.
- The DDBD model present a greater ductility than the force model for every load pattern used. Also, in both model the ductility in the Y direction is the greatest.
- The based shear and displacement corresponding to the DBDD model are higher and lower respectively than the present in the force model confirming a better performance of the DDBD structure.
- The bolted connection increased the performances in steel structure by moving the plastic hinge location from the face of the column making the appearance of them with a higher shear than the obtained with a welded connection.

6.4. Conclusions of chapter 5.

- The pushover analysis in the case of the study case must consider the effects of the high modes due to the percentage of mass participation is less than 0.75; for this consideration was used a pattern of obtained of a combination SRSS with the modal modes until reaches the 90%
- The use of layer model for the shear wall is the best option to captor a more accurate representation because it is giving the behavior of the steel reinforcement and concrete.
- In figure 53 and 57, it exhibited a correct behavior strong column and weak beam; as well, it is shown that in Y direction the critical plastic hinges are present in the couple beam between the shear walls in the axe 8.
- The structure presents a live safe performance level in both directions according the performance objectives establish in VISION 2000.
- The added damping selected for both directions was the same 40% to avoid torsion problems; also, this helps to reduce the displacement in the another orthogonal direction consider in the time history analysis.

- The FNA in the study case reduce the analysis time comparing with the normal time history analysis allowing the analysis of more configuration; also, it permits a modal analysis of the structure with the influence of the dampers and the study of the plastic behavior of the principal earthquake-resistant structure.
- The best location in which the dampers presents the best efficiency is in the perimeter of the building. This was proved that that the added damping by the dampers was less than the computed at the beginning. However, in other case in which the dampers were located in other locations the dampers present elevated damper coefficients because the efficiency of them were lower.
- The energy capture by the nonlinear hysteretic damping with the damper were null, and the damper captures the higher percent of the input seismic energy 77%. Also, the dampers reduced the number of plastic hinges and increased the performances of the building.

7. Bibliography

Almansa, F. L. (06 de 2018). Class notes of Earthquake-resistant. Earthquake-resistant. Barcelona, España.

AMERICAN INSTITUTE OF STEEL CONSTRUCTION. (12 de May de 2016). Prequalified Connections for Special and Intermediate Steel Moment Frames for Seismic Applications. *ANSI/AISC 358-16*. Chicago, Illinois, United State.

Brown, A., M. Uno, J., Thompson, & Stratford, J. (8 de 11 de 2015). Seismic and Financial Performance of Fluid Viscous Dampers relative to BRBs: A Case Study. Sydney, Australia.

Castro, G. V., & Sánchez, M. D. (2016). *EDIFICACIONES CON DISIPADORES VISCOSOS.* Trujillo: Editora & Imprenta Gráfica Norte S.R.L.

Chopra, K., & Goel, K. (2001). Direct Displacement*Based Design: Use of Inelastic Design Spectra vs Elastic Design Spectr. *Earthquake Spectra*, 47-64.

Colunga, T. (2003). Disipasion Pasiva de Energia en México: un Estado del Arte. *Congreso Nacional de Ingenieria Sismica.* Barquisimeto .

Dogariu, A. (01 de 2011). Obtenido de https://www.ct.upt.ro/suscos/files/2013-2015/1E07/Add%202%20NONLINEAR%20ANALYSIS%20AD.pdf

Federal Emergency Management, A. a. (November de 2000). PRESTANDARD AND COMMENTARY FOR THE SEISMIC REHABILITATION OF BUILDINGS. Washington, D.C., USA.

Fernandex, J. O. (October de 2015). Diseno sismico basado en desplzamiento de estructuras de hormigon armado aporticadas y estructuras con muro de corte. Quito, Pichincha, Ecuador.

Ghorbanie-Asl, M. (April de 2007). PERFORMANCE-BASED SEISMIC DESIGN (Doctoral thesis). Ottawa, Canada.

GIANNOPOULOS, I. P. (21 de 10 de 2009). Seismic Assessment of a RC Building. Cambridge, United Kingdon.

KARIMZADA, N. A. (July de 2015). *PERFORMANCE-BASED SEISMIC DESIGN OF REINFORCED CONCRETE FRAME BUILDINGS: A DIRECT DISPLACEMENT-BASED APPROACH (MASTER OF SCIENCE THESES)*. İZMİR, Turquía.

Narkhede, D. I., & Sinha, R. (2012). Shock Vibration Control of Structures using Fluid. *15 World Conferences on Earthquake Engineering (15 WCEE)*. Lisbon.

Priestley, M., Calvi, G., & Kowalsky,, M. (2007). *Displacement-based Seismic Design of Structures*. PAiva: IUSS Press.

SaiChethan, K., Srinivas, K., & Ranjitha, K. (June de 2017). SEISMIC PERFORMANCE EVALUATION OF FLUID VISCOUS DAMPERS. *IJRET: International Journal of Research in Engineering and Technology*.

Symans, M. D., Constantinou, M. C., Taylor, D. P., & Garnjost, K. D. (2012). SEMI-ACTIVE FLUID VISCOUS DAMPERS FOR SEISMIC RESPONSE CONTROL. New York, New York, United State.

Teresa, G. (1999). Dynamics of SDOF Systme whti Nonlinear Viscous Daping. *Journal of Engineering Mechanics*.

Vega, L. d. (25 de 04 de 2015). *ABC*. Obtenido de https://www.abc.es/sociedad/20150425/abci-cronologia-peores-terremotos-201504251527.html#disqus_thread

Villani, A. (2009). *Critical Assessment of Seismic Design Procedures fo Steel MRF*. Pavia: IUSS.

Wilson, E. L. (1995). Three-Dimensional Static and Dynamic Analysis of Structures. Berkeley, California, USA.

8. Annex

Performance point DDBD model DDBD load pattern x direction.

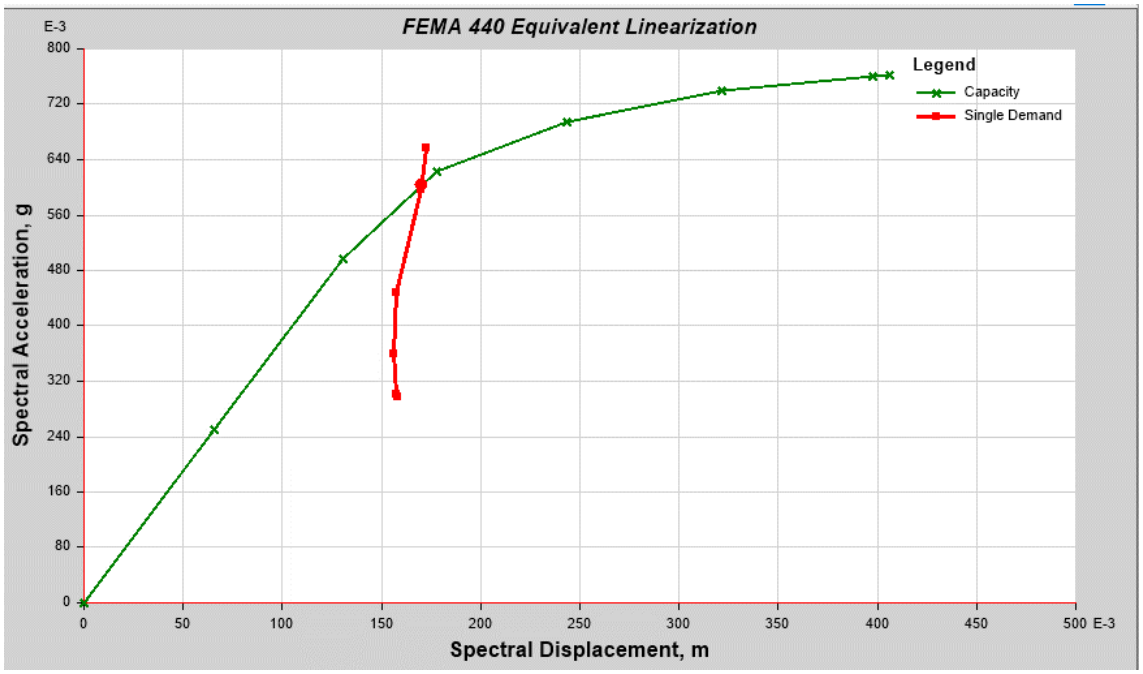

Performance point DDBD model first mode load pattern x direction.

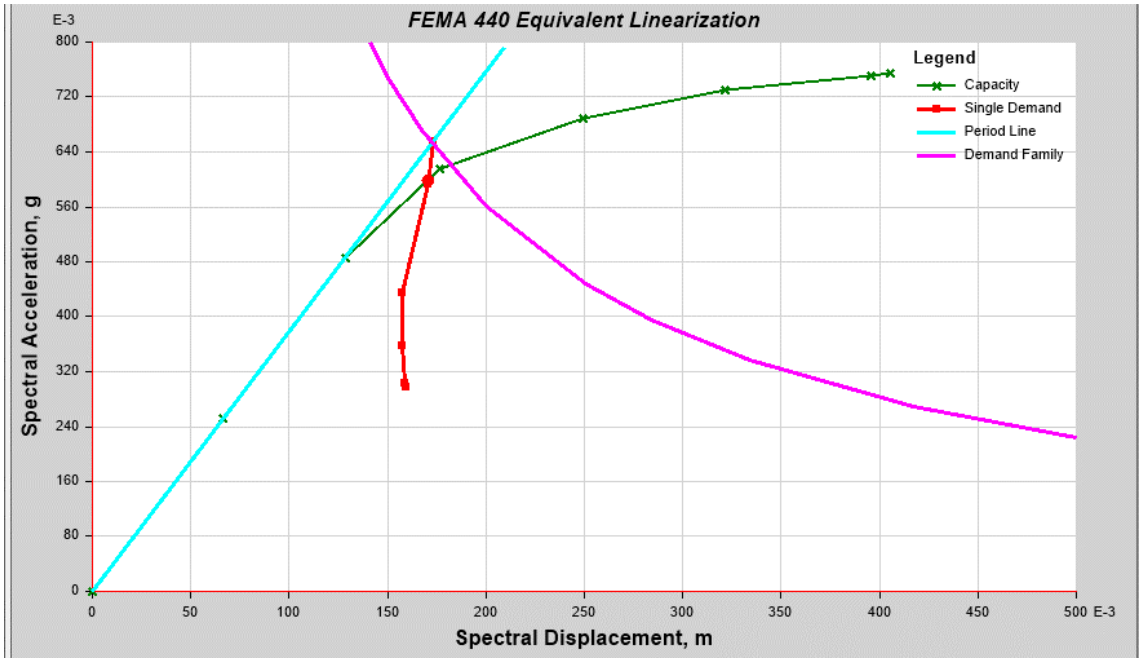

Performance point DDBD model triangular load pattern x direction.

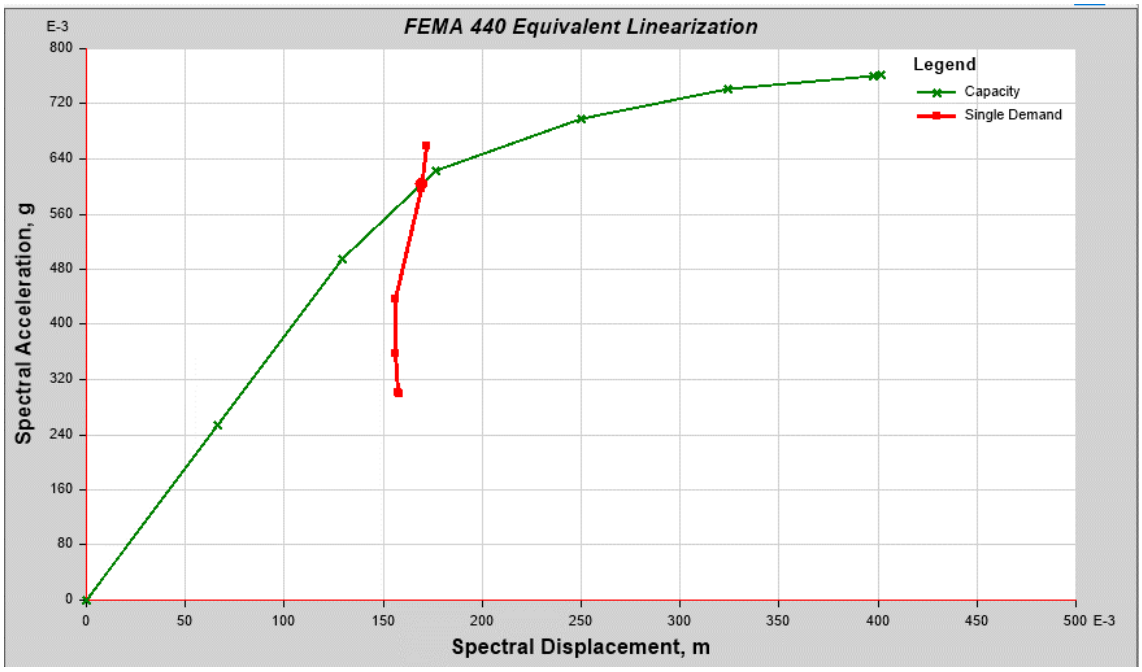

Performance point force model DDBD load pattern x direction.

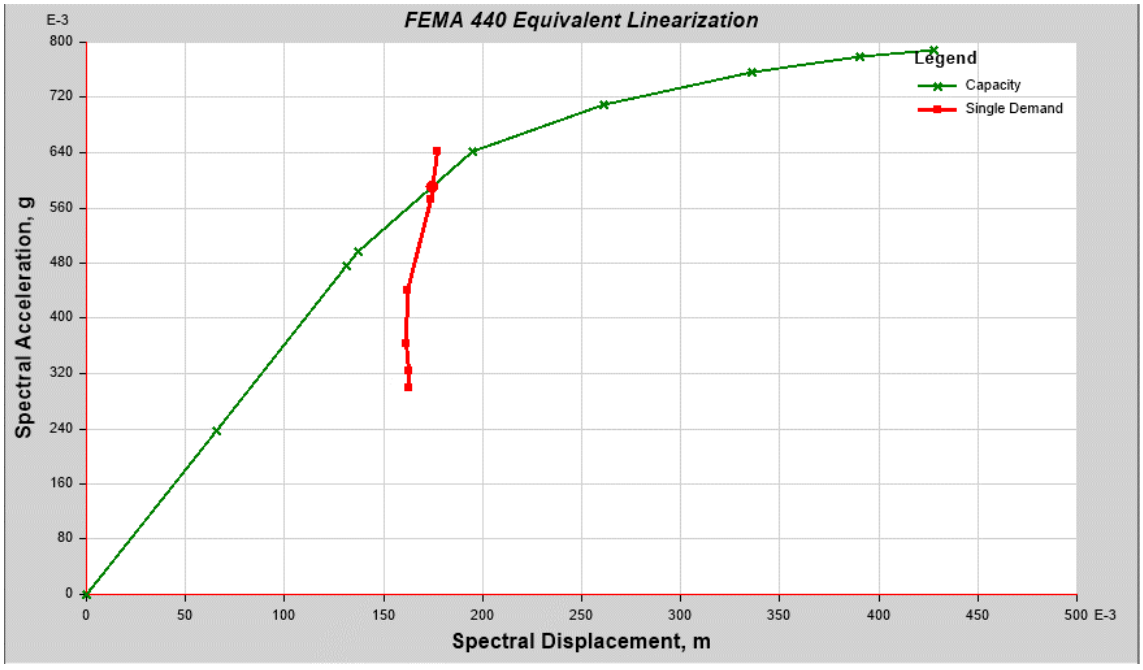

Performance point force model first mode load pattern x direction.

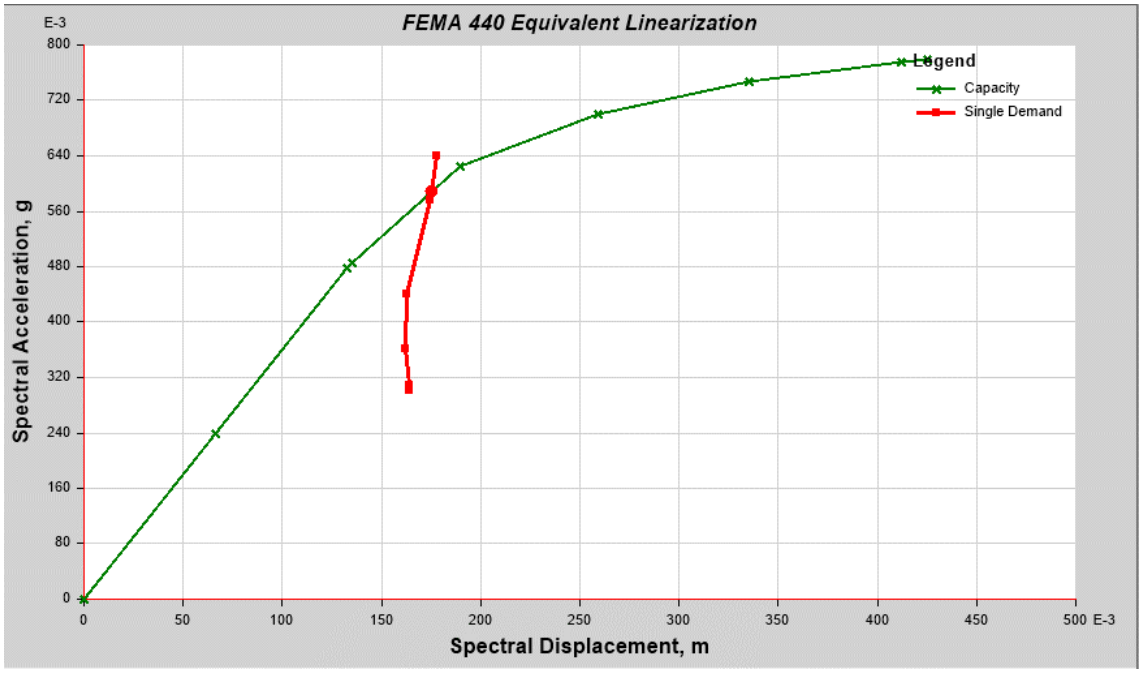

Performance point force model triangular load pattern x direction.

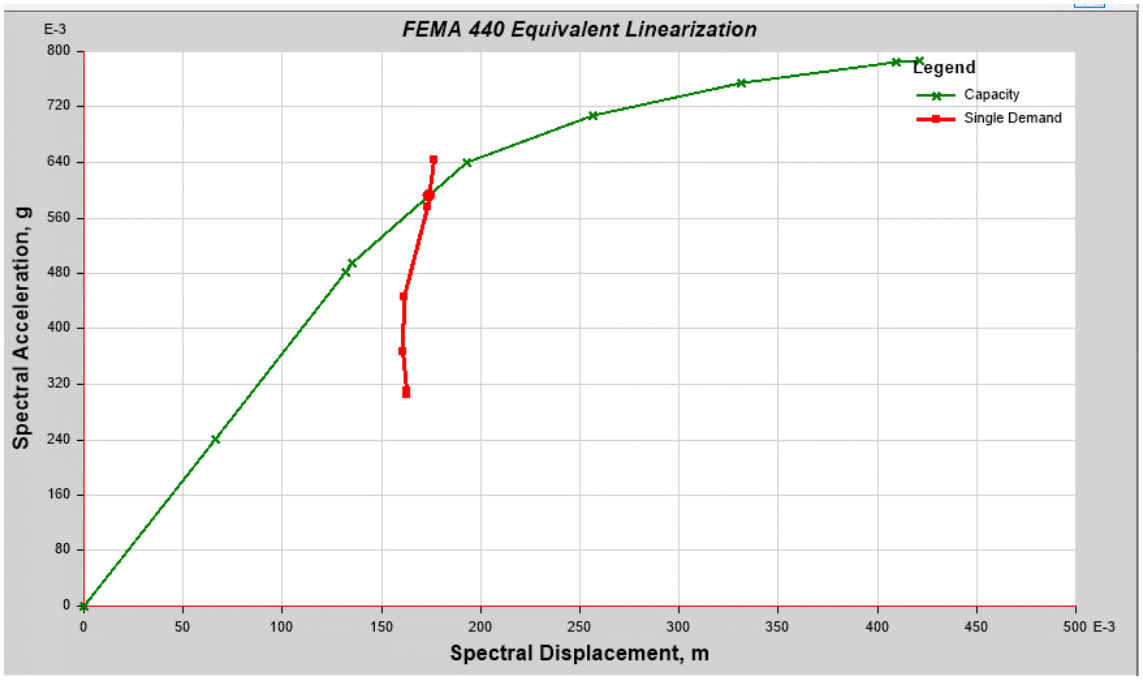

Performance point DDBD model DDBD load pattern y direction.

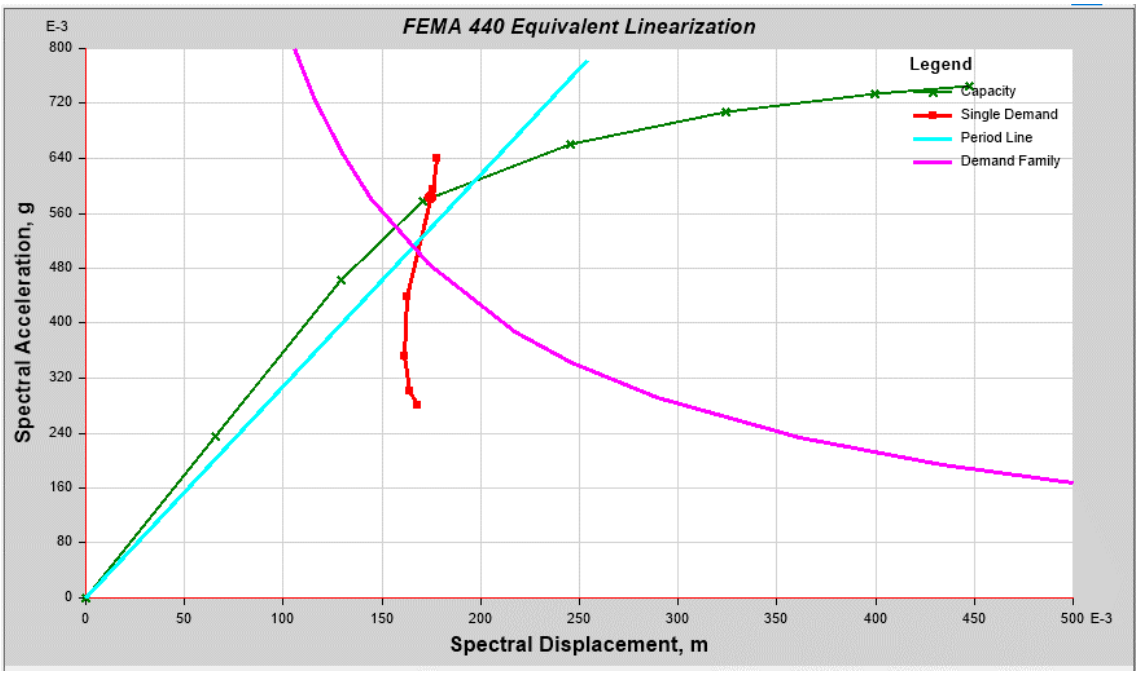

Performance point DDBD model First mode load pattern y direction.

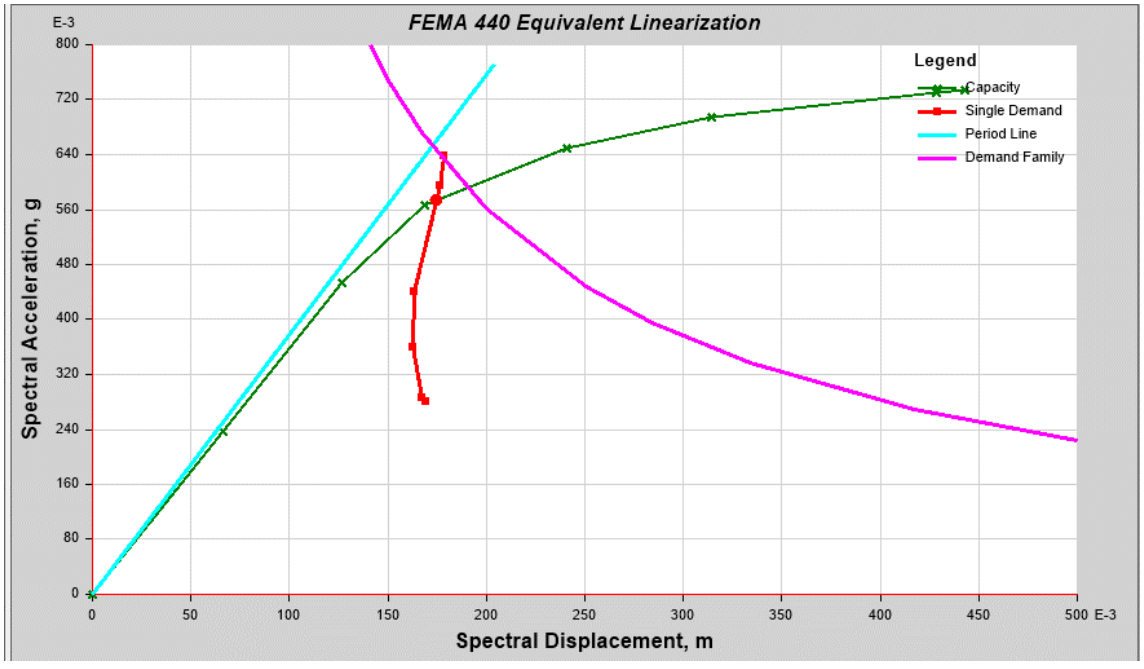

Performance point DDBD model triangular load pattern y direction.

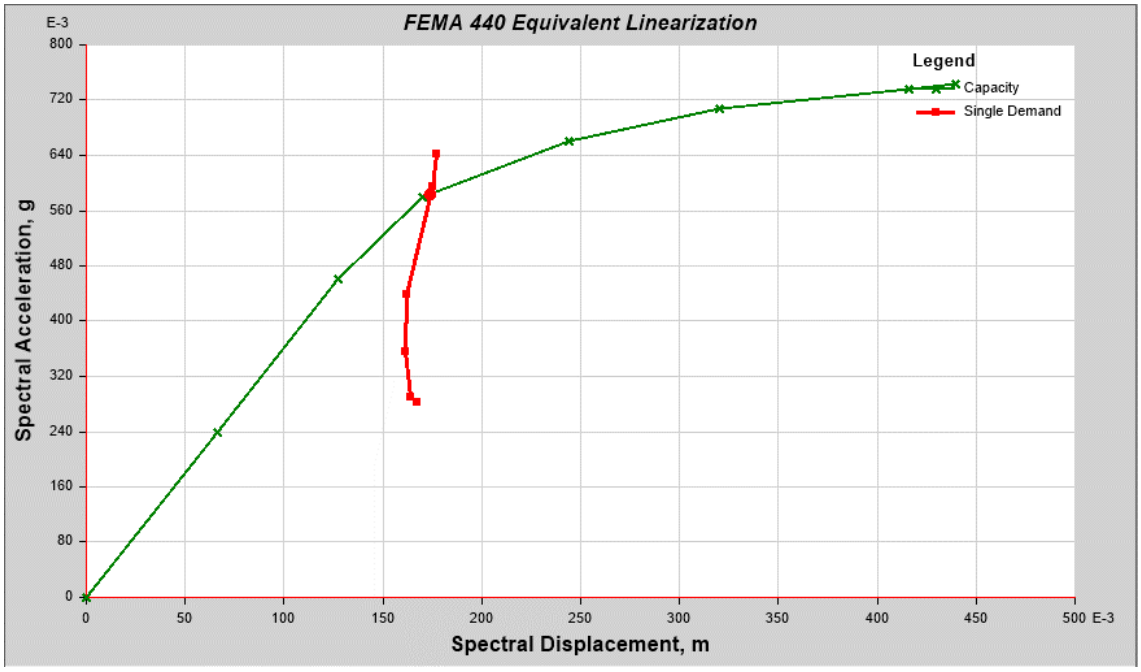

Performance point force model DBDD load pattern y direction.

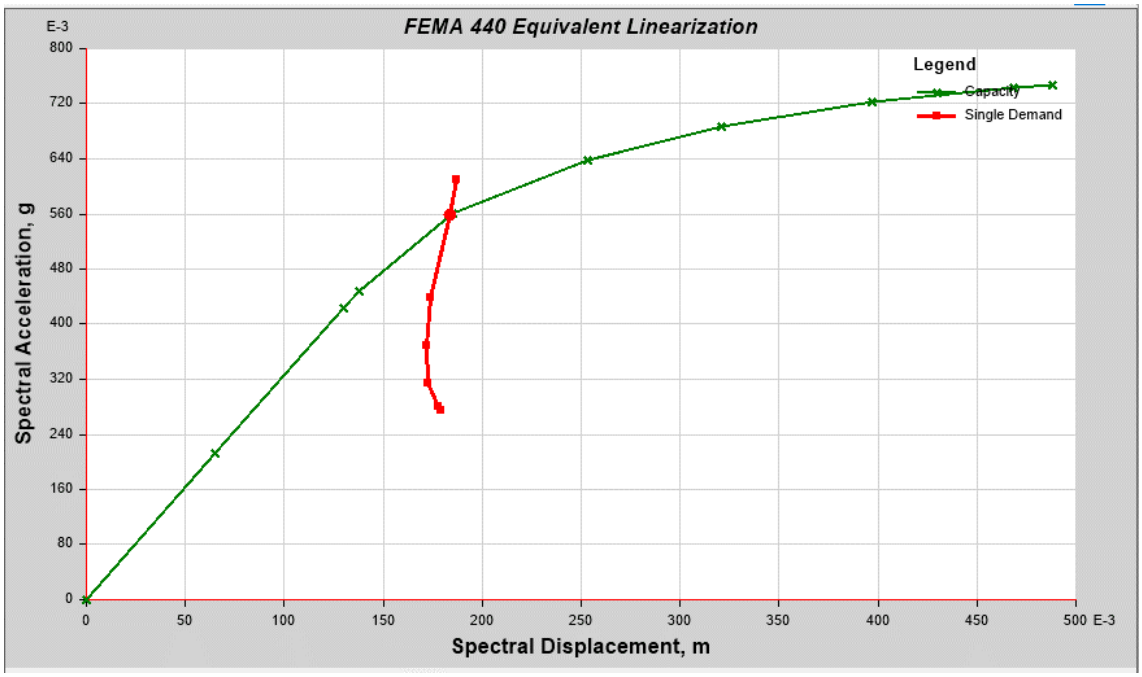

Performance point force model first mode load pattern y direction.

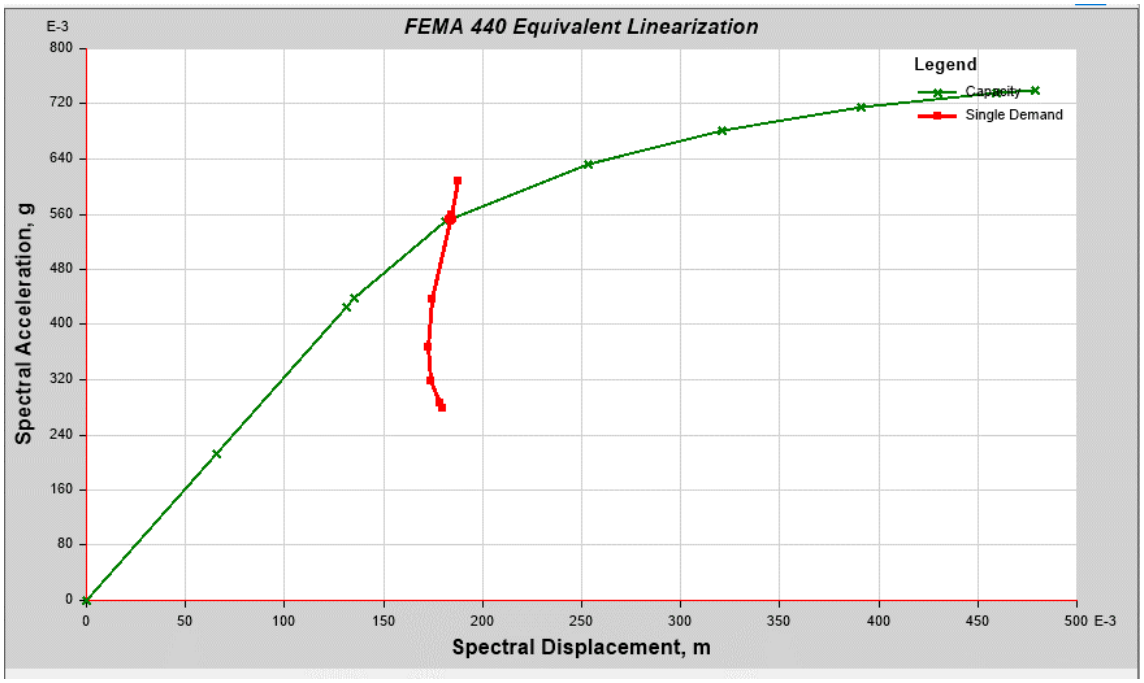

Performance point force model triangular load pattern y direction.